RICE UNIVERSITY

On the Parametrization of Ill-posed Inverse Problems Arising from Elliptic Partial Differential Equations

by

Fernando Guevara Vasquez

A THESIS SUBMITTED
IN PARTIAL FULFILLMENT OF THE
REQUIREMENTS FOR THE DEGREE
Doctor of Philosophy

Approved, Thesis Committee:

Liliana Borcea, Chair
Associate Professor of
Computational and Applied Mathematics

Frank Jones
Noah G. Harding Professor of Mathematics

Danny C. Sorensen
Noah G. Harding Professor of
Computational and Applied Mathematics

William W. Symes
Noah G. Harding Professor of
Computational and Applied Mathematics

Houston, Texas
July 2006

Abstract

On the Parametrization of Ill-posed Inverse Problems

Arising from Elliptic Partial Differential Equations

by

Fernando Guevara Vasquez

Electric impedance tomography (EIT) consists in finding the conductivity inside a body from electrical measurements taken at its surface. This is a severely ill-posed problem: any numerical inversion scheme requires some form of regularization. We present inversion schemes that address the instability of the problem by proper sparse parametrization of the unknown conductivity.

To guide us, we consider a consistent finite difference approach to an inverse Sturm-Liouville problem arising in EIT for layered media. The method first solves a model reduction problem for the differential equation where the reduced model parameters are essentially averages of the conductivity over the cells of a grid depending on the conductivity. Fortunately the dependence is weak. Thus one can efficiently estimate conductivity averages by using the grid for a reference conductivity. This simple inversion method converges to the true solution as the number of measurements increases. We analyze the sensitivity of the reduced model parameters to small changes in the conductivity, and introduce a Newton-type iteration to improve the reconstructions of the simple inversion method. As an added bonus, our method can benefit from a priori information if available.

We generalize both methods to the 2D EIT problem by considering finite volumes discretizations of size determined by the mesurement precision, but where the node locations are to be determined adaptively. This discretization can be viewed as a resistor network, where the resistors are essentially averages of the conductivity over grid cells. We show that the model reduction problem of finding the smallest

resistor network (of fixed topology) that can predict meaningful measurements of the Dirichlet-to-Neumann map is uniquely solvable for a broad class of measurements. We propose a simple inversion method that, as in the simple method for the inverse Sturm-Liouville problem, is based on an interpretation of the resistors as conductivity averages over grid cells, and an iterative method that improves such reconstructions by using sensitivity information on the changes in the resistors due to small changes in the conductivity. A priori information can also be incorporated to the latter method.

Acknowledgements

First of all I would like to thank my advisor Prof. Borcea for her invaluable guidance, help and support throughout my studies. I would also like to thank Prof. Jones; the clarity of his classes made going to them so much fun. He is a teaching model for me and anyone teaching mathematics. Also I am grateful to Prof. Sorensen for his excellent, down to earth advice and his immensely helpful teachings. I am also indebted to Prof. Symes for making hard things look easy and for his seminar classes that interested me and that taught me so much about inverse problems.

I am particularly indebted to my friend and colleague Vladimir; many of the ideas in this thesis would not have come to light without his help. Also he gave me the opportunity of working as an intern in the Summer 2005 at the Schlumberger-Doll research Math and Modelling group. Some of the results in this thesis are a direct answer to conversations I held with Tarek, Aria, Mikhail and many others. Many thanks to Leonid for granting me permission to use his optimal grid code; I learned a lot from it.

Back to my alma mater. I am grateful to Prof. Embree, Prof. Zhang, Prof. Heinkenschloß, Prof. Hintermüller and Prof. Tapia for their encouragements, helpful conversations and counsel.

I am also grateful to my friends and colleagues from CAAM, specially Agata, Anatoly, Denis, Eric, Fernando, Joanna, John, Michael and Mili; my studies would not have been fun without them. I am also specially indebted to Daria, Fran, Ivy and Margaret for making our grad student lives so much easier.

I am lucky for having long time, good friends in El Salvador (Pedro, Andrés, Napo, Mónica y Loïc, Loli,...) and in France (Palmo et Ingrid, Stoub et Julie, Johanna, Doudoule et Laure, Alexis, Romain, Karine et Mathieu, François,...), that were supportive all along and despite the distance.

I am also thankful for having such a wonderful and supportive family: my parents Lorena and Fernando, my sisters Bea and Patty, my brother José, my grandmother, and all my nephews, nieces, cousins, aunts, uncles, and in-laws.

I dedicate this work to my dear wife Alexandra for all her patience and love.

This work was supported in part by NSF grant DMS-0305056, and was compiled from revisions tex:599, bib:599.

Contents

1 Introduction and background **1**
1.1 Electrical Impedance Tomography 3
1.1.1 Uniqueness results for EIT 5
1.1.2 The inherent instability of EIT 6
1.2 Adaptive discretizations for ill-posed inverse problems 7
1.2.1 Distinguishability 8
1.2.2 A local resolution estimate 10
1.2.3 Multilevel inversion 12

2 A consistent finite difference approach to an inverse spectral problem **15**
2.1 The inverse spectral problem and its link to EIT 16
2.1.1 An inverse spectral problem arising in EIT for layered media . 16
2.1.2 Review of existing results for inverse spectral problems 19
2.2 Optimal grids for the inverse spectral problem 22
2.2.1 The discretization and its relation to the resistor network reduced model 23
2.2.2 The inverse problem for the resistor network 27
2.2.3 Optimal grid construction 29
2.2.4 The inverse problem for the conductivity 30
2.3 Sensitivity analysis of the optimal grid inversion 32
2.3.1 Sensitivity of the Jacobi Inverse Eigenvalue Problem 33
2.3.2 Sensitivity of the spectrum to the conductivity 35
2.3.3 Sensitivity of the resistors to the conductivity 39
2.4 A Newton type iterative algorithm for the inverse spectral problem . 41
2.4.1 The Gauss-Newton iteration 42
2.4.2 Numerical results for the Gauss-Newton iteration 44
2.4.3 Introducing a priori information 51
2.4.4 Numerical results with a priori information 52

3 Electrical impedance tomography with circular planar graphs **56**
3.1 Finite volumes discretization 58
3.1.1 The staggered finite volume grids 58

3.1.2 The finite volumes scheme 59
3.2 From continuum DtN maps to resistor networks 63
3.2.1 The measured DtN map 64
3.2.2 Uniqueness of the resistor network reduced model 66
3.2.3 Consistency of the measurements with the R-net model 70
3.2.4 The resistor finding problem 75
3.2.5 The resistor network for noisy measurements 75
3.3 From resistor networks to conductivity averages 78
3.3.1 Optimal grid construction for layered conductivities 79
3.3.2 Reconstructing averages of the conductivity 81
3.3.3 Does the grid depend weakly on the conductivity? 85
3.4 A Newton-type iterative algorithm for the inverse problem 90
3.4.1 The Gauss-Newton iteration 91
3.4.2 Numerical experiments for the Gauss-Newton algorithm 94
3.4.3 Introducing a priori information about the solution 99
3.4.4 Numerical experiments with a priori information 101
3.4.5 Comparison of our method to output least squares 102

4 Summary and future work **106**
4.1 Summary 106
4.2 Future work 107

A Optimal finite difference grids for the forward problem **109**

B Working with DtN map measurements **111**
B.1 The singular functions of the DtN map difference do not always become smoother as the singular values increase 111
B.2 Converting NtD map measurements to DtN map measurements with convex duality 112
B.3 The mollified DtN map 116
B.4 Lumping of the measurements 117

C Supplement for the two dimensional numerical experiments **120**
C.1 Conductivity definitions 120
C.2 The smoothed box function 121

List of Figures

2.1 Preview of the finite volumes discretization of Chapter 3. 26
2.2 Grids obtained by rational approximation of the impedance function. 30
2.3 Sensitivity functions of the resistors to perturbations in the conductivity. 40
2.4 Convergence history for Algorithm 2.12 on a piecewise constant conductivity. 48
2.5 More reconstruction examples for Algorithm 2.12. 49
2.6 Conditioning of the Jacobian $D\widetilde{\Gamma}_n[\sigma]$ and of the sensitivities of the spectrum to changes in the conductivity. 50
2.7 Reconstructions from spectral data using Algorithm 2.13 with a TV penalty functional, for a piecewise constant conductivity. 55
2.8 Reconstructions from spectral data using output least squares with a TV regularization term, for a piecewise constant conductivity. 55

3.1 Representative examples of the two kinds of grids we use. 60
3.2 A cell in the finite volume discretization. 61
3.3 Physically, the measured DtN map $\mathcal{M}_n(\Lambda_\sigma^{DtN})$ can be thought of as measurements taken with electrodes at the boundary. 65
3.4 Examples of $C(l,n)$ resistor networks. Here $l=(n-1)/2$ so that the network is critical, and thus uniquely recoverable. 66
3.5 Explanation of the Y-Δ transformation for resistor networks. 68
3.6 Critical graphs for an even number n of boundary points. 69
3.7 The R-net coming from linear triangular finite elements is not critical. 70
3.8 Singular values and functions of the NtD difference map. 78
3.9 The finite volume discretization for $\sigma \equiv 1$. 81
3.10 The conductivities used in the two dimensional numerics. See Appendix C for a precise definition. 84
3.11 Reconstructions of local averages of a smooth conductivity. 86
3.12 Reconstructions of local averages of a piecewise constant conductivity. 87
3.13 Reconstructions of local averages of a piecewise constant conductivity from noisy measurements. 88
3.14 Reconstructions of local averages of a smooth conductivity from noisy measurements. 89

3.15 Sensitivity functions for the reconstructed averages of Algorithm 3.15 to perturbations in the conductivity. 93
3.16 Convergence history for Algorithm 3.17 on a smooth conductivity. . . 97
3.17 Convergence history for Algorithm 3.17 on a piecewise constant conductivity. 98
3.18 Typical convergence history of the SQP algorithm for the minimization in Algorithm 3.18 with a TV penalty functional. 103
3.19 Reconstructions from noiseless data using Algorithm 3.18 with TV penalty functional. 104
3.20 Comparison of the method of Section 3.4.3 with traditional output least squares. 105

B.1 Singular values of the DtN map difference for Example B.1. 113
B.2 Singular values and functions of the DtN map difference. 114
B.3 How n measurement functions ϕ_i for the DtN map could be obtained from $2n$ measurement functions ψ_k of the NtD map. 116

C.1 The smoothed box function $\phi(t)$ we use to define the measured DtN map, rescaled to have values in $[0, 1]$. 122

List of Tables

3.1 Network sizes for inversion found by the method discussed in Section 3.2.5. 85
3.2 Condition number of $D\Gamma_n[\sigma]$ compared to that of $D\mathcal{M}_n[\sigma]$. 96

Chapter 1

Introduction and background

This Thesis focuses on the numerical solution of inverse problems arising in elliptic partial differential equations, where one wishes to determine the coefficients in the equation from boundary measurements. Specifically we look at the Electrical Impedance Tomography (EIT) problem, where the goal is to determine the conductivity function inside a domain Ω from simultaneous measurements of electric currents and voltages at the boundary of the domain. As we see in Section 1.1, this problem is known to be uniquely solvable, but is severely ill-posed, meaning that the conductivity does not depend continuously on the data. Therefore any numerical reconstruction method needs some form of regularization. We introduce reconstruction methods that obtain fast and stable reconstructions using proper sparse parametrizations of the unknown conductivity.

Clearly, any numerical inversion method for the EIT problem requires some parametrization of the unknown conductivity. Since the EIT problem is severely ill-posed, noise in the measurements severely limits the number of parameters that we can hope to recover. The idea of regularization by means of sparse representation of the unknown in some preassigned basis of functions has been proposed for linear inverse problems [37]. But the question remains how to choose a good basis of functions,

specially when we do not have any a priori information about the unknown quantity. We looked at bases consisting of characteristic functions of cells in a grid partitioning the domain Ω, where the size of the grid is to be determined from the noise in the measurements and the location of the grid points is to be determined *adaptively* as part of the inverse problem. Adaptivity is key because we know from resolution studies (see Section 1.2) that the resolution at which we can expect to reconstruct the conductivity is higher close to the surface of measurements than deep inside the domain.

To guide us in the solution of the EIT problem, we consider in Chapter 2 an inverse Sturm-Liouville problem (a type of inverse spectral problem) arising in EIT for layered media. We improve the method of Borcea, Druskin and Knizhnerman [19, 20], which is a consistent finite differences based approach that is probably the first rigorous result for finding a parametrization that takes into account the resolution limits of the problem. By rigorous we mean that convergence to the true solution as the number of measurements increases has been established [20]. In a nutshell, the method first finds the parameters of a reduced model for the differential equation. The parameters can be viewed as averages on a grid that alas depends on the conductivity. Fortunately, the dependence is weak, i.e. changing the conductivity does not change significantly the grid. This leads to a simple inversion procedure based on interpreting the averages on the precomputed grid for a reference conductivity. Our contribution is to use a sensitivity analysis of the reduced model parameters to perturbations in the conductivity, in the context of a Newton-type iterative procedure, to improve the reconstructions of [19, 20] when only a limited number of measurements are available. Moreover, our method can incorporate a priori information about the conductivity if it is available in the form of a penalty functional.

Then in Chapter 3, we extend the inversion methods of Chapter 2 to the EIT

problem in dimension two. First we solve the model reduction problem of finding the smallest resistor network of fixed topology that can predict meaningful measurements of the Dirichlet-to-Neumann map. We have established that for a broad class of measurements, this model reduction problem admits a unique solution. Then as in [19, 20] we interpret the reduced model parameters, i.e. the resistors, as averages of the conductivity over the grid cells of a finite volume discretization. Assuming the grid depends weakly on the conductivity, we estimate averages of the conductivity on a precomputed grid. However, we must be careful because unlike the inverse spectral problem, the EIT problem is severely ill-posed. Thus no matter how many measurements we take, the measurement precision severely limits the number of parameters we hope to recover. So we limit the size of the network according to the measurement precision. Finally we show that the same Newton-type iterative technique can be used to improve the reconstructions of this simple method and to incorporate a priori information about the true solution.

Chapters 2 and 3 have few cross-references and are meant to be standalone. Therefore, there is some overlap in the explanations of both chapters, specially for the Newton-type iterative method. Finally we conclude in Chapter 4 with some remarks and ideas for future work.

1.1 Electrical Impedance Tomography

The goal of Electrical Impedance Tomography (EIT) is to infer electrical properties (such as the conductivity) inside of a body from measurements of the voltages and the electric current density on its boundary. Among the applications for this inverse problem are: medical imaging [27], geophysical prospection [92] and non-destructive testing of materials [69].

This Thesis focuses on a static (DC) setup for EIT, which we now describe. Let Ω be a simply connected, bounded and open domain of $\mathbb{R}^d$ with $d \geq 2$ and let the (electric) conductivity $\sigma(\mathbf{x})$ be a positive, bounded function defined in $\overline{\Omega}$. The electric potential u satisfies the following elliptic second order partial differential equation inside the domain Ω,

$$\nabla \cdot [\sigma \nabla u] = 0, \tag{1.1}$$

which means neither current sinks nor current sources exist inside Ω. The *Dirichlet-to-Neumann (DtN) map* $\Lambda_\sigma^{DtN} : H^{1/2}(\partial\Omega) \to H^{-1/2}(\partial\Omega)$ maps Dirichlet boundary conditions (voltages at the boundary) to the resulting current density at the boundary:

$$\Lambda_\sigma^{DtN} V = \mathbf{n} \cdot (\sigma \nabla u) \,|_{\partial\Omega}, \tag{1.2}$$

where u is the potential satisfying (1.1) with Dirichlet boundary condition $u|_{\partial\Omega} = V$ and $\mathbf{n}(\mathbf{x})$ is the outward pointing, unit normal vector to the boundary at $\mathbf{x} \in \partial\Omega$. The DtN map is well-defined because the potential at the interior is uniquely determined by Dirichlet boundary conditions. We can now pose the *EIT problem*.

Problem 1.1. *Find the conductivity σ inside the domain Ω from the Dirichlet-to-Neumann map Λ_σ^{DtN}.*

Equivalently, the DtN map in Problem 1.1 can be exchanged by the *Neumann-to-Dirichlet (NtD) map* $\Lambda_\sigma^{NtD} : H^{-1/2}(\partial\Omega) \to H^{1/2}(\partial\Omega)$ that maps current densities at the boundary (Neumann boundary conditions) satisfying the *compatibility condition* $\int_{\partial\Omega} I(\mathbf{x}) d\mathbf{x} = 0$ to voltages at the boundary,

$$\Lambda_\sigma^{NtD} I = u|_{\partial\Omega}, \tag{1.3}$$

where the potential u satisfies (1.1) with Neumann boundary condition $\mathbf{n} \cdot (\sigma \nabla u) \,|_{\partial\Omega} = I$.

With such boundary conditions, the potential is defined up to an additive constant (or rather grounding potential), which we choose by requiring that $\int_{\partial\Omega} u|_{\partial\Omega}(\mathbf{x})d\mathbf{x} = 0$.

Formulating Problem 1.1 with either the NtD or the DtN map is equivalent because the NtD map is the generalized pseudo-inverse of the DtN map, so the two maps carry the same information. Next we show through a review of the main theoretical results for EIT, that although under certain conditions the EIT problem admits a unique solution, it is a severely ill-posed problem.

1.1.1 Uniqueness results for EIT

The question of uniqueness for the EIT problem was first addressed in the landmark paper by Calderón [23], where the injectivity of the linearized DtN map is established. For the non-linear problem, Kohn and Vogelius [71] proved that an infinitely smooth bounded conductivity is uniquely identifiable at the boundary from the DtN map. Thus for analytic conductivities (or even piecewise analytic [72]), uniqueness at the interior is guaranteed in $\mathbb{R}^2$. Independently, Druskin [43, 48] proved uniqueness for piecewise constant and piecewise analytic conductivities in a unbounded domain of $\mathbb{R}^3$, with measurements given on a two dimensional plane.

Sylvester and Uhlmann [107] used Calderón's complex exponential harmonic functions to show uniqueness for the nonlinear problem in dimension three and higher, provided the conductivity is infinitely smooth. Their result was later extended to less smooth conductivities (e.g. [88, 22]), always in dimension three and higher.

In dimension two, the focus of Chapter 3, the first results (e.g. [106, 103, 104, 105]) were *local* in nature, i.e. only valid for conductivities belonging to very particular classes of functions and sufficiently close conductivities. Nachman [89] brought forward the first global result in dimension two by producing a constructive uniqueness proof for $W^{2,p}$ conductivities with $p > 1$. Very recently the uniqueness question

in dimension two was laid to rest by Astala, Päivärinta, and Lassas [8] since they established uniqueness for L^∞ conductivities.

Our account of uniqueness results for EIT is not meant to be exhaustive. We point instead to the thorough reviews of e.g. Uhlmann [111] or Borcea [18].

1.1.2 The inherent instability of EIT

The EIT problem is ill-posed in the sense that the conductivity in the interior does not depend continuously on the data (which can be either the DtN or NtD map). There are several ways to exhibit the discontinuity of the inverse map, but to fix ideas we start with a heuristic reasoning. In order to find the conductivity σ, we first need to find the potential u inside Ω. Actually the potential u solves the Cauchy problem for the elliptic equation (1.1), with the Neumann and Dirichlet conditions acting as initial data. Such problems are known to be *exponentially ill-posed* as the classical example of Hadamard [57] shows (see e.g. [51, p54]).

An example in dimension two due to Alessandrini [2] shows that the inverse map $\Lambda_\sigma^{DtN} \to \sigma$ is not continuous by giving a sequence of simple conductivities that are piecewise constant and radially symmetric on the unit disk, so that the DtN map can be computed explicitly. The sequence is such that $\Lambda_{\sigma^{(k)}}^{DtN}$ converges to Λ_1^{DtN} in the $H^{1/2}(\partial\Omega) \to H^{-1/2}(\partial\Omega)$ norm but $\|\sigma^{(k)} - 1\|_{L^\infty(\Omega)} = C > 0$. A similar conclusion can be reached for the NtD map. For example Dobson [40] used homogenization techniques to show the discontinuity of the inverse map $\Lambda_\sigma^{NtD} \to \sigma$ in the topology induced by the $L^2(\partial\Omega) \to L^2(\partial\Omega)$ norm for the NtD map and the $L^\infty(\Omega)$ norm for the conductivity.

A quantitative estimate of the discontinuity of the inverse map was given by Alessandrini [2] in the form of logarithmic estimates for $\Lambda_\sigma^{DtN} \to \sigma$ when the conductivities are smooth enough in dimension three and higher. His results were sub-

sequently generalized to encompass dimension two and less regular conductivities by Liu [76] and Barceló et al. [12]. The logarithmic estimates by Alessandrini [2] and Liu [76] state that for $d \geq 2$ there are constants $C > 0$ and $\delta \in (0, 1)$ such that[1]

$$\|\sigma_1 - \sigma_2\|_{L^\infty(\Omega)} \leq C \left(\ln \left(1 + \left\| \Lambda_{\sigma_1}^{DtN} - \Lambda_{\sigma_2}^{DtN} \right\|^{-1}_{H^{1/2}(\partial\Omega), H^{-1/2}(\partial\Omega)} \right) \right)^{-\delta}, \tag{1.4}$$

for smooth enough conductivities σ_1 and σ_2. Furthermore, Alessandrini [4] gave an example where (1.4) is tight. Recently Mandache [80] proved that these logarithmic estimates are in fact optimal, and he gave bounds on the exponent δ.

Logarithmic estimates suggest one requires exponentially accurate data to get an acceptable $L^\infty(\Omega)$ error in the reconstructed conductivity. However, these estimates are too pessimistic because of their global nature. For example, the conductivity is determined at the boundary in a stable way from the measurements [71, 108, 88]. Additionally, one can expect to distinguish better the values of the conductivity that are closer to the boundary than deep inside Ω, as we see next.

1.2 Adaptive discretizations for ill-posed inverse problems

We now review inversion methods for EIT (or related ill-posed inverse problems) where, as in the methods we introduce in this Thesis, the parametrization of the unknown quantity is chosen to account for the intrinsic resolution limits of the problem.

We start in Section 1.2.1 with the notion of *distinguishability*, which quantifies the resolution of EIT in the realistic case of noisy data and thus helps in determining a discretization for the conductivity. One way of estimating the distinguishability is described in Section 1.2.2. Then Section 1.2.3 is devoted to multilevel methods which solve the inverse problem on a coarse grid to help the inversion on a finer grid.

[1] Here the norm $\|\cdot\|_{H^{1/2}(\partial\Omega), H^{-1/2}(\partial\Omega)}$ is the operator norm from $H^{1/2}(\partial\Omega)$ to $H^{-1/2}(\partial\Omega)$.

In Chapter 3 we shall use an adaptive method for inverse Sturm-Liouville problems [19, 20] to guide us in finding adaptive discretizations for the conductivity in EIT. The review of the inversion algorithm [19, 20] is left to Section 2.2.

1.2.1 Distinguishability

How many details of the conductivity can we expect from an imperfect knowledge of the data in EIT? To understand this, Isaacson [65, 54] considered the set of perturbations $\delta\sigma$ that cannot be distinguished from a background conductivity σ^0 at a noise level δ in the measurements,

$$\mathcal{P}_\delta = \left\{ \delta\sigma \in L^\infty(\Omega) \text{ such that } \left\| \Lambda^{NtD}_{\sigma_0+\delta\sigma} - \Lambda^{NtD}_{\sigma_0} \right\|_{L^2(\partial\Omega),L^2(\partial\Omega)} < \delta \right\}. \tag{1.5}$$

For all practical purposes, the indistinguishable set[2] $\mathcal{P}_\delta$ is the nullspace of the forward map $\sigma \to \Lambda^{NtD}_\sigma$ at a measurement precision of δ.

To study the set $\mathcal{P}_\delta$, Isaacson [65] and independently Seagar et al. [96, 97] determined which circular inclusions are distinguishable from a constant background conductivity defined on the unit disk. For such simple conductivities, analytic formulas can be derived for the NtD maps with and without inclusion. For example if the inclusion is concentric, the analysis yields the singular values $s_k(r)$ of the "voltage difference map" $\Lambda^{NtD}_{\sigma_0+\delta\sigma} - \Lambda^{NtD}_{\sigma_0}$ for an inclusion of radius r. The radius r_1 of the smallest circular inclusion at the center distinguishable at a noise level δ can thus be found by solving $s_1(r) = \delta$, which gives $r_1 \approx \sqrt{\delta/(2+\delta)}$. The analysis by Seagar et al. [96, 97] covers circular inclusions that are not necessarily centered.

Moreover, Dobson [40, 41] gives upper and lower bounds to the indistinguishable

[2] In all generality, the operator norm in (1.5) should be replaced by the $H^{-1/2}(\partial\Omega), H^{1/2}(\partial\Omega)$ operator norm which is harder to manipulate than the norm used in (1.5). However, both norms give similar results if $\delta\sigma|_{\partial\Omega} = 0$ (see [54]).

set in the linearized EIT problem around a constant conductivity. The originality of his approach is to use a wavelet basis for capturing simultaneously information about the localization and the size of the largest indistinguishable perturbations. Specifically he confirms that the perturbations that are near the center are exponentially harder to distinguish than those near the boundary. However, there are no generalizations or implementations of Dobson's ideas, and this remains an open research area.

A heuristic for discretizing the conductivity based on distinguishability is proposed by Gisser, Isaacson, and Newell [54] and used in [26] for reconstructions from NtD map measurements collected on N uniformly spaced electrodes. The idea is to discretize the conductivity as a piecewise constant function on a grid that is uniform in angle with as many angular subdivisions as electrodes. The total number of degrees of freedom in the grid is chosen to be the number of independent measurements that can be done with N electrodes, i.e. $N(N-1)/2$.[3] The number N of electrodes can be estimated from the measurement precision by assuming the grid is uniform in the radial direction, with smallest radial subdivision being the radius r_1 given as above.

The use of distinguishability is taken further in the layer peeling algorithm of Somersalo et al. [99]. Basically, the conductivity is first estimated on a layer close to the boundary from the NtD map. Then the layer is peeled off by estimating the NtD map on the domain without the layer. Reiterating the procedure, one can estimate the conductivity layer by layer. To obtain good reconstructions, the radius r_k of layer k (counting outwards from the center) is in [99] the radius of the smallest feature at the center that can be distinguished by an excitation of frequency k. Clearly the radius r_k comes from the singular values $s_k(r)$ of the voltage difference map for circular inclusions by solving $s_k(r) = \delta$, since on closer inspection the singular

[3] The measured NtD map is an $N \times N$ matrix with zero row sum, so it is determined by $N(N-1)/2$ of its entries, e.g. its strict upper triangular part.

functions corresponding to $s_k(r)$ are the trigonometric functions $\cos(k\theta)$ and $\sin(k\theta)$. Positioning the layers in this way puts more layers close to the boundary than near the center, since higher frequencies penetrate less than lower frequencies. This is in concordance with the expected resolution loss away from the boundary.

The gridding techniques of this Section are heuristic, since they are based on distinguishability estimates of single inclusions on a constant background. However, the forward map $\sigma \to \Lambda_\sigma^{NtD}$ is non-linear, and hence the effect of several inclusions is not the sum of the effects of each inclusion considered separately.

1.2.2 A local resolution estimate

We review the study of MacMillan, Manteuffel, and McCormick [79] on the resolution limits of EIT and the discretization of the conductivity that can be derived from it.

Main theoretical results

Let σ and σ^* be conductivities belonging to a set where injectivity of the NtD map has been established (Section 1.1.1). In the following σ^* is understood as the true conductivity of the domain Ω, and σ as a trial conductivity. MacMillan et al. [79] start by defining a *local* norm on the set of conductivities by

$$\|\gamma\|_{\sigma^*} := \sup_{I_1, I_2 \in \mathcal{I}} \frac{\left| \int_\Omega \gamma \nabla u_1^* \cdot \nabla u_2^* d\mathbf{x} \right|}{\|I_1\|_{H^{-1/2}(\partial\Omega)} \|I_2\|_{H^{-1/2}(\partial\Omega)}}, \tag{1.6}$$

where u_1^* and u_2^* solve the PDE (1.1) with conductivity σ^* and Neumann boundary conditions $I_1 \in \mathcal{I}$ and $I_2 \in \mathcal{I}$ respectively. Here $\mathcal{I}$ represents the set of functions in $H^{-1/2}(\partial\Omega)$ that are orthogonal to the constants. The injectivity of the NtD map

together with the following inequalities guarantee that $\|\cdot\|_{\sigma^*}$ is indeed a norm [79]:

$$\eta_{\min}\|\sigma-\sigma^*\|_{\sigma^*} \leq \left\|\Lambda_\sigma^{NtD}-\Lambda_{\sigma^*}^{NtD}\right\|_{H^{-1/2}(\partial\Omega)\to H^{1/2}(\partial\Omega)} \leq \eta_{\max}\|\sigma-\sigma^*\|_{\sigma^*}, \qquad (1.7)$$

where

$$\eta_{\min}=\min_{\mathbf{x}\in\Omega}\frac{\sigma^*(\mathbf{x})}{\sigma(\mathbf{x})} \quad \text{and} \quad \eta_{\max}=\max_{\mathbf{x}\in\Omega}\frac{\sigma^*(\mathbf{x})}{\sigma(\mathbf{x})}.$$

The inequalities (1.7) rely on an identity due to Alessandrini [3] and can be thought of as a *coercivity bounds* for the NtD map. Moreover, the inequalities (1.7) have been generalized to encompass the loss of precision due to having a discrete set of measurements [79]. Strictly speaking (1.7) are not coercivity bounds for two reasons. First, the "constants" $\eta_{\min}$ and $\eta_{\max}$ depend on σ and σ^*, but given enough a priori information on σ^*, upper and lower bounds on $\eta_{\min}$ and $\eta_{\max}$ can be derived. In some situations, for instance high contrast media, such bounds may end up being too loose to be useful. Second, the norm used in the bound depends on σ^*, which is unknown.

The norm $\|\cdot\|_{\sigma^*}$ automatically incorporates resolution information about the problem. This is because the quantity $-\nabla u_1^*\cdot\nabla u_2^*$ that weights γ in (1.6) also appears in the linearization about σ^* of the quadratic form $Q_{\sigma^*}(I,J)=\left\langle I,\Lambda_{\sigma^*}^{NtD}J\right\rangle$, and from e.g. Dobson's [41] resolution studies of the linearized NtD map, the product $\nabla u_1^*\cdot\nabla u_2^*$ is larger close to the boundary than deep inside the domain.

Grid construction

The inequalities (1.7) readily give upper and lower bounds for the set of indistinguishable perturbations for the non-linear EIT problem. MacMillan et al. [79] construct grids for the conductivity based on these resolution estimates, which are meant to illustrate the resolution loss towards the center of the domain. To our knowledge there are no reconstruction methods using such grids.

The proposed representation for the conductivity in [79] is a piecewise constant function on a grid specified by angular and radial subdivisions of the unit disk, obtained by taking $\sigma \equiv 1$ and $\sigma^* = \sigma + \delta\sigma$ in (1.7), where the perturbations $\delta\sigma$ are the characteristic functions of grid cells. The radial dimension of a cell is essentially determined as the smallest such that $\delta\sigma$ is distinguishable in the sense of estimate (1.7), whereas the angular dimension comes from fixing the cell's "aspect ratio".

Instead of using the grid described here to represent the conductivity, MacMillan et al. [78] solve an optimization problem with a functional obtained with the so-called *first order system least squares* (FOSLS) method. The functional incorporates resolution limits because of a weighting term similar to the one weighting γ in (1.6).

1.2.3 Multilevel inversion

We review inversion methods that use a coarse discretization to stabilize the inversion on a finer discretization.

Multigrid methods

Borcea [17] devised a non-linear multigrid method for imaging in EIT. Her method starts by finding a very good guess of the impedance on a coarse grid. This step in itself is relatively stable. Then full multigrid (nested iteration) is used to solve on a finer grid the first-order necessary optimality conditions for an output least squares type functional, taking as initial guess the coarse grid reconstruction. The numerical results are backed by a convergence proof [17]. Other applications of multigrid to the EIT are those of McCormick and Wade [83] for the linearized EIT problem and Ascher and Haber [7] who speed up the computations in a Newton-type method for EIT by solving the linearized problem with multigrid.

In the methods described above, the finest discretization at which the conductivity

can be obtained is fixed a priori, without accounting for the measurement precision. Thus we may end up estimating too many degrees of freedom, making the problem harder than it is. For ill-posed linear inverse problems, Kaltenbacher [66] gives rules for choosing the finest discretization level in full multigrid (nested iteration) in such a way that optimal rates can be achieved for convergence of the reconstructed solution to the true one, when the noise level δ in the data tends to zero. Kaltenbacher and Schicho [67] extended this multigrid method to non-linear inverse problems. Numerical results have been reported for ground water filtration [66, 67] (an inverse problem close in formulation to EIT) and an electromagnetic inverse problem [68].

Ascher and Haber [6] have an indirect approach to stabilize inversion with a coarser grid: they estimate the regularization parameter in an output least squares type functional on a coarse grid, to use it later for fine grid computations.

We remark that none of the methods above explicitly discretizes the conductivity with more degrees of freedom where they are needed the most (i.e. the boundary in EIT), which is what the following methods do.

Grid refinement

Grid refinement strategies could also be classified as multilevel methods. The main idea is to reconstruct the conductivity on a coarse grid, and then use information about the obtained solution to refine the grid locally.

Ben Ameur et al. [15, 14] propose a grid refinement method for estimating the hydraulic transmissivity in groundwater filtration. They represent the hydraulic transmissivity (akin to the conductivity in EIT) as a piecewise constant function that is supposed to take a limited number of distinct and unknown values. Then they introduce refinement and coarsening indicators that give the first order effect on an output least squares type functional of adding or removing degrees of freedom to a

given discretization. Numerical results are presented in [15, 14].

A simple grid refinement strategy for the conductivity in EIT was adopted by Molinari et al. [87, 86]. First the conductivity is computed on a coarse grid, then the grid is refined where the conductivity is steep ($|\nabla\sigma|$ large), and the new grid is used for reconstructions. Numerically, this method gives visually good results for piecewise constant conductivities, but the rationale behind it needs to be further investigated.

Chapter 2

A consistent finite difference approach to an inverse spectral problem

Our main contribution in this Chapter is to improve a finite differences based reconstruction method [19, 20] for finding an unknown coefficient function in a Sturm-Liouville problem from information about the spectrum of the differential operator. This so-called *inverse Sturm-Liouville problem* is a well-known inverse spectral problem and we dedicate Section 2.1 to reviewing classic theoretical results as well as reconstruction methods. We concentrate our review on inversion methods that first discretize the Sturm-Liouville problem with e.g. finite differences and then estimate the unknown coefficient by solving a discrete inverse eigenvalue problem. Unfortunately, there are fundamental discrepancies in the spectral asymptotics of the continuum differential operator and its finite differences discretization. Thus the solution to the discrete inverse eigenvalue problem often does not approximate well the true continuum solution.

The inversion method [19, 20] that we review in Section 2.2 overcomes this difficulty by solving the inverse eigenvalue problem for a Jacobi matrix that can be assimilated to Kirchhoff's matrix for a resistor network, where the resistors are in some sense averages of the unknown coefficient over grid cells. Then to estimate the

unknown coefficient, the averages are interpreted on a grid that is determined a priori to give exact reconstructions for a reference coefficient function. Convergence of this simple procedure to the true solution as the number of measurements increases is established in [20], but we are interested in the realistic case where only a finite amount of data is available.

To improve upon the method of Section 2.2, we start in Section 2.3 with a sensitivity analysis of its reconstructions to small perturbations in the unknown coefficient. Then we use this extra information to define a Newton like iterative method in Section 2.4. The novelty of our approach is to view the inversion method of Section 2.2 as a non-linear transformation of the data that preconditions the iterations and helps with the convergence. In addition, this iterative procedure enables us to introduce a priori information about the conductivity by simply adding a correction in the orthogonal complement of the sensitivity functions.

2.1 The inverse spectral problem and its link to EIT

Inverse spectral problems guide us in developing reconstruction methods for the Electrical Impedance Tomography problem, as we see in Chapter 3. Therefore we connect the EIT problem for layered media to an inverse Sturm-Liouville problem in Section 2.1.1. Then we dedicate Section 2.1.2 to quickly review classical approaches to solving this and closely related inverse spectral problems.

2.1.1 An inverse spectral problem arising in EIT for layered media

Let us consider the EIT problem on the unit disk $\Omega \subset \mathbb{R}^2$, where the unknown conductivity is assumed to be layered (i.e. $\sigma(r,\theta) \equiv \sigma(r)$). Rewriting the EIT

equation (1.1) in polar coordinates and using the change of variables $z = -\ln(r)$, gives

$$\frac{1}{\sigma(z)}\frac{\partial}{\partial z}\left(\sigma(z)\frac{\partial u}{\partial z}(z,\theta)\right) + \frac{\partial^2 u}{\partial \theta^2}(z,\theta) = 0, \quad \text{for } z > 0. \tag{2.1}$$

At the boundary $\partial\Omega$, we impose to (2.1) the Neumann data (or electric current density) $j(\theta)$ satisfying the compatibility condition $\int_0^{2\pi} j(\theta)d\theta = 0$,

$$-\sigma(0)\frac{\partial u}{\partial z}(0,\theta) = j(\theta), \quad \text{for } \theta \in [0, 2\pi). \tag{2.2}$$

Then Fourier transforming (2.1) and (2.2) with respect to θ we obtain,

$$\begin{aligned} \frac{\partial}{\partial z}\left(\sigma(z)\frac{\partial U}{\partial z}(z,\omega)\right) - \omega^2\sigma(z)U(z,\omega) = 0, \quad \text{for } z > 0, \\ -\sigma(0)\frac{\partial U}{\partial z}(0,\omega) = J(\omega), \end{aligned} \tag{2.3}$$

where ω is the variable in frequency space corresponding to θ, and upper-case letters denote the Fourier transform of quantities that are periodically extended to $\mathbb{R}$ in θ, for example

$$U(z,\omega) = \int_{\mathbb{R}} u(z,\theta)e^{-i\omega\theta}d\theta.$$

To be precise, $U(z,\omega)$ is determined in (2.3) up to an additive constant that we fix so that $U(0,0) = 0$, i.e. we fix the grounding potential with $\int_0^{2\pi} u(0,\theta)d\theta = 0$.

The action of the Neumann-to-Dirichlet map Λ_σ^{NtD} on the current density $j(\theta)$ is

$$(\Lambda_\sigma^{NtD} j)(\theta) = u(0;\theta) = \frac{1}{2\pi}\int_{\mathbb{R}} F^\sigma(\omega)J(\omega)e^{i\omega\theta}d\omega,$$

where $F^\sigma(\omega)$ is known as the *impedance function*. For layered media, this function completely determines the NtD map. Thus the EIT problem for layered media is equivalent to finding the conductivity σ given the impedance function $F^\sigma(\omega)$.

The inverse spectral problem

We now relate (2.3) to the inverse spectral problem that will occupy us in this Chapter. Clearly, the bounded solution to (2.3) decays exponentially in z so, for all practical purposes, we can simplify the problem by truncating the domain to $z \in [0, Z]$, $Z < \infty$ and setting the boundary condition $U(Z, \omega) = 0$. After the rescaling z/Z, we may set the domain to be $[0, 1]$. After these modifications and by a slight abuse of notation we also call the new impedance function $F^\sigma(\omega) = v(0; \omega)$, where $v(z; \omega)$ solves the Sturm-Liouville problem

$$\begin{aligned} \frac{d}{dz}\left(\sigma(z)\frac{dv(z;\omega)}{dz}\right) - \omega^2\sigma(z)v(z;\omega) = 0, \quad \text{for } z \in [0,1], \\ -\sigma(0)\frac{dv(0;\omega)}{dz} = 1, \quad v(1;\omega) = 0. \end{aligned} \tag{2.4}$$

Let $\{-\omega_i^2\}_{i=1}^\infty$ be the eigenvalues of the differential operator in (2.4) sorted in decreasing order, and $\{y_i\}_{i=1}^\infty$ its eigenfunctions normalized such that $\|y_i\|_\sigma^2 = 1$, where the norm is induced by the weighted inner product,

$$\langle f, g\rangle_\sigma = \int_0^1 \sigma(z) f(z) g(z) dz, \quad \text{for arbitrary } f, g \in L^2([0,1]). \tag{2.5}$$

Then the impedance function can be expressed as a rational function,

$$F^\sigma(\omega) = v(0;\omega) = \sum_{i=1}^\infty \frac{y_i(0)^2}{\omega_i^2 + \omega^2}. \tag{2.6}$$

The inverse spectral problem we consider consists in finding the conductivity from poles and residues of the impedance function (2.6). More precisely our goal is to solve the following inverse problem.

Problem 2.1. *Image the conductivity σ from the spectral data $\{-\omega_i^2, y_i(0)^2\}_{i=1}^n$.*

Remark 2.2. As opposed to the EIT problem that is addressed in Chapter 3, the inverse spectral problem is a well-posed problem. Actually by using spectral data directly, we elude the ill-posed analytic continuation step of finding the spectral data from the impedance function. Therefore in this Chapter, ill-posedness of Problem 2.1 is not an issue. Our emphasis here is on efficient discrete methods that converge to the true solution. We deal with the ill-posedness of EIT (see Section 1.1.2) later in Section 3.2.5, when we generalize the reconstruction methods of Sections 2.2 and 2.4 to two dimensions.

The spectral measurements of Problem 2.1 are known as *truncated measure* measurements. Other types of measurements are conceivable, for example measurements based on Padé approximants of the impedance function [19, 20]. However, we concentrate on the truncated measure measurements.

2.1.2 Review of existing results for inverse spectral problems

We focus our review on three aspects: uniqueness results, stability results, and reconstruction methods. Many of the results we review are for inverse Sturm-Liouville problems that are equivalent to Problem 2.1 through well-known transformations, when the coefficients are smooth enough. For example, with $q = (\sqrt{\sigma})''/\sqrt{\sigma}$ the differential operator

$$Lu = \frac{d^2u}{dz^2} - q(z)u, \tag{2.7}$$

with boundary conditions $u'(0) = u(1) = 0$, has eigenvalues $-\omega_i^2$ and eigenfunctions $u_i = \sqrt{\sigma}y_i$, where the $-\omega_i^2$ and y_i are the eigenvalues and associated eigenfunctions of the differential operator in (2.4). Therefore the inverse problem of finding the coefficient q from spectral data of L is essentially equivalent to Problem 2.1.[1] The

[1] To be precise, equivalence holds only if $\sigma(0)$ and $\sigma'(0)$ are given.

operator in (2.7) is said to be in *Liouville normal form*. For in depth reviews of this and other related inverse Sturm-Liouville problems we refer to e.g. Dym and McKean [49], Pöschel and Trubowitz [94], McLaughlin [84], Levitan [75] or Rundell in [25].

Uniqueness results

Some of the earliest uniqueness results for inverse Sturm-Liouville problems are due to Borg [21], Levinson [74], Marčenko [81], and Gel′fand and Levitan [53]. In general, the eigenvalues of (2.4) alone are not enough information to determine the unknown coefficient. Additional spectral information is needed, such as the eigenvalues of the operator under different boundary conditions. For a survey of the different data sets that give uniqueness, see for example Rundell in [25] or McLaughlin [84]. The spectral data we use for Problem 2.1 gives uniqueness as is shown by Coleman and McLaughlin [32], who refer to the $y_i(0)^2$ as "norming constants" for the eigenfunctions.

Stability results

It is known that inverse Sturm-Liouville problems such as Problem 2.1, are stable problems. This means that one can derive bounds for the norm of small perturbations of the unknown coefficient (e.g. the conductivity σ for Problem 2.1, or the function q in the Liouville normal form (2.7)) in terms of the norm of perturbations in the spectral data. Examples of such bounds can be found in [61, 85] for the spectral problem in Liouville normal form. Hochstadt [61] gives bounds for the L^∞ norm of perturbations in the function q of (2.7) arising from small perturbations in finitely many eigenvalues. For the same problem, McLaughlin [85] bounds the L^2 norm of perturbations in q with the ℓ^2 norm of spectral data perturbations.

For Problem 2.1 with a different type of spectral data, McLaughlin [85] gives bounds for the L^∞ norm of perturbations in the conductivity in terms of the ℓ^∞ norm

of perturbations in the spectral data. See Remark 2.2 to contrast this well-posedness result with the exponential instability of the EIT problem.

Finally we point to the recent review of stability results for inverse Sturm-Liouville problems by Marletta and Weikard [82]. Additionally, they answer the question of stability when only finitely many Dirichlet-Dirichlet and Dirichlet-Neumann eigenvalues of (2.7) are known to within a certain precision [82]. This is an important question that arises in any numerical reconstruction method.

Reconstruction methods

The celebrated Gel′fand and Levitan [53] uniqueness proof is constructive because it leads to an integral equation that can be used to recover the unknown coefficient. Symes [109] exhibited the equivalence between the Gelf′and-Levitan inverse spectral problem and a coefficient determination problem for a hyperbolic differential equation, thus giving a physical interpretation (with the wave equation) of the Gelf′and-Levitan integral equation. Other reconstruction techniques that are based on similar integral equation formulations of the inverse Sturm-Liouville problem are those of Rundell and Sacks [95] and Coleman and McLaughlin [32].

When only a finite amount of spectral data is available, Hald [59] approximates the unknown q in the Liouville normal form (2.7) by solving finitely many non-linear equations coming from the Rayleigh-Ritz quotient, and proves a local convergence result for his method.[2] Non-linear equation and optimization techniques can also be used to find a function q matching the known spectral data [98, 13, 77].

Another way of solving inverse Sturm-Liouville problems is by approximating the differential operator with finite differences or finite elements, and then solving a (discrete) inverse eigenvalue problem (see e.g. the recent book by Chu and Golub [31]).

[2]With restrictions on a certain norm of the unknown q.

Such an approach is useless since on an ad-hoc (e.g. uniform) grid, the discrete and continuum differential operators have different asymptotics [31, p19]. To compensate for these discrepancies, the so-called asymptotic correction methods (see e.g. the recent review by Andrew [5]) add terms to the spectral data, resulting in a significant improvement in the accuracy of the reconstructions.

However, it is not always true that the asymptotics of the discrete and continuum differential operators differ; actually the discrepancy is an artifact of the choice of the grid used to discretize the differential operator. Indeed, one can choose a grid such that the discrete difference operator has the right asymptotics. This is the basic idea of the optimal grid method [19, 20] that we describe next.

2.2 Optimal grids for the inverse spectral problem

The method we propose in Section 2.4 is based on the inversion scheme of Borcea, Druskin and Knizhnerman [19, 20] which we review here. Their method relies on a reduced model of the differential equation (2.4). The reduced model dictates a discrete difference operator that is uniquely recoverable from the spectral data. The conductivity can then be estimated from the reduced model, giving reconstructions that are guaranteed to converge to the true conductivity as the number of measurements increases.

The discrete difference operator is obtained with the finite difference scheme described in Section 2.2.1. Actually, the reduced model for equation (2.4) is a resistor network with resistors given by averages of the unknown conductivity. The resistors can be determined uniquely and efficiently from the data, as is shown in Section 2.2.2. Then for a given conductivity, we show in Section 2.2.3 how to find a grid on which by design the discrete difference operator matches the spectral data. Finally in Sec-

tion 2.2.4, we show how to estimate averages of the unknown conductivity by using the grid for a known reference conductivity and state the convergence result [20]. Later in Section 2.4 we shall improve the reconstructions obtained with this method, when only a finite amount of data is available. Optimal grids were originally conceived to obtain efficient forward solvers. This use is briefly reviewed in Appendix A, but is technically out of the scope of this Thesis.

2.2.1 The discretization and its relation to the resistor network reduced model

The Sturm-Liouville equation (2.4) is discretized on a staggered grid, with $n+1$ primary nodes z_j, and $n+1$ dual nodes $\widehat{z}_j$, that are to be found as part of the inverse problem. The primary nodes serve to discretize the potential v, while its derivatives are discretized at the dual nodes. Since this is a staggered grid, primary and dual nodes are expected to alternate:

$$0 = \widehat{z}_0 = z_1 < \widehat{z}_1 < z_2 < \ldots < z_n < \widehat{z}_n < z_{n+1}. \tag{2.8}$$

Let v_i be the approximation of $v(z_i;\omega)$. Discretizing (2.4) on this grid gives,

$$\begin{aligned} &\frac{1}{\widehat{\gamma}_i}\left[\frac{v_{i+1}-v_i}{\gamma_i} - \frac{v_i - v_{i-1}}{\gamma_{i-1}}\right] - \omega^2 v_i = 0, \quad i = 2, \ldots n, \\ &\frac{1}{\widehat{\gamma}_1}\left[\frac{v_2 - v_1}{\gamma_1} + 1\right] - \omega^2 v_1 = 0, \ v_{n+1} = 0, \end{aligned} \tag{2.9}$$

where γ_i and $\widehat{\gamma}_i$ are essentially harmonic and algebraic averages over grid cells of the conductivity σ,

$$\gamma_i = \frac{h_i}{\widehat{\sigma}_i} = \int_{z_i}^{z_{i+1}} \frac{dz}{\sigma(z)}, \quad \text{and} \quad \widehat{\gamma}_i = \widehat{h}_i \sigma_i = \int_{\widehat{z}_{i-1}}^{\widehat{z}_i} \sigma(z) dz. \tag{2.10}$$

In linear system form, the discretization (2.9) can be rewritten as

$$(\mathbf{L} - \omega^2 \mathbf{I})\mathbf{v} = -\frac{1}{\widehat{\gamma}_1}\mathbf{e}_1, \tag{2.11}$$

where $\mathbf{I}$ is the $n \times n$ identity matrix, $\mathbf{v} = (v_1, \cdots, v_n)^T$, $\mathbf{e}_1$ is the first canonical basis vector of $\mathbb{R}^n$ and $\mathbf{L}$ is the tridiagonal $n \times n$ matrix, with entries

$$L_{ij} = \begin{cases} -\dfrac{1}{\widehat{\gamma}_i}\left(\dfrac{1}{\gamma_i} + \dfrac{1}{\gamma_{i-1}}\right)\delta_{i,j} + \dfrac{1}{\widehat{\gamma}_i\gamma_i}\delta_{i+1,j} + \dfrac{1}{\widehat{\gamma}_i\gamma_{i-1}}\delta_{i-1,j}, & 1 < i \leq n \text{ and } 1 \leq j \leq n, \\ -\dfrac{1}{\widehat{\gamma}_1\gamma_1}\delta_{j,1} + \dfrac{1}{\widehat{\gamma}_1\gamma_1}\delta_{j,2}, & i = 1 \text{ and } 1 \leq j \leq n, \end{cases} \tag{2.12}$$

where $\delta_{i,j}$ denotes the Kronecker delta.

Properties of the discrete differential operator

We collect the spectral properties of $\mathbf{L}$, which are analogous to those of the continuum problem (2.4), in the following Lemma.

Lemma 2.3. *The matrix* $\mathbf{L}$ *is diagonalizable with* $\mathbf{LY} = \mathbf{YD}$*, such that*

i. The eigenvalues are simple and real so that $\mathbf{D} = \operatorname{diag}(-\omega_{1,n}^2, \ldots, -\omega_{n,n}^2)$ *with* $-\omega_{1,n}^2 > \cdots > -\omega_{n,n}^2$.

ii. The matrix $\mathbf{Y}$ *of eigenvectors is orthonormal with respect to the weighted inner product*[3] $\langle \mathbf{a}, \mathbf{b} \rangle_{\widehat{\gamma}} = \sum_{p=1}^{n} \widehat{\gamma}_p a_p b_p$*, for all* $\mathbf{a}, \mathbf{b} \in \mathbb{R}^n$.

Proof. Notice the matrix $\mathbf{L}$ is similar to a Jacobi matrix[4]

$$\widetilde{\mathbf{L}} = \operatorname{diag}(\widehat{\gamma}_1^{1/2}, \ldots, \widehat{\gamma}_n^{1/2})\ \mathbf{L}\ \operatorname{diag}(\widehat{\gamma}_1^{-1/2}, \ldots, \widehat{\gamma}_n^{-1/2}). \tag{2.13}$$

[3] Notice the similarity to the continuum weighted inner product $\langle \cdot, \cdot \rangle_\sigma$ in (2.5).

[4] A Jacobi matrix is a tridiagonal, real and symmetric matrix with positive off-diagonal elements [30, 110, 39]

A straightforward calculation reveals that the eigenvalues of $\mathbf{L}$ are negative since for any nonzero $\mathbf{v} \in \mathbb{R}^n$,

$$\mathbf{v}^T \widetilde{\mathbf{L}} \mathbf{v} = -\frac{v_n^2}{\widehat{\gamma}_n \gamma_n} - \sum_{i=1}^{n-1} \left(\frac{v_i}{\sqrt{\widehat{\gamma}_i \gamma_i}} + \frac{v_{i+1}}{\sqrt{\widehat{\gamma}_{i+1} \gamma_i}} \right)^2 < 0.$$

The eigenvalues of $\mathbf{L}$ are simple because $\widetilde{\mathbf{L}}$ is a Jacobi matrix. Finally the orthogonality of the eigenvectors of $\mathbf{L}$ in the weighted inner product follows from the symmetry of $\widetilde{\mathbf{L}}$. □

Using Lemma 2.3, we can define an impedance function $F_n^\sigma(\omega)$ for (2.11) that as the continuum impedance function (2.6), is a rational function

$$F_n^\sigma(\omega) = \mathbf{e}_1^T \mathbf{v} = \sum_{j=1}^{n} \frac{(Y_{1,j})^2}{\omega^2 + \omega_{j,n}^2}. \tag{2.14}$$

Remark 2.4. When e.g. the first n poles and residues of the discrete impedance function (2.14) match those of the continuum impedance (2.6), the discrete impedance converges to the true impedance as $n \to \infty$. Thus the finite difference scheme can be seen as a reduced model of the continuum problem (2.4), where the reduced model parameters are $\gamma_i, \widehat{\gamma}_i$. The quality of the approximation greatly depends on the choice of the poles and residues in the discrete impedance. For example, the approximation is greatly improved if the discrete impedance is chosen to be a Padé-Chebyshev rational approximant of the true impedance [45].

The finite difference scheme as a resistor network

Alternatively, the finite difference scheme (2.11) with n nodes can be derived from a finite volumes discretization of the EIT equation (1.1) on the unit disk with the layered conductivity $\sigma(-\ln(r))$. Here we only sketch the discretization, since it is discussed in

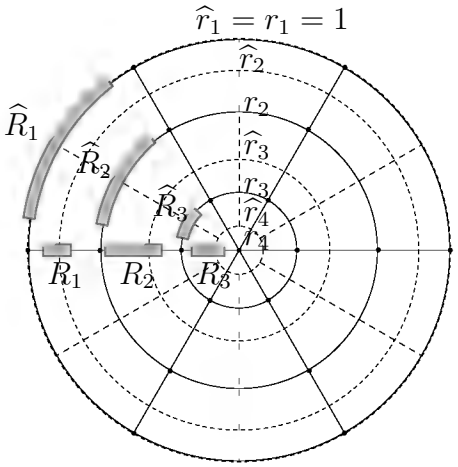

Figure 2.1: Preview of the finite volumes discretization of Chapter 3. The control volumes are in dotted lines and the underlying resistor network is in solid line. Since the conductivity $\sigma(-\ln(r))$ is layered, the network can be obtained by rotating the pattern of resistors highlighted in gray about the origin.

more detail in Section 3.1. Roughly speaking, the discretization is done on a staggered grid that is the tensor product of a uniform grid in the angular direction and of a grid in the radial direction, with radii given by $r_i = \exp(-z_i)$ and $\widehat{r}_i = \exp(-\widehat{z}_i)$. In the notation of Section 3.1, the discretization is of type $\mathcal{G}(2n, 4n+1)$, and an example is given in Figure 2.1.[5]

As we explain in Remark 3.1, the resulting discrete operator is precisely Kirchhoff's matrix for a resistor network of type $C(2n, 4n+1)$ (to be defined in Section 3.2.2) with resistors $R_{i,j}$, $\widehat{R}_{i,j+1/2}$. Here the index i is associated with the radial direction and j with the angular direction. Since the medium is layered, we can drop the dependence on the angular parameter j and use R_i, $\widehat{R}_i$ instead, which are also depicted in Figure 2.1.

We arrive to the difference scheme (2.11) from the resistor network by taking a discrete Fourier transform. The process is analogous to going from the 2D EIT

[5]The number $4n+1$ of radii in the network is chosen so that the network is uniquely recoverable from electrical measurements at the boundary (see Section 3.2.2). To eliminate the clutter in Figure 2.1, we reduced the number of radii that are represented.

equation for layered media to the Sturm-Liouville equation (2.4), in Section 2.1.1. The end result is that the $\gamma_i, \widehat{\gamma}_i$ we encountered in (2.11) are given in terms of the resistor in the network by

$$\widehat{\gamma}_i = \frac{h_\theta^2}{\widehat{R}_i} \quad \text{and} \quad \gamma_i = R_i,$$

where $h_\theta = 2\pi/(4n+1)$. This justifies the "resistor" name for the reduced model parameters $\gamma_i, \widehat{\gamma}_i$. We shall see in the next Section that the $\gamma_i, \widehat{\gamma}_i$ are determined uniquely by the spectral data of Problem 2.1.[6]

2.2.2 The inverse problem for the resistor network

The discrete (2.14) and continuum (2.6) impedance functions are both rational functions of ω^2, with poles and residues determined by the eigenvalues and eigenfunctions of the differential operator in (2.4) and the matrix $\mathbf{L}$ in (2.11). Therefore, we can determine the discrete operator $\mathbf{L}$ and, implicitly, the resistor network which is our reduced model, by solving a rational approximation problem for the impedance function. How this is done, depends on what measurements we have. Recall the spectral measurements of Problem 2.1 consist of the first n poles and residues of the continuum impedance, therefore we seek a discrete operator with spectrum

$$-\omega_{i,n}^2 = -\omega_i^2 \quad \text{and} \quad (Y_{1,i})^2 = (y_i(0))^2, \quad \text{for } i = 1, \ldots, n. \tag{2.15}$$

With this choice, the convergence of the discrete impedance function (2.14) to the true impedance (2.6) is guaranteed with the algebraic rate: $F_n^\sigma(\omega) - F^\sigma(\omega) = \mathcal{O}(1/n)$. Exponential convergence rates can be achieved when the discrete operator is chosen such that the discrete impedance is a Padé approximant of the true impedance [45, 19].

[6] The same conclusion can be reached by using graph theory (see Section 3.3.1), spectral functions of beaded strings [64] and complex analysis [64].

Solving the Jacobi Inverse Eigenvalue Problem

Now let us shift our attention to finding the matrix $\mathbf{L}$ from the spectral data (2.15). Equivalently, we can find the Jacobi matrix $\widetilde{\mathbf{L}}$ from the spectral data (see Lemma 2.3). This is known as the Jacobi Inverse Eigenvalue Problem (JIEP) [39, 16, 29, 30, 31].

Once we know $\widetilde{\mathbf{L}}$, we have solved the inverse problem for the resistor network since the resistors $\gamma_i, \widehat{\gamma}_i$ follow immediately from (2.12) and (2.13). Additionally, it can be proved that there is a one-to-one correspondence between the spectral data and the resistors (see e.g. [39]). The JIEP can be solved efficiently by for example, Stieltjes's method [101, 102] or Lanczos's method [30, 110, 39]. Here we limit the discussion to the latter, because it is the method we use in the numerics.

Let us denote the entries of the Jacobi matrix $\widetilde{\mathbf{L}}$ as follows,

$$\widetilde{L}_{i,i} = \alpha_i, \text{ for } i = 1, \ldots, n, \quad \text{and} \quad \widetilde{L}_{i+1,i} = \beta_i, \text{ for } i = 1, \ldots, n-1, \tag{2.16}$$

and let $\mathbf{Q}$ be an orthonormal matrix of eigenvectors of $\widetilde{\mathbf{L}}$. Then we have

$$\widetilde{\mathbf{L}}\mathbf{Q} = \mathbf{Q}\mathbf{D}, \tag{2.17}$$

where $\mathbf{D} = \operatorname{diag}(-\omega_1^2, -\omega_2^2, \cdots, -\omega_n^2)$ is given as data for the inverse problem. The other available data are the quantities $(Y_{1,i})^2$, which define the vector $\mathbf{q}_1 \equiv \mathbf{Q}^T\mathbf{e}_1$ since from (2.13) and because $\mathbf{Q}$ is orthonormal we get

$$\mathbf{q}_1 = \mathbf{Q}^T\mathbf{e}_1 = \frac{\mathbf{Y}^T\mathbf{e}_1}{\|\mathbf{Y}^T\mathbf{e}_1\|_2}.$$

Then to find $\alpha_1, \cdots, \alpha_n$ and $\beta_1, \cdots, \beta_{n-1}$, equate the rows in $\widetilde{\mathbf{L}}\mathbf{Q} = \mathbf{Q}\mathbf{D}$ to obtain

$$\mathbf{D}\mathbf{q}_i = \beta_{i-1}\mathbf{q}_{i-1} + \alpha_i\mathbf{q}_i + \beta_i\mathbf{q}_{i+1},$$

for $i = 1 \cdots n-1$, and with $\beta_0 \mathbf{q}_0 \equiv \mathbf{0}$. Then recurrence relations for α_i, β_i, and $\mathbf{q}_{i+1}$ follow. One note of caution: in floating point arithmetic the unmodified Lanczos recurrence gives an eigenvector matrix $\mathbf{Q}$ with poor orthogonality. This can be fixed by reorthogonalizing, and we do it in our implementation. For more details on reorthogonalization see e.g. [55, §9.2.3].

2.2.3 Optimal grid construction

Let us assume for the moment that the conductivity σ is given. The idea here is to determine grid points such that when we discretize equation (2.4) with finite differences as in Section 2.2.1, we get an exact matching of the spectral measurements. This is possible because the resistors $\gamma_i, \widehat{\gamma}_i$ can be computed from the spectral measurements (2.15) by solving the JIEP. Moreover from (2.10), the resistors are averages of σ on a grid that can be recovered using e.g. a non-linear equation solver.

Algorithm 2.5. Inputs: Conductivity σ and resistors $\{\gamma_j, \widehat{\gamma}_j\}_{j=1}^n$. **Outputs:** Grid nodes $\{z_{j+1}, \widehat{z}_j\}_{j=0}^n$.

i. Set $\widehat{z}_0 = z_1 = 0$.

ii. For $j = 1, \ldots, n$, find $\widehat{z}_j$ and z_{j+1} (recall (2.10)) such that,

$$\int_0^{\widehat{z}_j} \sigma(s)ds = \sum_{p=1}^{j} \widehat{\gamma}_p \quad \text{and} \quad \int_0^{z_{j+1}} \frac{ds}{\sigma(s)} = \sum_{p=1}^{j} \gamma_p,$$

The grid nodes are defined uniquely by the above relations because σ is positive, bounded above and below, so that the functions $\int_0^z \sigma(s)ds$ and $\int_0^z (\sigma(s))^{-1}ds$ are monotonically increasing.

In general, it is not known if the optimal grid for σ is properly speaking a grid.

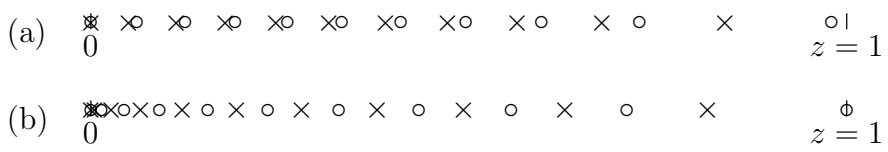

Figure 2.2: Grids obtained by approximating the impedance function $F^\sigma(\omega)$ for $\sigma = 1$ with: (a) largest 10 poles and residues (see (2.15)) and (b) Padé-Chebyshev interpolant with 10 poles and residues. Primary nodes are ($\circ$), and dual nodes ($\times$).

In particular, the question of interleaving of primary and dual nodes

$$0 = \widehat{z}_0 = z_1 < \widehat{z}_1 < z_2 < \ldots < z_n < \widehat{z}_n < z_{n+1},$$

has not been proved for the general case, but it has been observed in all numerical experiments. Also, the grid is known to fill the space [19], meaning that grid nodes are dense in $[0, 1]$ as $n \to \infty$. For the homogeneous medium ($\sigma \equiv 1$) and with the spectral measurements (2.15), an explicit expression of the grid is known [20]. For other smooth enough conductivities, the grid for σ is asymptotically close to the grid for $\sigma^0 \equiv 1$ when $n \to \infty$ [20].

We show in Figure 2.2 the optimal grid for the homogeneous medium for different spectral measurements, to illustrate that the grid depends strongly on the type of spectral measurements used. Notice that the last primary node z_{n+1} is not located at $z = 1$. However, we have $z_{n+1} \to 1$ as $n \to \infty$ with the same rate as that of the convergence of the discrete impedance function to the true impedance [19].

2.2.4 The inverse problem for the conductivity

As we saw in the previous Section, if we knew the optimal grid for σ and the resistors $\gamma_i, \widehat{\gamma}_i$, then we would be able to compute *exactly* the averages $\sigma_i, \widehat{\sigma}_i$ defined in (2.10). Obviously, this is not a viable inversion method, since the optimal grid depends on

the unknown conductivity σ.

Fortunately, it has been shown in [20] that the grid constructed in Section 2.2.3 depends weakly on the conductivity, meaning that changes in the conductivity do not change significantly the grid.[7] So we can interpret the averages (2.10) on a grid precomputed for a reference conductivity σ^0, that is "sufficiently similar" to the unknown conductivity σ. For the spectral measurements[8] (2.15), this inversion procedure is summarized in Algorithm 2.6.

Algorithm 2.6. Inputs: $\{-\omega_i^2, (y_i(0))^2\}_{i=1}^n$ (spectral data (2.15)). **Outputs:** $\{\sigma_i, \widehat{\sigma}_i\}_{i=1}^n$ (approximate averages of σ).

i. Calculate the grid $z_i^0, \widehat{z}_i^0$ for $\sigma^0 \equiv 1$ using Algorithm 2.5.

ii. Find $\gamma_i, \widehat{\gamma}_i$ from the spectral data (2.15) by solving the JIEP with e.g. Lanczos method.

iii. Obtain the approximate averages $\sigma_i, \widehat{\sigma}_i$ by substituting the grid $z_i^0, \widehat{z}_i^0$, and the resistors $\gamma_j, \widehat{\gamma}_j$ into (2.10), i.e.

$$\sigma_i = \frac{\widehat{\gamma}_i}{\widehat{z}_i^0 - \widehat{z}_{i-1}^0} \quad \text{and} \quad \widehat{\sigma}_i = \frac{z_{i+1}^0 - z_i^0}{\gamma_i}, \text{ for } 1 \leq i \leq n.$$

Algorithm 2.6 was originally proposed by Borcea and Druskin [19] and is a computationally cheap $\mathcal{O}(n^2)$ inversion scheme, since the bulk of the work is in finding the resistors $\gamma_i, \widehat{\gamma}_i$ from the spectral measurements. Moreover, Algorithm 2.6 has been proved to give reconstructions that converge to the true conductivity σ, under

[7] A more precise definition of the weak dependence of the grid on the conductivity is given in Corollary 6.2 in [20].

[8] By considering other types of spectral measurements (e.g. Padé-Chebyshev approximations of the continuum impedance [19]), reconstructions of smooth conductivities with Algorithm 2.6 can be improved. However, the only convergence result available [20] is for the measurements (2.15).

regularity assumptions on σ and as the number of spectral measurements increases [20]. The next theorem is a simplified version of the convergence result in [20].

Theorem 2.7 ([20]). *Suppose $\sigma \in \mathcal{S}$, where $\mathcal{S}$ is some compact set in $L^1[0,1]$ (resp. in $L^\infty[0,1]$) of conductivities containing $\sigma^0 = 1$. Let $\{-(\omega_i)^2, (y_i(0))^2\}_{i=1}^\infty$ and $\{-(\omega_i^0)^2, (y_i^0(0))^2\}_{i=1}^\infty$ be the spectral data for σ and σ^0 respectively. If there is a constant $\alpha > 0$ such that,*

$$\omega_i - \omega_i^0 = \mathcal{O}\left(\frac{1}{i^\alpha \log i}\right) \quad \text{and} \quad (y_i(0))^2 - (y_i^0(0))^2 = \mathcal{O}\left(\frac{1}{i^\alpha}\right), \text{ as } i \to \infty, \quad (2.18)$$

then a piecewise constant interpolation $\sigma^{(n)}$ of the approximate averages σ_i, $\widehat{\sigma}_i$ (obtained with Algorithm 2.6) on the grid $z_i^0, \widehat{z}_i^0$, satisfying $\sigma^{(n)}(z_i) = \sigma_i$ and $\sigma^{(n)}(\widehat{z}_i) = \widehat{\sigma}_i$ converges to $\sigma(z)$ in $L^1[0,1]$ (resp. in $L^\infty[0,1]$) as $n \to \infty$.

2.3 Sensitivity analysis of the optimal grid inversion

In this Section we determine how the reconstructions of Algorithm 2.6 are affected by small perturbations in the conductivity. In other words, we make a sensitivity analysis of the mapping that takes us from the conductivity to the spectral data, and then to the reconstructions of Algorithm 2.6. We make this linearization with an eye on Section 2.4, where the derivatives are used in a Newton-like method to improve the reconstructions.

We break up the analysis in the following natural steps, that can be easily pieced together using the chain rule. First in Section 2.3.1 we review explicit sensitivity formulas [20, 47] for the Jacobi Inverse Eigenvalue Problem (or JIEP, used in Algorithm 2.6 to compute the reduced model from the spectral data, see Section 2.2.2). Then in Section 2.3.2 we analyze the sensitivity of the spectral data of Problem 2.1 with respect to changes in the conductivity. Finally we collect in Section 2.3.3 in-

teresting properties of the complete conductivity-to-reconstructions of Algorithm 2.6 mapping.

2.3.1 Sensitivity of the Jacobi Inverse Eigenvalue Problem

The first evidence of continuous dependence of the Jacobi matrix with respect to its eigenvalues is due to Hochstadt [60], which was followed by the sensitivity bounds of Hald [58]. Since the JIEP can be solved by Lanczos method (see e.g. Section 2.2.2), bounds can also be obtained from the perturbation analysis for Lanczos recurrences of Greenbaum [56]. Here we review the recent analysis of Borcea, Druskin and Knizhnerman [20, 47], who use a discrete Gelf′and-Levitan theory [90] to derive *explicit* formulas for the sensitivity of the Jacobi matrix to its spectrum.

Let $\mathbf{T}^0 \in \mathbb{R}^{n\times n}$ be a symmetric tridiagonal matrix with positive entries, i.e. a Jacobi matrix. Let $\mathbf{Q}^0 = [\mathbf{q}_1, \mathbf{q}_2, \ldots, \mathbf{q}_n]$ be an orthonormal matrix of eigenvectors of $\mathbf{T}^0$, and $\lambda_1^0, \ldots, \lambda_n^0$, the corresponding eigenvalues.[9] Then we have

$$\mathbf{T}^0\mathbf{Q}^0 = \mathbf{Q}^0\mathbf{D}^0,$$

where $\mathbf{D}^0 = \mathrm{diag}\,(\lambda_1^0, \cdots, \lambda_n^0)$.

Recall from Section 2.2.2 that the entries of $\mathbf{T}^0$ can be uniquely recovered from the spectral data $\mathbf{e}_1^T\mathbf{Q}^0$ and $\mathbf{D}^0$. Now, let us define the perturbed spectral data $\mathbf{D} = \mathbf{D}^0 + \delta\mathbf{D}$ and $\mathbf{e}_1^T\mathbf{Q} = \mathbf{e}_1^T\mathbf{Q}^0 + \mathbf{e}_1^T\delta\mathbf{Q}$ corresponding to the perturbed matrix $\mathbf{T} = \mathbf{T}^0 + \delta\mathbf{T}$. Our convention is to write reference unperturbed quantities with a superscript 0 and perturbed quantities without a superscript. The letter δ stands for small perturbations.

As in (2.16), the $\alpha_1, \ldots, \alpha_n$ are the diagonal entries of a Jacobi matrix $\mathbf{T}$, and the

[9] This notation for the eigenvalues is meant to simplify the $-(\omega_{k,n}^0)^2$ notation of Lemma 2.3.

$\beta_1, \ldots, \beta_{n-1}$ its off-diagonal entries. Furthermore, we use a vector notation for the spectral data: $\boldsymbol{\eta} \equiv \mathbf{Q}^T \mathbf{e}_1$ and $\boldsymbol{\lambda} \equiv (\lambda_1, \ldots, \lambda_n)^T$.

Before stating the results of [47] in Lemma 2.8, let us introduce vectors $\mathbf{a} \in \mathbb{R}^n$ and $\mathbf{b} \in \mathbb{R}^{n-1}$, that are in some sense discrete primitives of $\delta\alpha_j$ and of $\delta\beta_j$. Specifically they are defined by

$$\mathbf{a} = \begin{bmatrix} \delta\alpha_1 \\ \delta\alpha_1 + \delta\alpha_2 \\ \vdots \\ \sum_{j=1}^{n} \delta\alpha_j \end{bmatrix} \quad \text{and} \qquad \mathbf{b} = \begin{bmatrix} \delta\beta_1/\beta_1^0 \\ \delta\beta_1/\beta_1^0 + \delta\beta_2/\beta_2^0 \\ \vdots \\ \sum_{j=1}^{n-1} \delta\beta_j/\beta_j^0 \end{bmatrix}. \tag{2.19}$$

Once we know the expressions for $\mathbf{a}$ and $\mathbf{b}$, the perturbations of the entries of the matrix $\mathbf{T}$ arising from perturbations in the spectrum follow. Indeed we have $\delta\alpha_1 = a_1$, $\delta\beta_1 = \beta_1^0 b_1$ and $\delta\alpha_i = a_i - a_{i-1}$, $\delta\beta_i = \beta_i^0(b_i - b_{i-1})$, for $i = 2, \ldots, n$.

Lemma 2.8 (Druskin, Borcea, and Knizhnerman [47])**.** *The sensitivity of the entries of a Jacobi matrix to small perturbations $\delta\boldsymbol{\eta}$ and $\delta\boldsymbol{\lambda}$ in the spectrum can be written in terms of the "discrete primitives" $\mathbf{a}$ and $\mathbf{b}$ of $\delta\alpha_j$ and of $\delta\beta_j$ respectively* (2.19)*:*

$$\mathbf{a} = \mathbf{A}_{\boldsymbol{\lambda}}\delta\boldsymbol{\lambda} + \mathbf{A}_{\boldsymbol{\eta}}\delta\boldsymbol{\eta}, \quad \textit{and} \quad \mathbf{b} = \mathbf{B}_{\boldsymbol{\lambda}}\delta\boldsymbol{\lambda} + \mathbf{B}_{\boldsymbol{\eta}}\delta\boldsymbol{\eta},$$

where $\mathbf{A}_{\boldsymbol{\lambda}}, \mathbf{A}_{\boldsymbol{\eta}} \in \mathbb{R}^{n\times n}$ and $\mathbf{B}_{\boldsymbol{\lambda}}, \mathbf{B}_{\boldsymbol{\eta}} \in \mathbb{R}^{n-1\times n}$. The entries of the matrices $\mathbf{A}_{\boldsymbol{\lambda}}$ and $\mathbf{A}_{\boldsymbol{\eta}}$ are given for $i = 1, \ldots, n-1$ and $j = 1, \ldots, n$ by,

$$\begin{aligned} A_{\boldsymbol{\lambda}}^{ij} &= 1 + \beta_i^0 \sum_{\substack{p=1 \\ p\neq j}}^{n} \frac{1}{\lambda_j^0 - \lambda_p^0} \left[2Q_{ip}^0 Q_{i+1p}^0 - \frac{Q_{1p}^0}{Q_{1q}^0}(Q_{ip}^0 Q_{i+1q}^0 + Q_{i+1p}^0 Q_{iq}^0) \right], \quad A_{\boldsymbol{\lambda}}^{nj} = 1, \\ A_{\boldsymbol{\eta}}^{ij} &= 2\beta_i^0 \frac{Q_{i+1j}^0 Q_{ij}^0}{Q_{1j}^0}, \quad A_{\boldsymbol{\eta}}^{nj} = 0. \end{aligned} \tag{2.20}$$

The entries of the matrices $\mathbf{B}_{\boldsymbol{\lambda}}$ *and* $\mathbf{B}_{\boldsymbol{\eta}}$ *are for* $i = 1, \ldots, n-1$ *and* $j = 1, \ldots, n$,

$$\begin{aligned} B^{ij}_{\boldsymbol{\lambda}} &= \sum_{\substack{p=1 \\ p\neq j}}^{n} \frac{1}{\lambda^0_j - \lambda^0_p} \left[\left(Q^0_{i+1p}\right)^2 - \frac{Q^0_{1p}}{Q^0_{1j}} Q^0_{i+1p} Q^0_{i+1j} \right], \\ B^{ij}_{\boldsymbol{\eta}} &= \frac{\left(Q^0_{i+1j}\right)^2}{Q^0_{1j}}. \end{aligned} \tag{2.21}$$

2.3.2 Sensitivity of the spectrum to the conductivity

Now we perform a linearization study of the Sturm-Liouville problem (2.4) we described in Section 2.1.1. Let σ^0 be the reference conductivity. Recall from Section 2.1.1 that $y^0_k(z)$ are the normalized (with respect to the weighted inner product (2.5)) eigenfunctions of (2.4). The associated eigenvalues are denoted by λ^0_k.[10]

Let $\delta\sigma$ be a small perturbation of σ^0, the perturbed conductivity is $\sigma = \sigma^0 + \delta\sigma$. We additionally assume that $\delta\sigma(0) = 0$, which is equivalent to knowing $\sigma(0)$, but this can be relaxed. We denote by $\lambda_k = \lambda^0_k + \delta\lambda_k$ and $y_k = y^0_k + \delta y_k$ the perturbed eigenvalues and associated eigenfunctions. We aim to find the perturbations $\delta y_k(0)$ and $\delta\lambda_k$, in the linearized sense, of the residues and eigenvalues resulting from the perturbation $\delta\sigma$ of the conductivity. In other words, we are computing the Fréchet derivative of the eigenvalues and residues to changes in the conductivity.[11] We summarize the result in the following Lemma.

Lemma 2.9. *The sensitivity of the eigenvalue* λ^0_k *with respect to a small perturbation in the conductivity* σ *is,*

$$-\delta\lambda_k = \int_0^1 \delta\sigma(z)((y^0_k)'(z))^2 dz + \lambda^0_k \int_0^1 \delta\sigma(z)(y^0_k(z))^2 dz. \tag{2.22}$$

[10] This notation for the eigenvalues is different from the notation $-(\omega^0_k)^2$ of Section 2.1.1.

[11] The Fréchet differentiability of the eigenvalues and eigenfunctions with respect to the coefficient function can be found in e.g. [94, 32].

Moreover, the sensitivity of the residue $y_k^0(0)$ to the conductivity is given by,

$$\delta y_k(0) = -\int_0^1 \delta\sigma(z)(y_k^0)'(z)\frac{\partial}{\partial z}G_k(z,0)dz - \lambda_k^0\int_0^1 \delta\sigma(z)y_k^0(z)G_k(z,0)dz \\ -\frac{1}{2}y_k(0)\int_0^1 \delta\sigma(z)(y_k^0)^2(z)dz, \quad (2.23)$$

where $G_k(z,s)$ has the series expansion,

$$G_k(z,s) = -\sum_{\substack{j=1\\ j\neq k}}^{\infty}\frac{y_j^0(z)y_j^0(s)}{\lambda_j^0-\lambda_k^0}. \quad (2.24)$$

Proof. Write (2.4) with the perturbed quantities, neglect the higher-order terms and cancel out the $\mathcal{O}(1)$ terms, to find the differential equation satisfied by δy_k and $\delta\lambda_k$:

$$\begin{cases} (\sigma^0\delta y_k')' - \lambda_k^0\sigma^0\delta y_k = \delta\lambda_k\sigma^0 y_k^0 + \lambda_k^0\delta\sigma y_k^0 - (\delta\sigma(y_k^0)')' \\ (\delta y_k)'(0) = \delta y_k(1) = 0. \end{cases} \quad (2.25)$$

Multiply (2.25) by y_k^0 on both sides and integrate over $[0,1]$ to obtain, after applying Green's identity, the expression for $\delta\lambda_k$ in terms of $\delta\sigma$.

Call f the right-hand side in (2.25). Since the above calculation shows that $\int_0^1 f(s)y_k^0(s)ds = 0$, the solution to (2.25) can be found using a generalized Green's function. The series expansion for the Green's function can be constructed as in e.g. [33, pp. 344–346] by finding the equations satisfied by the Fourier coefficients of δy_k on the basis of eigenfunctions $\{y_j^0\}_{j=1}^{\infty}$.

Hence the solution to (2.25) has the form,

$$\delta y_k(s) = -\int_0^1 f(s)G_k(z,s)dz + c_k y_k^0(s). \quad (2.26)$$

The Fourier coefficient $c_k = \int_0^1 \sigma^0(z)\delta y_k(z)y_k^0(z)dz$ is entirely determined by re-

quiring the perturbed eigenfunction $y_k^0+\delta y_k$ has norm one in the norm of the perturbed inner product. That is,

$$\int_0^1 (\sigma^0(z)+\delta\sigma(z))(y_k^0(z)+\delta y_k(z))^2(z)dz = 0. \tag{2.27}$$

After neglecting the higher-order terms and canceling the $\mathcal{O}(1)$ terms,

$$c_k = \int_0^1 \sigma^0(z)\delta y_k(z) y_k^0(z)dz = -\frac{1}{2}y_k^0(0)\int_0^1 \delta\sigma(z)(y_k^0)^2(z)dz.$$

Now in the integral (2.26), the orthogonality of the $\{y_j^0\}_{j=1}^\infty$ in the weighted inner product (2.5) makes the term $\delta\lambda_k\sigma^0 y_k^0$ of the right-hand side f vanish. The final expression for $\delta y_k(0)$ follows from integrating by parts and evaluating at $s=0$. □

In the case where $\sigma^0 \equiv 1$, we can sum explicitly the series of the Green's function (2.24), when its second argument is zero. This is the purpose of the next Lemma.

Lemma 2.10. *The following identity for the Green's function defined in* (2.24) *holds,*

$$G_k(s,0) \equiv -\sum_{\substack{j=1\\ j\neq k}}^{\infty} \frac{y_j^0(s)y_j^0(0)}{(\omega_k^0)^2-(\omega_j^0)^2} = \frac{(s-1)\sin(\omega_k^0 s)}{\omega_k^0} + \frac{\cos(\omega_k^0 s)}{2(\omega_k^0)^2}.$$

Proof. Elementary calculations show that for $\sigma^0 \equiv 1$,

$$\omega_k^0 = \pi\left(k-\frac{1}{2}\right) \quad \text{and} \quad y_k^0(z) = \sqrt{2}\cos(\omega_k z).$$

For $-\omega^2$ not an eigenvalue of the operator $\frac{\partial^2}{\partial z^2}$, the Green's function,

$$G(s,z) = \begin{cases} \dfrac{1}{\omega\cos(\omega)}\sin(\omega(1-z))\cos(\omega s) & \text{for } s<z, \\ \dfrac{1}{\omega\cos(\omega)}\sin(\omega(1-s))\cos(\omega z) & \text{for } s>z, \end{cases}$$

solves the differential equation,

$$\begin{cases} \dfrac{\partial^2}{\partial s^2}G(s,z) + \omega^2 G(s,z) = -\delta(s-z) \\ \qquad \dfrac{\partial}{\partial s}G(0,z) = G(1,z) = 0. \end{cases}$$

Moreover, the series expansion of this Green's function is,

$$G(s,z) = -\sum_{j=1}^{\infty} \frac{y_j^0(s)y_j^0(z)}{\omega^2 - (\omega_j^0)^2}.$$

By evaluating at $z = 0$ and subtracting the $k-$th term in the last sum, we obtain

$$\begin{aligned} -\sum_{\substack{j=1 \\ j\neq k}}^{\infty} \frac{y_j^0(s)y_j^0(0)}{\omega^2 - (\omega_j^0)^2} &= G(s,0) + \frac{y_k^0(s)y_k^0(0)}{\omega^2 - (\omega_k^0)^2} \\ &= \frac{\sin(\omega(1-s))}{\omega\cos(\omega)} + \frac{2\cos(\omega_k^0 s)}{\omega^2 - (\omega_k^0)^2}. \end{aligned}$$

Then the expression of $G_k(s,0)$ follows by taking the limit as $\omega \to \omega_k^0$,

$$G_k(s,0) = \lim_{\omega\to\omega_k} \frac{\sin(\omega(1-s))}{\omega\cos(\omega)} + \frac{2\cos(\omega_k^0 s)}{\omega^2 - (\omega_k^0)^2}. \qquad \square$$

From the integrals of Lemma 2.9, we can identify sensitivity functions $D\lambda_k[\sigma^0](z)$ and $D(y_k(0))[\sigma^0](z)$ such that,

$$\delta\lambda_k = \int_0^1 D\lambda_k[\sigma^0](z)\delta\sigma(z)dz \quad \text{and} \quad \delta y_k = \int_0^1 D(y_k(0))[\sigma^0](z)\delta\sigma(z)dz.$$

By Lemma 2.10, one can derive analytic formulas for these sensitivity functions in terms of what are essentially trigonometric functions. These formulas are stated without proof in the next Lemma.

Lemma 2.11. *The sensitivity functions for perturbations of the spectrum arising*

from perturbations of the conductivity are for $\sigma^0 \equiv 1$ *and with* $\omega_k^0 = \pi(k - 1/2)$,

$$D\lambda_k[\sigma^0](z) = 2(\omega_k^0)^2 \cos(2\omega_k^0 z), \quad \textit{and}$$
$$D(y_k(0))[\sigma^0](z) = \sqrt{2}\omega_k^0(z-1)\sin(2\omega_k^0 z) - \frac{1}{\sqrt{2}}\cos(2\omega_k^0 z).$$

2.3.3 Sensitivity of the resistors to the conductivity

We do not delve in the details of the calculation of the sensitivities of the resistors with respect to the conductivity. We only note that these can be obtained *explicitly* with the chain rule from the sensitivity results of previous Sections and the relationship between the resistors and the entries of the Jacobi matrix (2.13). We limit ourselves to describing properties of the sensitivity functions that are useful later in Section 2.4.

Let the resistors corresponding to the reference conductivity σ^0 be γ_i^0 and $\widehat{\gamma}_i^0$, and those for the perturbed conductivity $\sigma = \sigma^0 + \delta\sigma$ be $\gamma_i = \gamma_i^0 + \delta\gamma_i$ and $\widehat{\gamma}_i = \widehat{\gamma}_i^0 + \delta\widehat{\gamma}_i$. Then we can compute functions $D\gamma_i[\sigma^0](z)$ and $D\widehat{\gamma}_i[\sigma^0](z)$ such that for small perturbations $\delta\sigma$ of the conductivity we have the formal expansions, for $i = 1, \ldots, n$,

$$\begin{aligned} \gamma_i &= \gamma_i^0 + \int_0^1 D\gamma_i[\sigma^0](z)\delta\sigma(z)dz + \cdots, \\ \widehat{\gamma}_i &= \widehat{\gamma}_i^0 + \int_0^1 D\widehat{\gamma}_i[\sigma^0](z)\delta\sigma(z)dz + \cdots. \end{aligned} \tag{2.28}$$

These sensitivity functions are linear combinations of the sensitivity functions for the spectrum that are discussed in Section 2.3.2. For the conductivity $\sigma^0 \equiv 1$, Lemma 2.11 entails that the functions $D\gamma_i[\sigma^0]$ and $D\widehat{\gamma}_i[\sigma^0]$ are essentially trigonometric functions. We computed the latter sensitivity functions and report them in Figure 2.3.

We can gather some insight on the meaning of the sensitivity functions by recalling that the resistors $\gamma_i, \widehat{\gamma}_i$ of equation (2.10) are essentially averages of the conductivity over the cells of the optimal grid $z_i, \widehat{z}_i$ for the perturbed conductivity σ (see Sec-

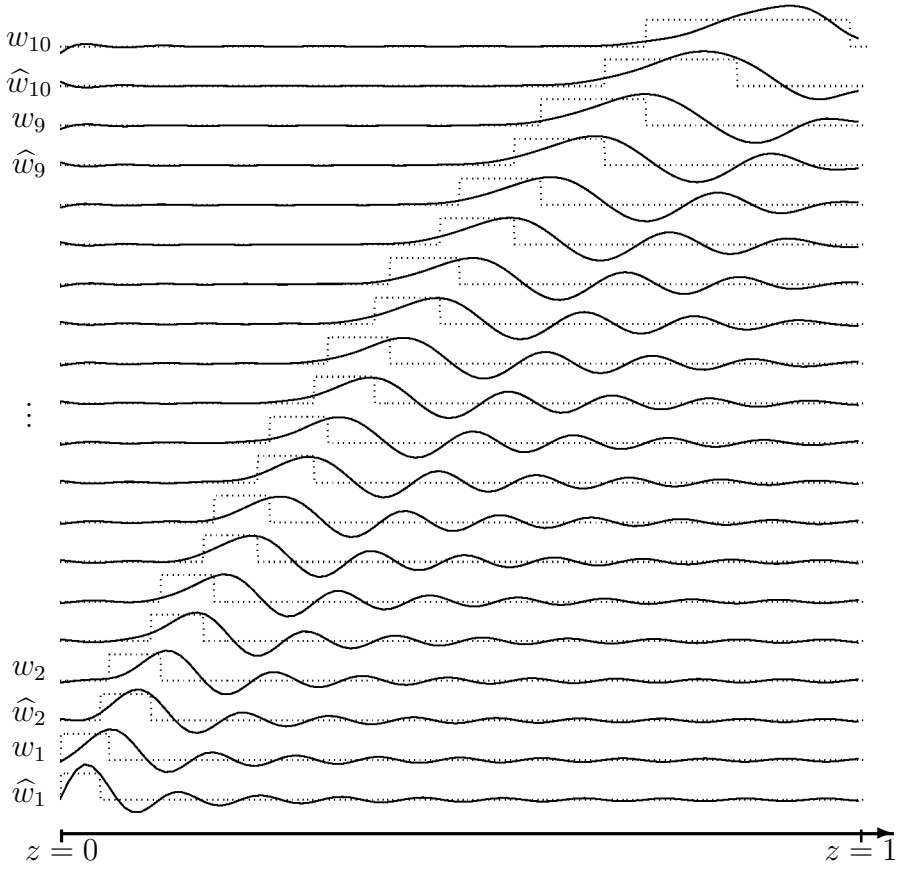

Figure 2.3: The sensitivity functions $w_i(z) \equiv -D\gamma_i[\sigma^0](z)$ and $\widehat{w}_i(z) \equiv D\widehat{\gamma}_i[\sigma^0](z)$ are plotted in solid line. For comparison with w_i (respectively $\widehat{w}_i$) the characteristic function of the optimal grid interval $[z_i^0, z_{i+1}^0]$ (respectively $[\widehat{z}_{i-1}^0, \widehat{z}_i^0]$) figures in dotted line. Here the number of spectral measurements is $n = 10$ and $\sigma^0 \equiv 1$.

tions 2.2.1 and 2.2.3). Linearizing at σ^0 the relations (2.10) gives,

$$\begin{aligned} \delta\gamma_i &= \int_{z_i^0}^{z_{i+1}^0} \frac{-\delta\sigma(s)}{(\sigma^0(s))^2} ds + \mathcal{O}(\delta(z_{i+1} - z_i)) \quad \text{and} \\ \delta\widehat{\gamma}_i &= \int_{\widehat{z}_{i-1}^0}^{\widehat{z}_i^0} \delta\sigma(s) ds + \mathcal{O}(\delta(\widehat{z}_i - \widehat{z}_{i-1})), \end{aligned} \tag{2.29}$$

where the last term in the sums accounts for changes in the grid. As is explained in Section 2.2.3 (see also [20]), the grid depends weakly on the conductivity therefore we expect the terms in (2.29) accounting for grid changes to be small. By neglecting these

terms and extending the domain of integration to $[0,1]$, we obtain by identification the following approximations to the sensitivity functions

$$D\gamma_i[\sigma^0] \approx \frac{-\chi_{[z_i^0, z_{i+1}^0]}}{(\sigma^0)^2} \quad \text{and} \quad D\widehat{\gamma}_i[\sigma^0] \approx \chi_{[\widehat{z}_{i-1}^0, \widehat{z}_i^0]}, \tag{2.30}$$

where $\chi_{[a,b]}(z)$ stands for the characteristic function of the interval $[a,b]$. We have observed numerically that these approximations hold, at least in some weak sense:

- The sensitivity functions are localized in some weak sense to the support of the box functions predicted by (2.30) (e.g. when integrating times some smooth function, the integrals are close). The localization stands out particularly well in the intervals $[0, z_{i+1}]$ and $[0, \widehat{z}_i]$, as appears from the comparison done in Figure 2.3 for $\sigma^0 \equiv 1$.

- For $\sigma^0 \equiv 1$, the functions $-D\gamma_i[\sigma^0]/\gamma_i^0$ and $D\widehat{\gamma}_i[\sigma^0]/\widehat{\gamma}_i^0$ integrate like the box functions of (2.30),

$$\begin{aligned} \frac{-1}{\gamma_i^0}\int_0^1 D\gamma_i[\sigma^0](s)ds \approx \frac{1}{\gamma_i^0}\int_0^1 \chi_{[z_i^0, z_{i+1}^0]}(s)ds = 1 \quad \text{and} \\ \frac{1}{\widehat{\gamma}_i^0}\int_0^1 D\widehat{\gamma}_i[\sigma^0](s)ds \approx \frac{1}{\widehat{\gamma}_i^0}\int_0^1 \chi_{[\widehat{z}_{i-1}^0, \widehat{z}_i^0]}(s)ds = 1. \end{aligned}$$

  For $D\widehat{\gamma}_1[\sigma^0]/\widehat{\gamma}_1^0$, the approximation above is actually an equality. The proof follows by using the identity $\widehat{\gamma}_1 = 1/\sum_{i=1}^n (y_i(0))^2$.

2.4 A Newton type iterative algorithm for the inverse spectral problem

We improve the reconstructions of Algorithm 2.6 by using the sensitivity information we derived earlier in Section 2.3. One way of achieving this is to seek a conductiv-

ity that minimizes the misfit with the spectral measurements. This approach has been implemented before in e.g. [98, 13, 77]. Our idea is to capitalize on the fast inversion Algorithm 2.6 by viewing it as a non-linear transform of the spectral data. So instead of minimizing the misfit in the spectral data, we minimize the misfit in the reconstructions of Algorithm 2.6. Our method is presented in Section 2.4.1 and followed by numerical evidence in Section 2.4.2 that this non-linear transformation is beneficial to the convergence of the iterations, because it acts as a preconditioner, in some sense.

After the iterative procedure we have a conductivity that fits the data. To first order approximation, we may add to the conductivity elements of the orthogonal complement of the sensitivity functions without significantly changing the data fit. We apply this idea in Sections 2.4.3 and 2.4.4 to introduce a priori information about the conductivity *after* the data fitting.

2.4.1 The Gauss-Newton iteration

Let us start by defining the mapping $\Gamma_n : \mathcal{S} \to \mathbb{R}^{2n}$ which takes a conductivity to its spectral measurements and then to the reconstructions of Algorithm 2.6.[12] Here the conductivity is assumed to belong to the set $\mathcal{S}$ of positive functions. Since the reconstructions of Algorithm 2.6 are close to the true conductivity, the mapping Γ_n ought to be close to the identity, in some sense.

The basic idea here is to find a conductivity σ^* minimizing,

$$\min_{\sigma \in \mathcal{S}} \frac{1}{2} \left\| \Gamma_n(\sigma) - \Gamma_n(\sigma_{true}) \right\|_2^2 . \tag{2.31}$$

The minimization problem (2.31) is constrained to positive conductivities. We deal

[12] The ordering of the $2n$ approximate averages $\sigma_i, \widehat{\sigma}_i$ to form a vector of $\mathbb{R}^{2n}$ is irrelevant, as long as we keep the same ordering throughout.

with this constraint by using the change of variables $\kappa = \ln(\sigma)$ (sometimes called "geometric programming"). To make the new mapping as close to the identity as possible, we measure the misfit in the logarithm of the reconstructions of Algorithm 2.6. Combining these two modifications, we substitute the minimization (2.31) by,

$$\min_{\kappa} \frac{1}{2} \left\| \widetilde{\Gamma}_n(\kappa) - \widetilde{\Gamma}_n(\kappa_{true}) \right\|_2^2, \tag{2.32}$$

where $\widetilde{\Gamma} \equiv \ln \circ \Gamma \circ \exp$ and $\kappa_{true} = \ln(\sigma_{true})$.

We minimize (2.32) with the Gauss-Newton method. The Jacobian of $\widetilde{\Gamma}(\kappa) = \ln(\Gamma(\exp(\kappa)))$ can be easily obtained with the chain rule from that of $\Gamma(\sigma)$, which in turn is given by the analysis of Section 2.3. The Gauss-Newton iteration boils down to finding the update step as the minimal L^2 norm solution to the linearization of the problem around the current iterate. In equations, if $\kappa^{(k)}$ is the current iterate, the next iterate $\kappa^{(k+1)}$ is

$$\kappa^{(k+1)} = \kappa^{(k)} + \left(D\widetilde{\Gamma}_n[\kappa^{(k)}] \right)^{\dagger} \left(\widetilde{\Gamma}_n(\kappa_{true}) - \widetilde{\Gamma}_n(\kappa^{(k)}) \right), \tag{2.33}$$

where $\left(D\widetilde{\Gamma}_n[\kappa^{(k)}] \right)^{\dagger}$ is the pseudo-inverse[13] of $D\widetilde{\Gamma}_n[\kappa^{(k)}]$.

Because the Gauss-Newton method is local, choosing a good first iterate can speed up the convergence of the iterations. We take for the first iterate a smooth interpolation of the reconstruction given by Algorithm 2.6, which we expect to be close to the true conductivity. We put together the iterative method as follows.

Algorithm 2.12. Inputs: Spectral measurements $\{(y_i(0))^2, -(\omega_i)^2\}_{i=1}^n$ for σ_{true}. **Outputs:** A reconstructed conductivity σ^*.

1. Compute $\kappa^{(0)} = \ln(\sigma^{(0)})$, where $\sigma^{(0)}$ is a smooth interpolation of the averages $\sigma_i, \widehat{\sigma}_i$

[13] The pseudo-inverse, also called the Moore-Penrose generalized inverse, can be defined in the context of Hilbert spaces. See e.g. [50, §2].

obtained by Algorithm 2.6 from the measurements $\{(y_i(0))^2, -(\omega_i)^2\}_{i=1}^n$.

2. For $k = 0, 1, \ldots$ do,

   (a) $\kappa^{(k+1)} \leftarrow \kappa^{(k)} + \left(D\widetilde{\Gamma}_n[\kappa^{(k)}]\right)^\dagger \left(\widetilde{\Gamma}_n(\kappa_{true}) - \widetilde{\Gamma}_n(\kappa^{(k)})\right)$

   (b) If $\left\|\widetilde{\Gamma}_n(\kappa^{(k+1)}) - \widetilde{\Gamma}_n(\kappa_{true})\right\|_2 < \epsilon$, stop.

3. $\sigma^* \leftarrow \exp(\kappa^{(k+1)})$.

2.4.2 Numerical results for the Gauss-Newton iteration

Numerical approximation of the Jacobian

We represent the conductivity by pointwise values on a uniform grid with $N = 100$ points. On the *same grid* as the conductivity, we need the values of the sensitivity functions for the spectrum to perturbations in the conductivity. According to Lemma 2.9, to construct these sensitivity functions we do not only require the eigenfunctions of the differential operator in (2.4) and the Green's functions (2.24), we also need their derivatives (on the same grid as the conductivity). However, we use the finite difference discretization of Section 2.2.1 which only approximates the values of these functions on the primary grid nodes. A quick fix is to work on a finer uniform grid with $2N$ primary nodes, which allows us to approximate the derivatives using central finite differences. Moreover, to approximate the Green's functions (2.24) we need to sum over all the $2N$ available eigenfunctions to obtain a good agreement with the exact formulas of Lemma 2.10. The values of the conductivity at the nodes where it is not defined are found by spline interpolation. Finally we note that most of the spectrum calculations are done with the Fortran 90 code of Knizhnerman [45].

Implementation of the Gauss-Newton algorithm

In our numerics, the number of spectral measurements $2n$ is much smaller than the number of parameters N used to discretize the log-conductivity κ. Thus the Gauss-Newton update (2.33) can be efficiently computed via the identity,

$$(D\widetilde{\Gamma}_n[\kappa^{(k)}])^\dagger = D\widetilde{\Gamma}_n^*[\kappa^{(k)}] \left(D\widetilde{\Gamma}_n[\kappa^{(k)}] D\widetilde{\Gamma}_n^*[\kappa^{(k)}] \right)^\dagger. \tag{2.34}$$

Furthermore, we observed that for the conductivities we considered, the Jacobian $D\widetilde{\Gamma}_n[\kappa^{(k)}]$ is full-rank to working precision and well-conditioned, so that the relatively small $2n \times 2n$ matrix $D\widetilde{\Gamma}_n[\kappa^{(k)}] D\widetilde{\Gamma}_n^*[\kappa^{(k)}]$ is invertible and the pseudo-inverse in (2.34) could be replaced by the inverse.

Since we assume all along that $\kappa(0) = 0$ is known (since $\sigma(0) = 1$), it is desirable for the update that $\delta\kappa(0) = 0$. However there is no guarantee that this is respected, due to the space of functions where we look for the update $\delta\kappa$, namely the span of the sensitivity functions (the "columns" of $D\widetilde{\Gamma}_n^*[\kappa^{(k)}]$). In fact numerically we have $D\gamma_i[\sigma^0 \equiv 1](0) \approx -1$ and $D\widehat{\gamma}_i[\sigma^0 \equiv 1](0) \approx 1$. We remedy this by looking for the update in the span of the sensitivity functions, shifted by a constant function such that they are zero at $z = 0$. This amounts to replacing all the occurrences of the adjoint in the identity (2.34) by its shifted version.

Note that Rundell in [25, p117] recommends to not compute the spectrum of the differential operator of (2.4) as part of an inversion method, simply because there are inversion methods at least an order of magnitude faster than that. Our method does require the computation of the spectrum (and eigenfunctions), of a tridiagonal matrix of size $2N \times 2N$. This is a relatively inexpensive operation that does not need to be carried out many times since the number of iterations to convergence has always been small in our results. Conceivably, one could use a "fixed" or "frozen" Newton's

method, i.e. use the Jacobian at the first iterate for all the iterations. However, we were not urged to try the modification, considering that with $N = 100$ an iteration took less than 2 seconds on a PowerPC G4 1GHz, 1GB RAM computer.

The iterations

We implemented the method and give a typical convergence history in Figure 2.4. Sample reconstructions for piecewise continuous conductivities inspired by [95] are included in Figure 2.5. All our reconstructions are based on synthetic spectral measurements generated on a uniform grid with $N = 500$ primary points. This grid is different from the one used for the conductivity reconstructions to avoid committing an inverse crime.

An indication that (2.32) is relatively easy to minimize is that it is not necessary to limit the size of the update (2.33) to converge. In optimization this is known as a globalization strategy (examples are line search or trust region methods) and it is usually built in the method to ensure global convergence.

We also note that numerical convergence is achieved in very few steps, with the largest update occurring at the first iteration. Moreover, we observed Gibb's like phenomena close to the discontinuity points of the true conductivity. This would be expected if we had sought the update in the span of the sensitivity functions for σ^0, since then the sensitivity functions are essentially trigonometric functions (Lemma 2.11).

A preconditioning of the Gauss-Newton iteration?

Finally we compare the condition number[14] of the Jacobian $D\widetilde{\Gamma}_n[\sigma]$ to that of the sensitivity functions of the spectrum to changes in the conductivity (Section 2.3.2).

[14]The condition number of a matrix (not necessarily square) is defined as the ratio of the largest singular value to the smallest one.

We recall that both functions span the same space, however it appears from the comparison of Figure 2.6 that the basis we use in our method is by far better conditioned, and does not increase significantly with the number of spectral measurements.

We should be careful to draw conclusions on a non-linear problem from its linearization. Indeed, there are examples of non-linear problems that are ill-posed but have well-posed linearizations and vice-versa [50, §10.1].

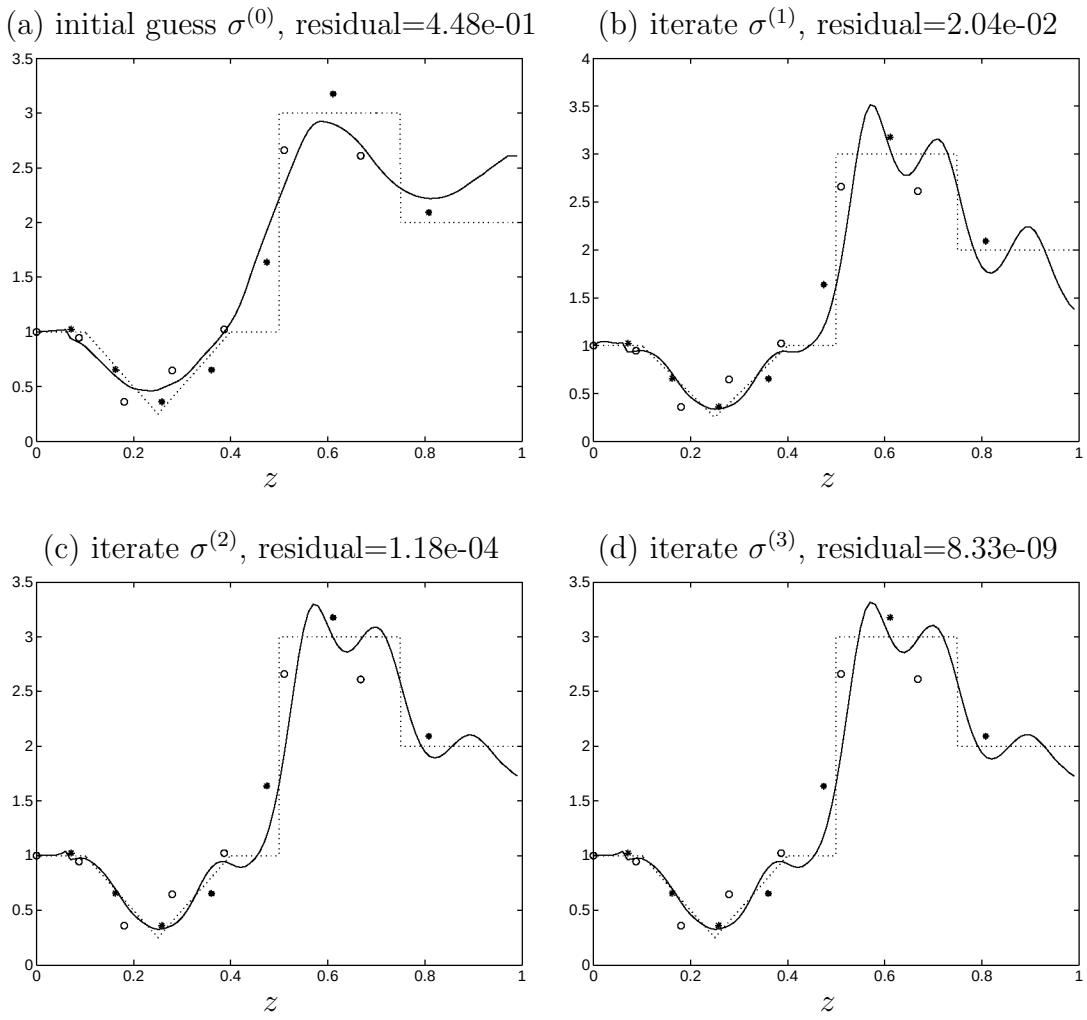

Figure 2.4: Convergence history for Algorithm 2.12 on a piecewise constant conductivity (dotted line) for $n = 7$ spectral measurements. Algorithm 2.6 gives the values indicated by ($\circ$) and ($*$) at the primary and dual grid points, respectively. The initial guess (a) is a smooth interpolation of these values. The reported residual is the log-resistor misfit $\|\widetilde{\Gamma}_n(\ln(\sigma)) - \widetilde{\Gamma}_n(\ln(\sigma_{true}))\|_2^2$.

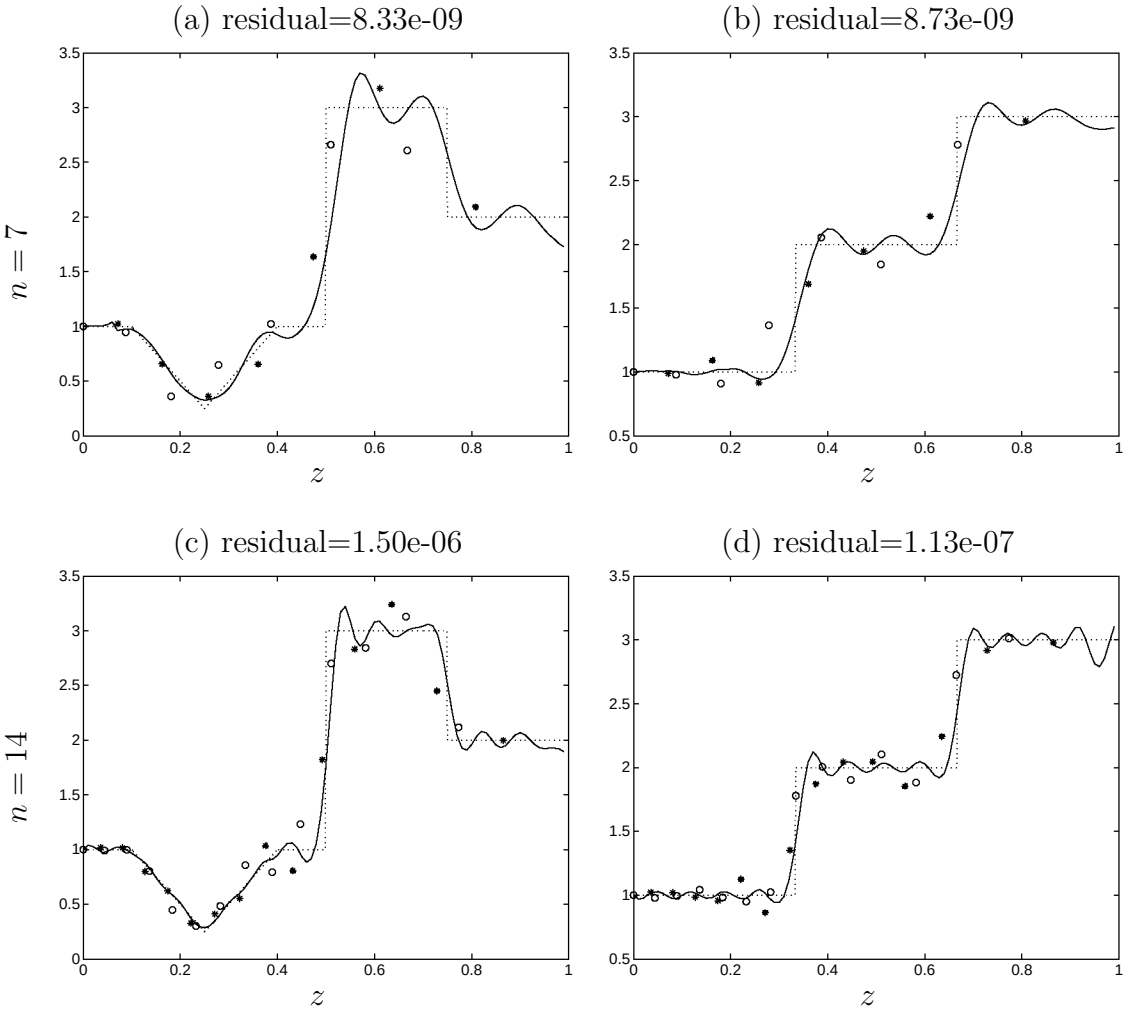

Figure 2.5: More reconstruction examples for Algorithm 2.12 with different conductivities and number of spectral measurements n. We show the third iterate and report the residual $\|\widetilde{\Gamma}_n(\ln(\sigma^{(3)})) - \widetilde{\Gamma}_n(\ln(\sigma_{true}))\|_2^2$. Algorithm 2.6 gives the values indicated by $(\circ)$ and $(*)$ at the primary and dual grid points, respectively. The true conductivity appears in dotted line.

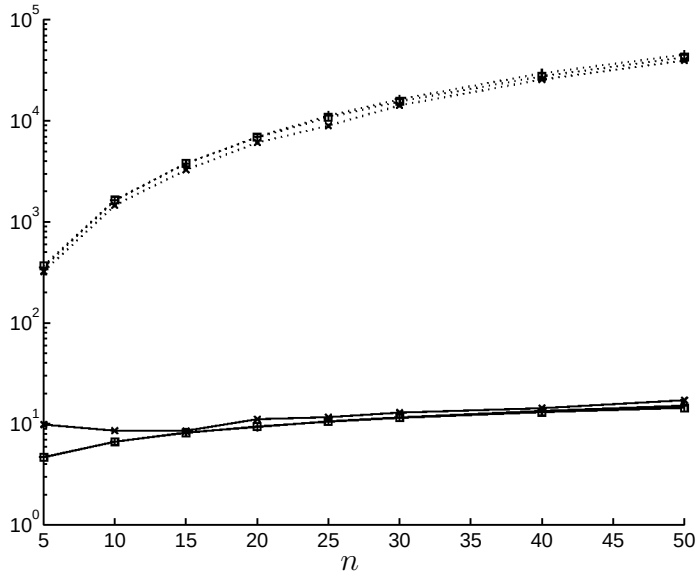

Figure 2.6: Conditioning of the Jacobian $D\widetilde{\Gamma}_n[\sigma]$ (solid lines) and of the sensitivities of the spectrum to changes in the conductivity (dotted lines) for different conductivities, which are: constant ($\square$), piecewise constant ($\times$) and piecewise linear ($+$). The sensitivities are discretized on a uniform grid with $N = 200$ primary nodes.

2.4.3 Introducing a priori information

Assume we have some a priori information about the true solution, in the form of some *penalty functional* $J(\sigma)$ that measures how far σ is from the desired prior. For example, if we know somehow that the true conductivity is piecewise constant, we can look specifically for conductivities with small total variation, i.e. that minimize $J(\sigma) = \mathrm{TV}(\sigma)$.

Recall from the numerics of Section 2.4.2 that the Gauss-Newton iteration converges fast. Actually, the largest correction happens during the first iteration. In subsequent iterations, the data fit is improved but the reconstruction does not change significantly. Let us then stop the iterations after the first iterate. Equivalently we find the minimal L^2 norm solution κ^{LS} to the linearized inverse problem,

$$D\widetilde{\Gamma}_n[\kappa^{(0)}](\kappa^{LS} - \kappa^{(0)}) = \widetilde{\Gamma}_n(\kappa_{true}) - \widetilde{\Gamma}_n(\kappa^{(0)}). \tag{2.35}$$

The basic idea of our method is to find a conductivity that minimizes the penalty functional while fitting the data. We relax the data fitting requirement by asking that it holds only in the linearized sense. To be precise, we seek a conductivity κ that minimizes the penalty functional and has the form $\kappa = \kappa^{LS} + \delta\kappa$, with $\delta\kappa \in \mathrm{null}\,(D\widetilde{\Gamma}_n[\kappa^{(0)}])$. Therefore, we view the introduction of a priori information as adding a correction in the orthogonal complement of the sensitivity functions. We look for a minimizer of the linearly constrained optimization problem,

$$\begin{aligned} \min_{\kappa} \quad & J(\kappa) \\ \text{subject to} \quad & D\widetilde{\Gamma}_n[\kappa^{(0)}](\kappa - \kappa^{LS}) = 0. \end{aligned} \tag{2.36}$$

We summarize the procedure as follows.

Algorithm 2.13. Inputs: $\{-\omega_i^2, (y_i(0))^2\}_{i=1}^n$ (spectral data (2.15)) and a penalty functional $J(\kappa)$ encoding the a priori information. **Outputs:** A reconstructed conductivity σ^*.

i. Compute $\kappa^{(0)} = \ln(\sigma^{(0)})$, where $\sigma^{(0)}$ is a smooth interpolation of the averages $\sigma_i, \widehat{\sigma}_i$ obtained by Algorithm 2.6 from the spectral measurements.

ii. Carry out the first iteration of Algorithm 2.12, that is compute the least squares solution to the linearized EIT problem with misfit measured in the reconstructions of Algorithm 2.6:

$$\kappa^{LS} \leftarrow \kappa^{(0)} + \left(D\widetilde{\Gamma}_n[\kappa^{(0)}]\right)^\dagger \left(\widetilde{\Gamma}_n(\kappa_{true}) - \widetilde{\Gamma}_n(\kappa^{(0)})\right).$$

iii. Find the reconstructed log-conductivity $\kappa^* = \ln(\sigma^*)$ as a minimizer of (2.36).

2.4.4 Numerical results with a priori information

We applied the method of the previous section to the functional J_{TV}, which favours piecewise constant reconstructions, and is defined as follows,

$$J_{TV}(\kappa) = TV(\kappa), \quad \text{where} \quad TV(\kappa) = \int_0^1 \left|\frac{d\kappa(z)}{dz}\right| dz.$$

Implementation strategies

Since the number of resistors we look for is small, the optimization problem (2.36) has only a few linear constraints. We exploit this structure by using an SQP (Sequential Quadratic Programming) method, with KKT (Karush-Kuhn-Tucker) systems solved by the range space approach [91, Chap. 18]. The globalization strategy we used was line search on an ℓ_1 type merit function [91, p544].

Moreover we approximated the non-linear functional J_{TV} with the standard smooth approximation of the absolute value:

$$\mathrm{TV}(\kappa) \approx \int_0^1 \sqrt{\left(\frac{d\kappa(z)}{dz}\right)^2 + \beta^2} dz, \tag{2.37}$$

with $\beta = 10^{-5}$. In order to regularize the Hessian systems to be solved at each iteration, we added 10^{-8} to their diagonal entries.

The resulting numerical method to minimize (3.24) with the J_{TV} functional is very similar to the so-called lagged diffusivity method [112, p136], modified to take into account the constraints.

Reconstructions

The stopping criterion for the iterations was that the gradient of the Lagrangian be reduced by 10^{-6}, which occurred in roughly 20 SQP iterations. Typical reconstructions are reported in Figure 2.7, and were computed using the same data and under the same conditions as the Gauss-Newton iterations of Section 2.4.2. The SQP iterations took as a whole less than one second for each reconstruction of Figure 2.7, under the same computational setup as in Section 2.4.2.

For comparison, we include in Figure 2.8 reconstructions obtained by minimizing a TV regularized output least squares (OLS) functional J_{ols} that measures the misfit in the spectral data,

$$J_{ols}(\kappa) = \frac{1}{2}\left\|\boldsymbol{\lambda}(\kappa) - \boldsymbol{\lambda}(\kappa_{true})\right\|_2^2 + \frac{1}{2}\left\|\boldsymbol{\eta}(\kappa) - \boldsymbol{\eta}(\kappa_{true})\right\|_2^2 + \mathrm{TV}(\kappa), \tag{2.38}$$

where $\boldsymbol{\lambda}(\kappa)$ denotes the vector of k eigenvalues of the differential operator of (2.4) for $\sigma = \exp(\kappa)$, and similarly $\boldsymbol{\eta}(\kappa)$ is the vector of the norming constants $y_i(0)^2$ for

the corresponding k eigenfunctions. The optimization is carried out with Newton's method with Armijo line search on exactly the same spectral data as our method. The TV functional was approximated using (2.37) with $\beta = 10^{-4}$ and we added 10^{-3} to the diagonal of the Hessian to stabilize the inversion. These parameters and the regularization parameter α were determined empirically by trying several values until obtaining satisfactory reconstructions. We report the number of iterations needed to reduce the gradient by a factor of 10^{-2}.

The reconstructions of both methods are very similar. The OLS method converges in less iterations than our method. However each OLS iteration is expensive because we have to compute the spectrum and derivatives, which is roughly the cost of an iteration of Algorithm 2.12. In our method we need to compute the spectrum and derivatives only once, which makes it faster.

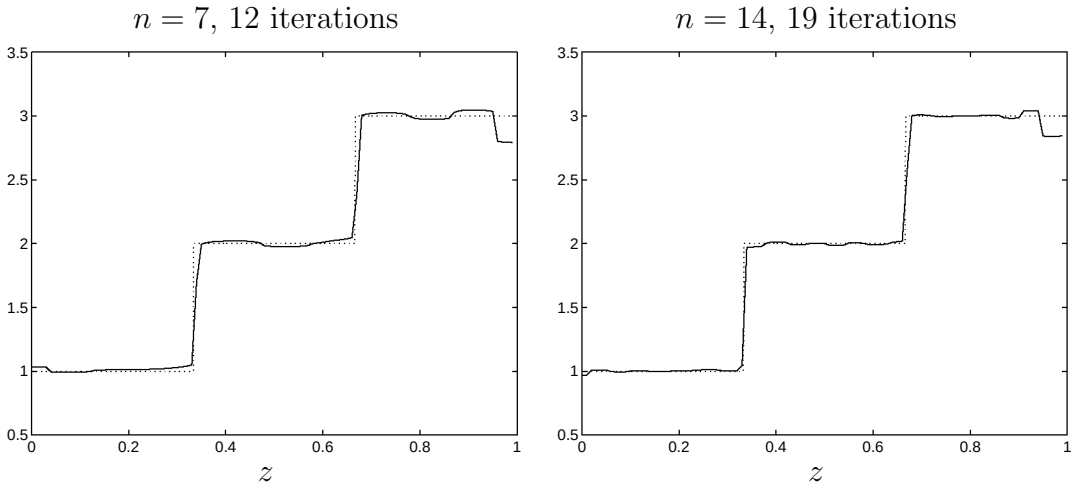

Figure 2.7: Reconstructions from spectral data using Algorithm 2.13 with a TV penalty functional, for a piecewise constant conductivity.

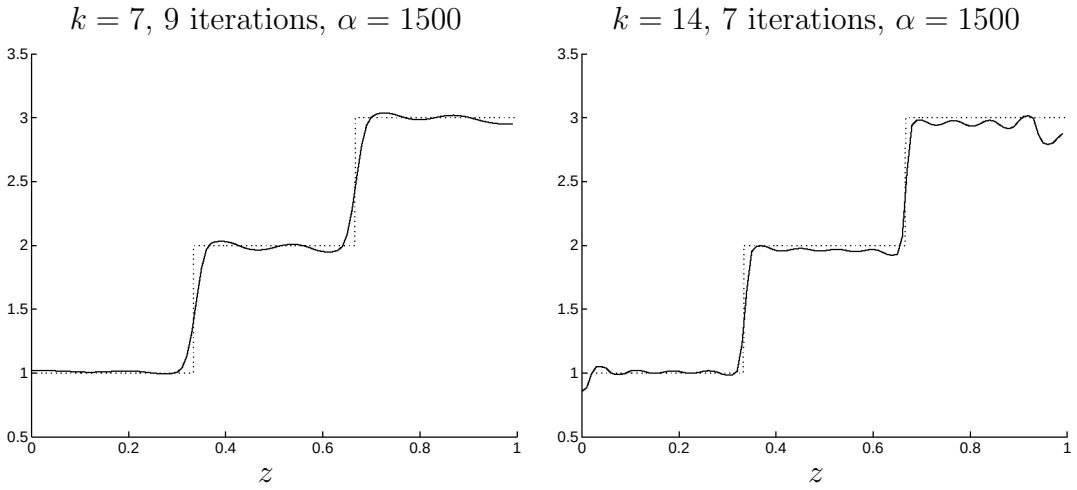

Figure 2.8: Reconstructions from spectral data using output least squares with a TV regularization term (2.38), for a piecewise constant conductivity. In wall-clock time the reconstruction took around 12 seconds for $k = 7$ and 16 seconds for $k = 14$.

Chapter 3

Electrical impedance tomography with circular planar graphs

In this Chapter we extend the ideas discussed in Chapter 2 for the one dimensional spectral problem (see Section 2.1) to the 2D Electrical Impedance Tomography (EIT) problem (see Section 1.1), on domains that can be conformally mapped to a disk. To estimate the unknown conductivity σ, we follow the same steps as for the one-dimensional problem. First we solve the model reduction problem of finding the smallest resistor network (of fixed topology) that can predict some meaningful measurements of the DtN map. Once we know the network, we estimate the unknown conductivity σ with a Gauss-Newton method.

While in inverse spectral problems the size of the resistor networks is determined by the number of measurements, the ill-posedness of EIT requires a different decision. Noise limits severely the amount of information about σ that is carried in the data, no matter how many measurement points we take. Typically, the high frequency responses are buried in the noise, so one can only rely on the low frequency components of the data and obtain, therefore, a low resolution image of σ.

This chapter is organized as follows: We start by describing in Section 3.1 a finite volumes discretization of the EIT problem that leads to resistor networks, our

reduced model of the elliptic partial differential equation satisfied by the potential. The topology of the networks is given by the discretization stencil and the resistors are determined by averages of the conductivity on the grid.

Then, in Section 3.2 we show how to determine these reduced models from measurements of the DtN map Λ_σ^{DtN}. Specifically, we define in Section 3.2.1 a broad class of measurements of the DtN map and prove that they correspond to DtN maps of resistor networks. The *sparsest* such network can be recovered *uniquely* from the meaningful measurements, by solving a discrete inverse problem, as we show in Section 3.2.2. By meaningful measurements we mean that when the data is contaminated with noise, only part of it carries real information about σ. We explain in Section 3.2.5 how to extract the meaningful data, which we then use to find the resistor network with size depending naturally on the level of noise.

Next, in Section 3.3, we recall the definition of the resistors in terms of averages of σ and we explain how we can estimate it on a precomputed grid, for a sufficiently similar reference conductivity σ^0. The assumption is that, as in the one dimensional case, the grids depend weakly on σ. It is difficult to show that the reconstructed σ on the reference grid converges to the true conductivity, in ideal situations and for smooth enough σ. We prove however in Section 3.3.3 that a necessary condition for convergence is to reconstruct on such reference grids.

The reconstructions of σ on the reference grids are used in Section 3.4 as starting points of a Gauss-Newton iteration that is designed to recover a low resolution image of the conductivity, which is the best that we can hope for realistic noise levels, in light of the ill-posedness of the problem. Finally, we show in Section 3.4.3 how to improve the resolution of the reconstruction by incorporating certain types of a priori information about σ.

3.1 Finite volumes discretization

We discretize the EIT equation using a finite volumes scheme on a staggered tensor product grid. We choose this discretization because it leads to reduced models that are uniquely recoverable from the measurements, as we explain in detail in Section 3.2.3.

For us the domain Ω is the unit disk $B(0,1) \subset \mathbb{R}^2$. In principle other simply connected bounded domains with C^2 boundary can be considered by conformally mapping the domain to $B(0,1)$, but this is not addressed here. The grids we use are described in Section 3.1.1. The finite volumes scheme is derived from the conservation of currents law in Section 3.1.2.

3.1.1 The staggered finite volume grids

For the discretization we use grids that are staggered, i.e. composed of a primary and dual grid as shown in Figure 3.1. Both primary and dual grids are tensor products of a uniform angular grid and an adaptive, not known a priori, radial grid. The dual grid angles are the bisectors of the primary grid angles and these are chosen according to the highest frequency that we wish to capture in the potential. The potential is discretized on the primary grid points and the current fluxes on the dual grid points.

Following [64], we denote the grids by $\mathcal{G}(l,n)$, where n is the number of boundary nodes and l is the number of primary grid "layers". A layer is defined as in [64], as a minimal subset of edges of the primary grid that is invariant under rotations of the grid about the origin by the angle $2\pi/n$. For example, the primary grid constructed by rotating n times the pattern "`0-1`" by an angle of $2\pi/n$ about the origin has 1 layer, "`0-|1`" has 2 layers, "`0-|-1`" has 3 layers, "`0-|-|1`" has 4 layers, etc. Here the symbol "`-`" represents an edge in the radial direction and "`|`" an edge in the angular direction.

In our discretizations, the innermost (closest to the origin) primary layer is always in the radial direction. The parity of the number of primary layers determines the type of the outermost (or boundary) primary layer: it is in the radial direction if and only if l is odd. The discretization is slightly different depending on the parity of l, as is illustrated with the examples in Figure 3.1.

We label the primary nodes starting from the boundary, so that the radii of the primary grid points are,

$$0 = r_{\lceil l/2 \rceil + 1} < r_{\lceil l/2 \rceil} < \cdots < r_2 < r_1 = 1,$$

where $\lceil m \rceil$ is the smallest integer larger or equal to m. Similarly, the radii of the dual cell boundaries are,

$$0 < \widehat{r}_{\lfloor l/2 \rfloor + 1} < \widehat{r}_{\lfloor l/2 \rfloor} < \cdots < \widehat{r}_2 < \widehat{r}_1 = 1,$$

where $\lfloor m \rfloor$ is the largest integer smaller or equal to m.

3.1.2 The finite volumes scheme

In a finite volumes scheme, we integrate equation (1.1) over the dual cells, and then use the divergence theorem to derive the balance of fluxes through the dual cell boundaries. These fluxes are approximated using finite differences, and the discrete equations can be interpreted as Kirchhoff's node law for a resistor network with topology given by the primary grid.

We denote by $u_{i,j}$ the approximation of the potential u at the primary grid nodes (r_i, jh_θ), for $1 \leq i \leq \lceil l/2 \rceil + 1$ and $1 \leq j \leq n$, and by I_j the approximation of the current density $I = \sigma \mathbf{n} \cdot \nabla u|_{\partial\Omega}$ at the boundary points $(1, jh_\theta)$, for $1 \leq j \leq n$. For

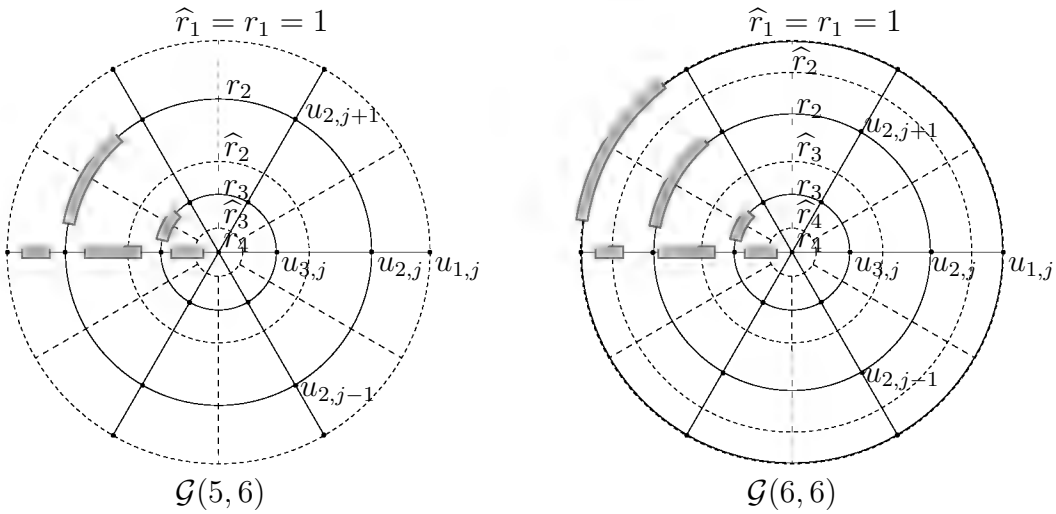

Figure 3.1: Representative examples of the two kinds of grids we use. The primary grid is in solid line and the dual grid in dotted line. In $\mathcal{G}(5,6)$, the primary boundary edges are in the radial direction, whereas in $\mathcal{G}(6,6)$ they are in the angular direction.

illustration purposes, let us zoom in the dual cell centered at primary node (r_i, jh_θ), depicted in Figure 3.2. The conservation law in this cell is

$$\begin{aligned}\int_{\text{cell}(i,j)} \nabla \cdot [\sigma \nabla u] d\mathbf{x} = & \int_{AD} \sigma \frac{\partial u}{\partial r} dS_{AD} - \int_{BC} \sigma \frac{\partial u}{\partial r} dS_{BC} \\ & + \int_{AB} \frac{\sigma}{r} \frac{\partial u}{\partial \theta} dS_{AB} - \int_{CD} \frac{\sigma}{r} \frac{\partial u}{\partial \theta} dS_{CD} = 0\end{aligned} \tag{3.1}$$

and the discretization of the fluxes is done as follows. On the cell boundary segment AD, we have

$$\begin{aligned}\int_{AD} \sigma \frac{\partial u}{\partial r} dS_{AD} &= \int_{(j-1/2)h_\theta}^{(j+1/2)h_\theta} \widehat{r}_{i-1} \sigma(\widehat{r}_{i-1}, \theta) \frac{\partial u}{\partial r}(\widehat{r}_{i-1}, \theta) d\theta \\ &\approx \left(\int_{(j-1/2)h_\theta}^{(j+1/2)h_\theta} \widehat{r}_{i-1} \sigma(\widehat{r}_{i-1}, \theta) d\theta \right) \frac{\partial u}{\partial r}(\widehat{r}_{i-1}, jh_\theta) \\ &= -\frac{\partial u}{\partial x_j}(\widehat{r}_{i-1}, jh_\theta) \\ &\approx -\frac{u(r_i, jh_\theta) - u(r_{i-1}, jh_\theta)}{x_j(r_i) - x_j(r_{i-1})},\end{aligned}$$

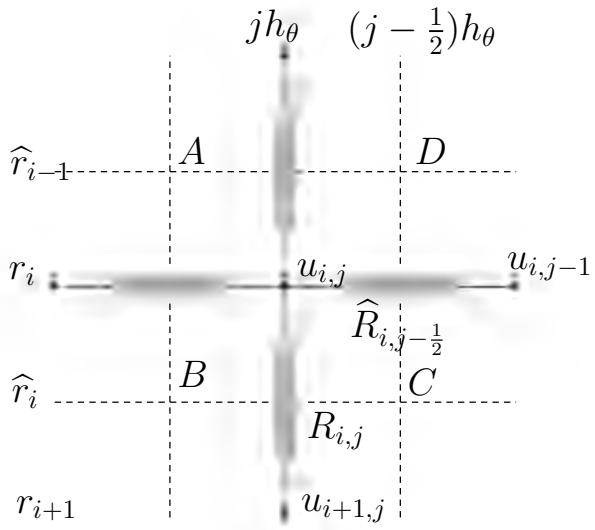

Figure 3.2: Cell (i, j) in the finite volume discretization. The primary grid appears in solid line and the dual grid in dotted line.

where the last approximation in the chain is made with finite differences and where we used the change of variables

$$x_j(r) = \int_r^1 \frac{dt}{t \displaystyle\int_{(j-1/2)h_\theta}^{(j+1/2)h_\theta} \sigma(t,\theta)d\theta}.$$

Similarly, on the segment AB, we have

$$\begin{aligned}
\int_{AB} \frac{\sigma}{r}\frac{\partial u}{\partial \theta} dS_{AB} &= \int_{\widehat{r}_i}^{\widehat{r}_{i-1}} \frac{\sigma(t,(j+1/2)h_\theta)}{t}\frac{\partial u}{\partial \theta}(t,(j+1/2)h_\theta)dt \\
&\approx \left(\int_{\widehat{r}_i}^{\widehat{r}_{i-1}} \frac{\sigma(t,(j+1/2)h_\theta)}{t}dt\right)\frac{\partial u}{\partial \theta}(r_{i-1},(j+1/2)h_\theta) \\
&= \frac{\partial u}{\partial \phi_i}(r_{i-1},(j+1/2)h_\theta) \\
&\approx \frac{u(r_{i-1},(j+1)h_\theta) - u(r_{i-1},jh_\theta)}{\phi_i((j+1)h_\theta) - \phi_i(jh_\theta)},
\end{aligned}$$

where we made the change of variables

$$\phi_i(\theta) = \int_0^\theta \frac{d\alpha}{\displaystyle\int_{\widehat{r}_i}^{\widehat{r}_{i-1}} dt \frac{\sigma(t,\alpha)}{t}}, \quad \text{for } i = 2, \ldots, \lfloor l/2 \rfloor + 1.$$

Let us define

$$\begin{aligned} R_{i,j} = x_j(r_{i+1}) - x_j(r_i) &= \int_{r_{i+1}}^{r_i} dt \left(t \int_{(j-1/2)h_\theta}^{(j+1/2)h_\theta} \sigma(t,\theta) d\theta \right)^{-1} \\ &= \frac{1}{\widehat{\sigma}_{i,j}} \frac{1}{h_\theta} \int_{r_{i+1}}^{r_i} \frac{dt}{t}, \end{aligned} \tag{3.2}$$

for $i = 1, \ldots, \lceil l/2 \rceil$, $j = 1, \ldots, n$ and

$$\begin{aligned} \widehat{R}_{i,j+1/2} = \phi_i((j+1)h_\theta) - \phi_i(jh_\theta) &= \int_{jh_\theta}^{(j+1)h_\theta} d\alpha \left(\int_{\widehat{r}_i}^{\widehat{r}_{i-1}} dt \frac{\sigma(t,\alpha)}{t} \right)^{-1} \\ &= \frac{1}{\sigma_{i,j+1/2}} h_\theta \left(\int_{\widehat{r}_i}^{\widehat{r}_{i-1}} \frac{dt}{t} \right)^{-1}, \end{aligned} \tag{3.3}$$

for $i = 2, \ldots, \lfloor l/2 \rfloor + 1$, $j = 1, \ldots, n$. The coefficients $\widehat{\sigma}_{i,j}$ and $\sigma_{i,j+1/2}$ are averages of the conductivity on the grid. We now write the discretization of (3.1).

We look first at dual cells containing primary grid nodes (r_i, jh_θ) that are neither on the boundary nor at the origin. This happens when $2 \le i \le \lceil l/2 \rceil$ and $1 \le j \le n$. On these cells, the finite volumes scheme is

$$\frac{u_{i-1,j} - u_{i,j}}{R_{i-1,j}} + \frac{u_{i+1,j} - u_{i,j}}{R_{i,j}} + \frac{u_{i,j+1} - u_{i,j}}{\widehat{R}_{i,j+\frac{1}{2}}} + \frac{u_{i,j-1} - u_{i,j}}{\widehat{R}_{i,j-\frac{1}{2}}} = 0, \tag{3.4}$$

where the operations $(+)$ and $(-)$ on the angular discretization parameter j are to be understood modulo n. The cell containing the origin is a special case, as it contains

only radial primary layers and the discretization is

$$\sum_{j=1}^{n} \frac{u_{\lceil l/2 \rceil, j} - u_{\lceil l/2 \rceil + 1, j}}{R_{\lceil l/2 \rceil, j}} = 0. \tag{3.5}$$

It remains to define the stencil for boundary nodes. The discretization is different at the boundary, depending on the number of layers l. In the case where l is odd (see Figure 3.1 on the left) the stencil is

$$\frac{u_{2,j} - u_{1,j}}{R_{1,j}} + I_j = 0, \quad \text{for } 1 \leq j \leq n. \tag{3.6}$$

When the number of layers l is even (see Figure 3.1 on the right) the stencil is,

$$\frac{u_{2,j} - u_{1,j}}{R_{1,j}} + \frac{u_{1,j+1} - u_{1,j}}{\widehat{R}_{1,j+\frac{1}{2}}} + \frac{u_{1,j-1} - u_{1,j}}{\widehat{R}_{1,j-\frac{1}{2}}} + I_j = 0, \quad \text{for } 1 \leq j \leq n. \tag{3.7}$$

Remark 3.1. Equations (3.4) through (3.7) are Kirchhoff's node law for a circular resistor network with topology given by the primary grid and with resistors $R_{i,j}$, $\widehat{R}_{i,j+1/2}$. The resistors are determined by averages of the conductivity on the grid, as stated in (3.2) and (3.3). Some resistors are shown in gray in Figures 3.1 and 3.2.

3.2 From continuum DtN maps to resistor networks

In this section we consider the model reduction problem of finding the sparsest resistor network that reproduces measurements of the continuum DtN map. We prove the solvability of this problem in a few steps. First, we define in Section 3.2.1 a general class of measurements of the continuum DtN map. Then, we show that these measurements belong to the set of DtN maps of well-connected networks. After proving this consistency result, we obtain the injectivity of the map that takes us from the

measurements to critical resistor networks. The resistor networks arising in our finite volume discretizations can be made critical by choosing appropriately the number of layers, for a given number of boundary nodes.

Although, in theory, the determination of the critical networks from the measurements has a unique solution, the problem is ill-posed and the instability gets worse as we increase the size of the network. We show however in Section 3.2.5 that, for noisy data, only the low frequency components carry information about σ and this allows us to lump the measurements into those corresponding to the DtN map of small resistor networks. The lumping limits naturally the resolution of the image for realistic noise levels and is detailed further in Appendix B.4.

3.2.1 The measured DtN map

We consider a general class of linear measurements $\mathcal{M}_n(\Lambda_\sigma^{DtN}) \in \mathbb{R}^{n\times n}$ of the DtN map that as we show in Section 3.2.3 define the DtN map of well-connected resistor networks.

Definition 3.2. Let $\phi_1, \ldots, \phi_n$ be a set of n nonnegative functions in $H^{1/2}(\partial\Omega)$, with disjoint supports numbered in circular order around the boundary and satisfying $\int_{\partial\Omega} \phi_i = 1$.[1] The *measured DtN map* $\mathcal{M}_n(\Lambda_\sigma^{DtN}) \in \mathbb{R}^{n\times n}$ is defined componentwise by,

$$\left(\mathcal{M}_n(\Lambda_\sigma^{DtN})\right)_{i,j} = \begin{cases} \left\langle \phi_i, \Lambda_\sigma^{DtN}\phi_j \right\rangle & \text{if } i \neq j \\ -\displaystyle\sum_{i=1, p\neq i}^{n} \left\langle \phi_i, \Lambda_\sigma^{DtN}\phi_p \right\rangle & \text{otherwise,} \end{cases} \tag{3.8}$$

where $\langle \cdot, \cdot \rangle$ is the $H^{1/2}(\partial\Omega), H^{-1/2}(\partial\Omega)$ duality pairing.

[1] The condition $\int_{\partial\Omega} \phi_i = 1$ on the ϕ_i makes $\mathcal{M}_n(\Lambda_\sigma^{DtN})$ an approximation of pointwise measurements of the kernel of the DtN map, as the $\operatorname{supp}\phi_i$ become small.

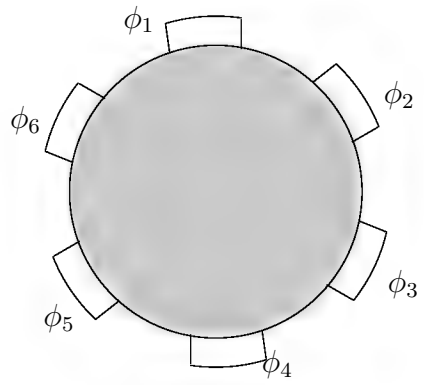

Figure 3.3: Physically, the measured DtN map $\mathcal{M}_n(\Lambda_\sigma^{DtN})$ can be thought of as measurements taken with electrodes at the boundary.

When the ϕ_i are box functions,[2] as shown in Figure 3.3, the measured DtN map corresponds precisely to the so called "shunt electrode model" [100]. Indeed, an electrode can be idealized by a perfect conductor, and so the potential is constant over the support of the electrode. Thus $\Lambda_\sigma^{DtN}\phi_j$ is the current density arising from a nonzero potential at electrode j. The current density is measured at electrode i by $\left\langle \phi_i, \Lambda_\sigma^{DtN}\phi_j \right\rangle$ which is the total current flowing out of electrode i.

Since the reduced model we use for the PDE is a resistor network, the diagonal elements of $\mathcal{M}_n(\Lambda_\sigma^{DtN})$ are chosen to agree with the compatibility condition for networks: the currents flowing out of the network sum to zero.

Remark 3.3. It is known that the shunt electrode model is a crude model because it does not account for the electrode effects on the medium that are observed in practice. Instead, one should interpret the readings with the "complete electrode model" [100], which does take account of the electrode effects, and then transform the readings to the shunt model. Moreover, the electrode models in [100] are actually defined for the NtD map, but by convex duality arguments appearing in Appendix B.2, NtD measurements can be transformed into DtN measurements.

[2]Box functions are not in $H^{1/2}(\partial\Omega)$, however they can be approximated by continuous functions to define $\mathcal{M}_n(\Lambda_\sigma^{DtN})$. Alternatively, some regularity of the kernel of the DtN map can be assumed.

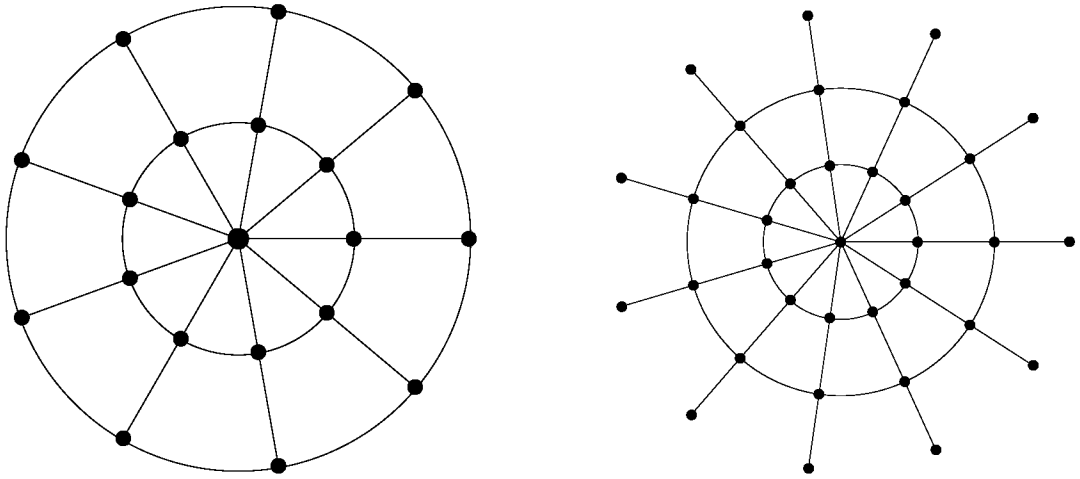

Figure 3.4: Examples of $C(l,n)$ resistor networks. Here $l = (n-1)/2$ so that the network is critical, and thus uniquely recoverable.

3.2.2 Uniqueness of the resistor network reduced model

In this section we review resistor networks results [34, 36, 35] that guarantee that the resistor networks we use are uniquely determined from their DtN map (Theorem 3.5).

The DtN map of circular resistor networks

A circular resistor network (R-net) is a planar graph that can be embedded in the plane, and that has a resistance value assigned to each edge. We shall consider R-nets with topology $C(l,n)$ given by the topology of the primary grid in the finite volume discretization $\mathcal{G}(l,n)$ defined in Section 3.1. Examples of such networks appear in Figure 3.4.

In a resistor network, the potentials at the nodes satisfy Kirchhoff's node law. The DtN map is defined as the linear mapping taking potentials at the boundary nodes to currents flowing out of the boundary nodes. Let us assume that the network has n boundary nodes labeled $v_1, v_2, \ldots, v_n$. We shall represent the DtN map as a matrix, where the $i-$th column contains the currents flowing out of the network through

nodes $v_1, \ldots, v_n$, when the potential is one at node v_i and zero at the other nodes.

A circular R-net is said to be *well-connected* if any two disjoint non-overlapping sets $P = \{p_1, \ldots, p_k\}$ and $Q = \{q_1, \ldots, q_k\}$ of k boundary nodes, appearing in the order $p_1, \cdots, p_k, q_k, \cdots, q_1$ on the boundary, are connected by k disjoint paths. Curtis et al. [36] proved that the DtN map for a well-connected circular resistor network with n boundary nodes and positive, bounded, resistors belongs to a subset Ω_n of $\mathbb{R}^{n\times n}$ defined as follows,[3]

Definition 3.4. The set Ω_n is the set of matrices $\mathbf{A} \in \mathbb{R}^{n\times n}$ such that,

i. The matrix A is symmetric.

ii. The matrix A has zero row sum, i.e. $\mathbf{A1} = \mathbf{0}$.

iii. All circular minors $\mathbf{M}$ of $\mathbf{A}$, that is all submatrices $\mathbf{M} = \mathbf{A}(p_1, \ldots, p_k; q_1, \ldots, q_k)$ where the distinct indices $p_1, \ldots, p_k, q_k, \ldots, q_1$ appear in order when $\{1, \ldots, n\}$ is laid down on a circle, are totally negative, or equivalently $\det(-\mathbf{M}) > 0$.[4]

We show later in Section 3.2.3 that the measurements $\mathcal{M}_n(\Lambda_\sigma^{DtN})$ of the DtN map, defined by (3.8), belong to Ω_n.

Recoverable resistor networks

A resistor network is said to be *recoverable* when its resistors can be *uniquely* recovered from its DtN map. A network is recoverable if and only if it is *critical* [36, Lemma 13.2], meaning that the network is well-connected and that the removal of any edge makes the network not well-connected.

In general it is not possible to find both the resistors and the topology of the network from the DtN map. This is because all graphs that are $Y-\Delta$ equivalent have

[3]The Ω_n notation is borrowed from [36] and should not be confused with the domain Ω.

[4]Since we work with well-connected networks only, we do not need to relax the determinantal inequality to a non-strict one, as is done in [36].

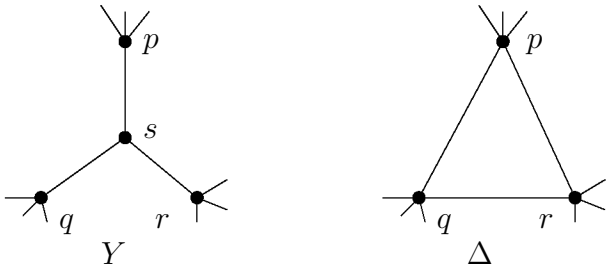

Figure 3.5: At the nodes p, q, r, the Y on the left is electrically equivalent to the Δ on the right. A R-net can be transformed through a sequence of these transformations into another R-net with the same DtN map (adapted from [36, §5]).

the same DtN map. Two graphs are $Y-\Delta$ equivalent if there is a sequence of $Y-\Delta$ or $\Delta-Y$ transformations taking one graph to the other. A $Y-\Delta$ transformation takes a Y at an interior node s (Figure 3.5 left) to a Δ (Figure 3.5 right). Both configurations are electrically indistinguishable at the nodes p, q, r. Also note that $Y-\Delta$ (or $\Delta-Y$) transformations preserve the number of edges.

The next theorem essentially shows that under certain assumptions on the number of layers, the resistor network underlying the finite volumes discretization of Section 3.1 is uniquely recoverable from its DtN map.

Theorem 3.5. *All recoverable resistor networks with an* odd *number n of boundary nodes are $Y-\Delta$ equivalent to a resistor network with topology $C(l=(n-1)/2, n)$.*

Proof. This follows from Proposition 2.3 and Corollary 9.4 in [35]. □

Note that the size of recoverable networks is fixed by the number of measurement points and that the number of resistors is $nl = n(n-1)/2$, which is exactly the number of "independent" measurements in the DtN map.[5]

The following elementary Lemma shows why we consider only an *odd* number of boundary points in Theorem 3.5.

[5]Since the DtN map of a R-net with n boundary nodes is symmetric and has zero row sum, all its entries are determined by the $n(n-1)/2$ entries above the diagonal.

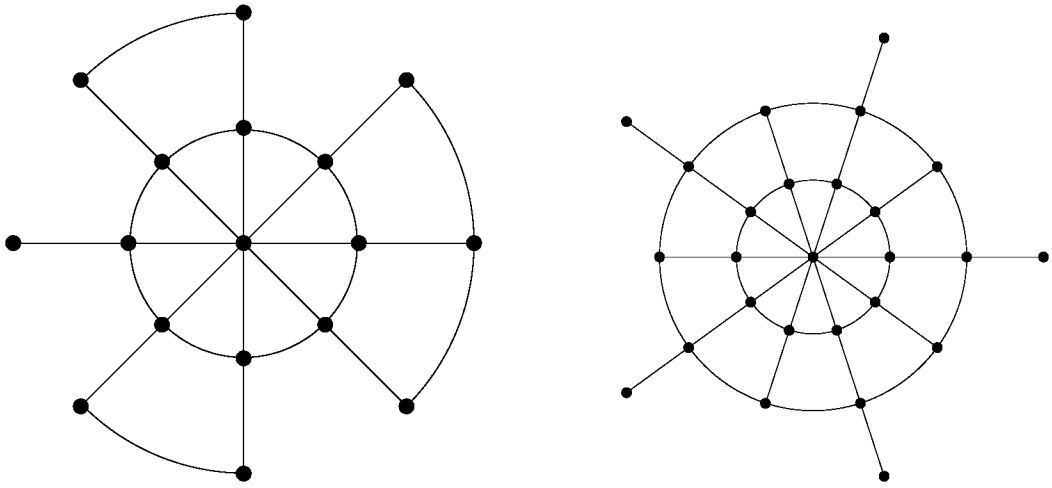

case $n \equiv 0 \bmod 4$ case $n \equiv 2 \bmod 4$

Figure 3.6: Critical graphs for an even number n of boundary points. The construction is slightly different depending on n mod 4 (taken from [35, pp20–24]).

Lemma 3.6. *For n even, there is no l such that $C(l, n)$ is a critical graph.*

Proof. A critical graph with n boundary nodes has $n(n-1)/2$ edges. This can be verified for the critical graphs with topologies given in Figures 3.4 and 3.6 by counting edges. Moreover, *all* critical graphs with n boundary nodes are $Y - \Delta$ equivalent (see [36, §5]), and therefore they all have the same number of edges.

If n is even, the number of edges in a critical graph with n boundary nodes is $n(n-1)/2 \equiv n/2 \bmod n$. However the number of edges in $C(l, n)$ is $nl \equiv 0 \bmod n$. Therefore $C(l, n)$ is not a critical graph when n is even. □

To illustrate Lemma 3.6, we give examples of critical graphs with an even number of boundary nodes in Figure 3.6.

Recoverable R-nets and the finite volumes discretization

We now justify our choice of a finite volumes discretization. Other discretization methods such as the finite elements method with P_1 triangular elements or Q_1 quadrilateral elements, yield networks that are not critical and thus not recoverable. This

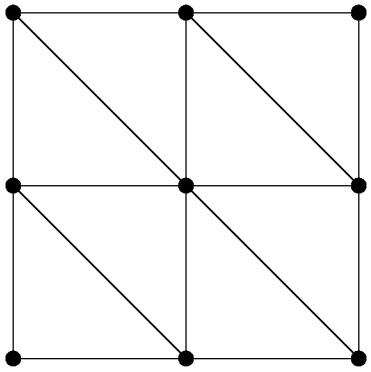

Figure 3.7: Part of the R-net coming from a P_1 (linear) finite element discretization with triangular elements. This discretization gives a R-net that is not critical, and therefore not recoverable. Specifically, the slanted edges are redundant.

is illustrated in Figure 3.7 for P_1 triangular finite elements. However through careful choice of the quadrature rule (mass lumping), one can transform certain finite element methods (e.g. Q_1 elements) into a difference scheme that can also be viewed as a $C(l, n)$ resistor network. By the uniqueness of the solution to the model reduction problem, such a scheme is equivalent to ours.

3.2.3 Consistency of the measurements with the R-net model

Here we prove the solvability of the model reduction problem, which we state as follows.

Theorem 3.7. *For a smooth enough positive, bounded conductivity σ, the measured DtN map $\mathcal{M}_n(\Lambda_\sigma^{DtN})$ (Definition 3.2), is the DtN map of a well-connected R-net.*

Now from the uniqueness results of Section 3.2.2 we deduce the following corollary involving the R-nets coming from the finite volumes discretization of Section 3.1.

Corollary 3.8. *For a smooth enough positive bounded conductivity σ, and for n odd, there is a unique resistor network of type $C(l = (n-1)/2, n)$ with DtN map $\mathcal{M}_n(\Lambda_\sigma^{DtN})$.*

Proof. This corollary is a direct consequence of Theorem 3.7 and Theorem 3.5. □

The proof of Theorem 3.7 proceeds by showing that the measured DtN map $\mathcal{M}_n(\Lambda_\sigma^{DtN})$ belongs to Ω_n, the set of DtN maps of well-connected R-nets defined in Definition 3.4. That $\mathcal{M}_n(\Lambda_\sigma^{DtN})$ is a symmetric $n \times n$ matrix with zero row sum follows trivially from Definition 3.2 and the self-adjointness of Λ_σ^{DtN}. The technical part is to show that all the circular minors of $\mathcal{M}_n(\Lambda_\sigma^{DtN})$ are *totally negative* (see e.g. [36, §10] for a definition), and the rest of this Section is devoted to proving this result.

To establish the total negativity of the circular minors of the measured DtN map, we use a characterization of the kernel of the DtN map due to Ingerman and Morrow [62]. Recall that the kernel $K_\sigma : \partial\Omega \times \partial\Omega \to \mathbb{R}$ of the DtN map is such that for $f \in H^{1/2}(\partial\Omega)$,

$$(\Lambda_\sigma^{DtN} f)(\mathbf{x}) = \int_{\partial\Omega} K_\sigma(\mathbf{x}, \mathbf{y}) f(\mathbf{y}) d\mathbf{y}.$$

We require some terminology to review the results in [62]. A set of $2n$ distinct points of $\partial\Omega$ $(\mathbf{x}_1, \ldots, \mathbf{x}_n; \mathbf{y}_1, \ldots, \mathbf{y}_n)$ is called a *circular pair* if $\mathbf{x}_1, \ldots, \mathbf{x}_n, \mathbf{y}_n, \ldots, \mathbf{y}_1$ are consecutive on the circle. Similarly, a set of $2n$ nonnegative functions $(X_1, \ldots, X_n; Y_1, \ldots, Y_n)$, with respective supports I_1, …, I_n, J_1, …, J_n in $\partial\Omega$, is called a *circular pair of functions* if their supports are disjoint and are consecutive on the circle when numbered $I_1, \ldots, I_n, J_n, \ldots, J_1$, and additionally if each function integrates to one.

Definition 3.9. A kernel $K : \partial\Omega \times \partial\Omega \to \mathbb{R}$ is said to have *Property* **(P1)** if and only if, for all circular pairs $(\mathbf{x}_1, \ldots, \mathbf{x}_n, \mathbf{y}_1, \ldots, \mathbf{y}_n)$ the following determinantal inequality holds

$$\det(\{-K(\mathbf{x}_i, \mathbf{y}_i)\}_{i,j=1,\ldots,n}) > 0. \tag{3.9}$$

Definition 3.10. A kernel $K : \partial\Omega \times \partial\Omega \to \mathbb{R}$ is said to have *Property* **(P2)** if and only if, for all circular pairs of functions $(X_1, \ldots, X_n, Y_1, \ldots, Y_n)$ the following

determinantal inequality holds

$$\det\left(\left\{-\int_{\partial\Omega\times\partial\Omega} X_i(\mathbf{x})Y_j(\mathbf{y})K(\mathbf{x},\mathbf{y})d\mathbf{x}d\mathbf{y}\right\}_{i,j=1,\ldots,n}\right)>0. \tag{3.10}$$

Note that both determinantal inequalities above are equivalent to saying that the matrices in the determinants are *totally positive*. Also, it is possible to take pointwise measurements of the kernel $K_\sigma(\mathbf{x},\mathbf{y})$ of the DtN map whenever the kernel is continuous away from the diagonal $\mathbf{x}=\mathbf{y}$, which occurs at least for C^2 conductivities (see [62]).

It is clear from Definition 3.2 that to show the total negativity of the circular minors of $\mathcal{M}_n(\Lambda_\sigma^{DtN})$, it suffices to show that the kernel of the DtN map satisfies **(P2)**. The main result in [62] is that the kernel K_σ of the DtN map for a conductivity $\sigma\in C^2(\Omega)$ satisfies **(P1)**. We have extended this result to more general measurements by showing the equivalence between **(P1)** and **(P2)**, which is stated in the next theorem.

Theorem 3.11. *Let $K:\partial\Omega\times\partial\Omega\to\mathbb{R}$ be some kernel continuous away from the diagonal, and such that $\lim_{\mathbf{y}\to\mathbf{x}} K(\mathbf{x},\mathbf{y})=-\infty$. Then **(P1)** holds for K if and only if **(P2)** holds for K.*

In order to prove Theorem 3.11, let us first show an intermediary Lemma involving the weaker properties **(WP1)** and **(WP2)**, which are obtained by replacing the strict inequalities in the Definitions 3.9 and 3.10 by non-strict inequalities. Note that the assumptions on K in the following lemma are relaxed compared to those of Theorem 3.11: the singularity of the kernel on the diagonal is not required.

Lemma 3.12. *Let $K:\partial\Omega\times\partial\Omega\to\mathbb{R}$ be some continuous kernel away from the diagonal. Then **(WP1)** holds for K if and only if **(WP2)** holds for K.*

Proof. We use the techniques of Lemma 6.1 in [62]. Let K be a kernel satisfying the assumptions of the theorem. Let us start by assuming **(WP1)** holds. If $(X_1, \ldots, X_n, Y_1, \ldots, Y_n)$ is some circular pair of functions, using the combinatorial definition of the determinant, and reducing the domain of integration to the support of the functions involved, we may write,

$$\det\left(\left\{-\int_{I_i\times J_j} X_i(\mathbf{x})Y_j(\mathbf{y})K(\mathbf{x},\mathbf{y})d\mathbf{x}d\mathbf{y}\right\}_{i,j=1,\ldots,n}\right)$$
$$=\sum_{\tau\in\Pi(1,\ldots,n)}\operatorname{sgn}(\tau)\prod_{i=1}^{n}\left(-\int_{I_i\times J_{\tau(i)}} X_i(\mathbf{x}_i)Y_{\tau(i)}(\mathbf{y}_{\tau(i)})K(\mathbf{x}_i,\mathbf{y}_{\tau(i)})d\mathbf{x}_i d\mathbf{y}_{\tau(i)}\right), \quad (3.11)$$

where $\Pi(1,\ldots,n)$ is the set of all $n!$ permutations of $1,\ldots,n$, and the sign of a permutation τ is defined by,

$$\operatorname{sgn}(\tau)=\begin{cases}+1 & \text{if } \tau \text{ is equivalent to an even number of transpositions,}\\ -1 & \text{if } \tau \text{ is equivalent to an odd number of transpositions.}\end{cases}$$

Now, we rewrite the product of integrals as one single integral, which with some reordering yields,

$$\sum_{\tau\in\Pi(1,\ldots,n)}\operatorname{sgn}(\tau)\int_{I_1\times J_1}\cdots\int_{I_n\times J_n}\left(\prod_{i=1}^{n}-K(\mathbf{x}_i,\mathbf{y}_{\tau(i)})\right)\left(\prod_{i=1}^{n}X_i(\mathbf{x}_i)Y_i(\mathbf{y}_i)\right)d\mathbf{x}_1 d\mathbf{y}_1\cdots d\mathbf{x}_n d\mathbf{y}_n.$$

Whereby identifying a determinant we get,

$$\det\left(\left\{-\int_{I_i\times J_j} X_i(\mathbf{x})Y_j(\mathbf{y})K(\mathbf{x},\mathbf{y})d\mathbf{x}d\mathbf{y}\right\}_{i,j=1,\dots,n}\right)$$
$$=\int_{I_1\times J_1}\cdots\int_{I_n\times J_n}\det(\{-K(\mathbf{x}_i,\mathbf{y}_j)\}_{i,j=1,\dots,n})\left(\prod_{i=1}^{n}X_i(\mathbf{x}_i)Y_i(\mathbf{y}_i)\right)d\mathbf{x}_1d\mathbf{y}_1\cdots d\mathbf{x}_nd\mathbf{y}_n. \tag{3.12}$$

Now $(\mathbf{x}_1,\dots,\mathbf{x}_n;\mathbf{y}_1,\dots,\mathbf{y}_n)$ is a circular pair of points because $\mathbf{x}_i\in I_i$ and $\mathbf{y}_i\in J_i$ and $I_1,\dots,I_n,\ J_n,\dots,J_1$ do not intersect and are consecutive when laid on a circle. Since K satisfies **(WP1)**, the determinant in the integrand is nonnegative, and so is the integrand itself, which proves **(WP1)** $\Rightarrow$ **(WP2)**.

To prove **(WP2)** $\Rightarrow$ **(WP1)**, construct a sequence of circular pairs of functions $(X_1^{(p)},\dots,X_n^{(p)};\ Y_1^{(p)},\dots,Y_n^{(p)})$ such that for $i,j=1,\cdots,n$, we have

$$\lim_{p\to\infty}\int_{\partial\Omega\times\partial\Omega}X_i^{(p)}(\mathbf{x})Y_j^{(p)}(\mathbf{y})K(\mathbf{x},\mathbf{y})d\mathbf{x}d\mathbf{y}=K(\mathbf{x}_i,\mathbf{y}_j).$$

Then **(WP1)** follows from continuity of the determinant. □

We can now write a proof of Theorem 3.11, which essentially follows from [62],

Proof of Theorem 3.11. Using (3.12) and strict inequalities in the argument for **(WP1)** $\Rightarrow$ **(WP2)** in Lemma 3.12, it follows that **(P1)** $\Rightarrow$ **(P2)**. Now assume **(P2)** holds for K, therefore **(WP2)** and by Lemma 3.12 also **(WP1)** hold for K. Moreover Ingerman and Morrow [62, §4], proved that provided K is a kernel continuous away from the diagonal and singular on the diagonal, we have **(WP1)** $\Rightarrow$ **(P1)**, which completes this proof. □

3.2.4 The resistor finding problem

For recovering the resistors in a critical R-net, we choose the algorithm introduced by Curtis et al. [34], which is basically a layer peeling algorithm: it determines the resistors layer by layer from the boundary to the interior of the network by mathematically peeling each of the layers.

We prefer the Curtis et al. [34] algorithm over other algorithms such as least squares minimization, because it is non-iterative, and we do not have to worry about local minima. Other advantages of the Curtis et al. [34] algorithm are that it is fast, simple to implement and reasonably stable when recovering small networks.

However, recovering the resistors in the network amounts to solving a Cauchy problem for the potential and is therefore an ill-posed (discrete) inverse problem in itself. The ill-posedness gets worse as the size of the network to be recovered increases: we have typically observed a loss of precision in the resistors of a factor of 10 by going from one layer to the next. In the presence of noise, we regularize the problem by keeping the network small, as we shall see next.

3.2.5 The resistor network for noisy measurements

We regularize the resistor finding problem by restricting the size of the network with a criterion based on the noise level of the measurements. To achieve this, we use the distinguishability ideas of Isaacson [65] (see also Section 1.2). The main idea is to determine which frequencies of the data carry information about the conductivity by looking at the singular value decomposition of the difference between the measured Neumann-to-Dirichlet (NtD) map and the NtD map for a reference conductivity σ^0. This criterion has also been implemented in [28].

The reduction in size per se is achieved by lumping measurements made on N

"electrodes" so as to obtain the DtN map of a resistor network with $n < N$ boundary nodes. The lumping can be seen as a low pass filtering of the data, because it essentially discards the higher frequencies in the data, which do not contain any valuable information about the conductivity. More details on the implementation of the lumping are available in Appendix B.4.

It is easier to carry the analysis of how much information is contained in the data with the NtD map. So far we have have worked with the DtN map, but we can always process the data to approximate NtD measurements as explained in Appendix B.2.

To determine the size of the R-net (i.e. discretization grid), let us look at excitations that are capable of distinguishing the unknown conductivity σ from a reference one σ^0, with noisy measurements. To this end, let us first consider the "voltage difference map" given by $\Lambda_\sigma^{NtD} - \Lambda_{\sigma^0}^{NtD}$. Let s_k be its singular values, and $I_k(\mathbf{x})$ its corresponding singular functions. Note that we need not distinguish between left and right singular functions because they are up to a sign the same for the NtD map, because it is symmetric.

It can be shown [54, AIII] that the singular values s_k of the voltage difference map decay exponentially fast, at least if σ and σ^0 agree in a neighborhood of the boundary. For example if σ and σ^0 are equal to one for $r \in [\alpha, 1]$, then the singular values are $\mathcal{O}\left(\alpha^{2k}/k\right)$. For a concrete example see Figure 3.8a.

Following Isaacson [65], in the presence of noise, we expect only a few singular values of the voltage difference map are above the noise level δ. This means that of all possible probing currents with unit $L^2(\partial\Omega)$ norm, only those that belong to the span of the singular functions I_k corresponding to singular values above the noise level ($s_k > \delta$) give voltage differences that are distinguishable from the measurements:

$$\left\|\Lambda_\sigma^{NtD} I - \Lambda_{\sigma^0}^{NtD} I\right\|_{L^2} > \delta, \quad \text{for all } I \in \operatorname{span}\{I_1, \ldots, I_{n_\delta}\}, \text{ with } \|I\|_{L^2} = 1,$$

and where n_δ is the largest integer k such that $s_k > \delta$. For all practical purposes, probing with the other singular functions $I_k(\mathbf{x})$, for $k > n_\delta$, does not add useful information. Cherkaeva and Tripp [28] sought the conductivity in span $\{\nabla u_i \cdot \nabla u_j\}_{i,j=1}^{n_\delta}$, where the u_j are the potentials that the leading n_δ singular functions I_j produce when the conductivity is σ^0. In our method, we use a similar idea to determine the size of our discretization of the conductivity (the resistor network).

The first n_δ singular modes of the voltage difference map are smooth (see for example Figure 3.8b), so they can be decomposed reasonably well in the first $\lfloor n_\delta/2 \rfloor$ harmonics $\{\cos(k\theta), \sin(k\theta)\}_{k=1}^{\lfloor n_\delta/2 \rfloor}$, where $\theta \in [0, 2\pi]$ is the angle. Actually, when the conductivity is layered (i.e. $\sigma(r, \theta) \equiv \sigma(r)$), the singular functions are precisely the harmonics. Therefore we choose a circular resistor network with n_δ boundary nodes.[6]

It follows from the discussion in Section 3.2.3, that when n_δ is odd, a recoverable network with topology $C(l, n_\delta)$, must have $l = (n_\delta - 1)/2$ layers. When n_δ is even, we take $n_\delta + 1$ instead. So the size of the network, or in other words, the number of parameters we solve for is determined by the noise level δ. Network sizes recommended by this method for typical noise levels are reported in Table 3.1.

Remark 3.13. As we explained in Section 3.1.2 and we discuss in detail next, in Section 3.3, the resistors of the small networks with topology $C(l_\delta, 2l_\delta + 1)$, with $l_\delta = \lfloor n_\delta/2 \rfloor$, are averages of the conductivity on a coarse grid $\mathcal{G}(l_\delta, 2l_\delta + 1)$. Therefore the level of noise limits naturally the resolution of the image.

Remark 3.14. We do not address the problem of estimating the level of noise in the measurements. For this purpose, it is possible to get a rough estimate of the noise level by determining where the singular values of the voltage difference map stop decaying exponentially.

[6] We show in Appendix B.1 that such analysis fails for DtN data, and we give some ideas to remedy this situation.

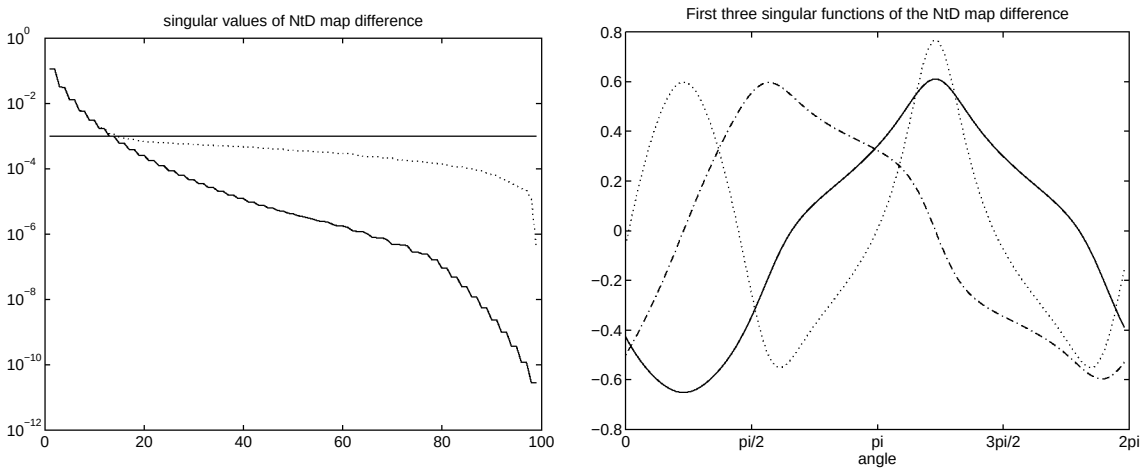

(a: Singular values) (b: Leading singular vectors)

Figure 3.8: (a) Singular values of the NtD difference map for conductivities `sigX` (defined in Appendix C) and $\sigma^0 \equiv 1$. We include singular values for the true (solid line) and noisy (dotted line) difference maps. The noise level $\delta = 10^{-3}$ is also displayed. (b) The three leading singular vectors, normalized such that $\|I_k\|_{L^2} = 1$. The leading singular function I_1 is in solid line, I_2 in dashed line and I_3 in dotted line.

3.3 From resistor networks to conductivity averages

Previously in Section 3.2 we established that a resistor network reduced model of the PDE problem can be found uniquely from measurements of the DtN map. Now we explain how averages of the conductivity can be estimated from the resistors in the network.

Given the discretization discussed in Section 3.1, the resistors that match the measurements can be interpreted as averages of some conductivity over the grid cells of the discretization. Regardless of the grid choice, such a conductivity would match the measurements by design. The key is to find a grid for which the averages we recover are close to the averages of the unknown conductivity.

We show in Section 3.3.1 how to find the grid for which the recovered averages match those of a known, layered conductivity (that is $\sigma(r, \theta) \equiv \sigma(r)$). We conjecture that the grid depends weakly on the conductivity, meaning that the averages obtained

by interpreting the resistors that fit measurements of the DtN map, on the grid for a layered (reference) conductivity, are close to the averages of the unknown conductivity on the same grid.

Our conjecture of weak dependence of the grid on the conductivity is in part justified by our numerical results and by showing in Section 3.3.3 that a necessary condition for convergence of our inversion scheme is that the grids used for inversion are asymptotically close to the precomputed grids for a reference conductivity.

3.3.1 Optimal grid construction for layered conductivities

Let us assume the layered conductivity $\sigma(r)$ is given. Let us take measurements of the DtN map $\mathcal{M}_n(\Lambda_\sigma^{DtN})$ (see Definition 3.2), with n functions $\phi_i \equiv \phi(\mathbf{x}-\mathbf{x}_i)$, where the $\mathbf{x}_i$ are n equally spaced nodes of $\partial\Omega$. If we further assume n is odd, the main result of Section 3.2 is that there is a unique resistor network of type $C(l=(n-1)/2,n)$ with $\mathcal{M}_n(\Lambda_\sigma^{DtN})$ as its DtN map. By the symmetries of the layered problem, the resistor network has to be layered,[7] meaning that the resistors $R_{i,j}, \widehat{R}_{i,j+1/2}$ do not depend on the angular parameter j. Call $R_i, \widehat{R}_i$ the resistors for the layered case and recall from equations (3.2) and (3.3) that they are given by,

$$\begin{aligned} R_i &= \frac{1}{h_\theta}\int_{r_{i+1}}^{r_i}\frac{dt}{t\sigma(t)} && \text{for } i=1,\dots,\lceil l/2\rceil, \\ \widehat{R}_i &= h_\theta\left(\int_{\widehat{r}_i}^{\widehat{r}_{i-1}} dt\frac{\sigma(t)}{t}\right)^{-1}, && \text{for } i=2,\dots,\lfloor l/2\rfloor+1, \end{aligned} \tag{3.13}$$

where $l=(n-1)/2$ so that the network is uniquely determined by the measurements.

Now, since the conductivity and the resistors are both known, the grid can be found from (3.13) with e.g. a nonlinear equation solver. The same idea is used to

[7] Note that Ingerman [64] arrived to the same conclusion for layered conductivities by transforming to an inverse spectral problem for beaded strings.

obtain the so-called "optimal grids" for a one dimensional inverse spectral problem in [63, 19, 20] (see also Section 2.2.3). The term optimal refers here to the fact that, by design, the discrete DtN map matches exactly the measurements $\mathcal{M}_n(\Lambda_\sigma^{DtN})$.

In our numerical reconstructions, we use the optimal grid for $\sigma(r) = 1$. This is given by,

$$\begin{aligned} r_1 &= \widehat{r}_1 = 1, \\ r_{k+1} &= \exp\left(-(R_1 + \cdots + R_k)/h_\theta\right), && \text{for } k = 1, \ldots, \lceil l/2 \rceil, \\ \widehat{r}_k &= \exp\left(-h_\theta \left((\widehat{R}_2)^{-1} + \cdots + (\widehat{R}_k)^{-1}\right)\right), && \text{for } k = 2, \ldots, \lfloor l/2 \rfloor + 1. \end{aligned} \tag{3.14}$$

Computed grids for $l = 5$ and 7 appear in Figure 3.9. To define the measurement operator $\mathcal{M}_n$, we used for ϕ a smoothed box function and we computed the integrals in (3.8) numerically with 200 uniformly spaced points on the boundary and the analytical kernel of the DtN map. Note that in our calculations, the grid does not appear to depend strongly on the choice of ϕ, so unless specified, we use the smoothed box functions specified in Appendix C.2 throughout this Thesis.

Also, remark that for the innermost (closest to the origin) layer of resistors to appear connected in the grid one would need $r_{\lceil l/2 \rceil + 1} = 0$, however in the grids we obtain $r_{\lceil l/2 \rceil + 1} > 0$, which could be thought of as a truncation of the domain close to the origin. Of course, in the resistor network the innermost branches are all electrically connected. Numerically we also observed that as $l \to \infty$, we have $r_{\lceil l/2 \rceil + 1} \to 0$.

To have a proper finite volumes discretization, the primary and dual grids need to interleave. Although we have not rigorously established this property, we have verified it numerically at least for $n \leq 31$. We conjecture that in exact arithmetic, proper finite volumes discretizations can be obtained through this method for larger n, however our reconstructions are coarse (by the very nature of the EIT problem

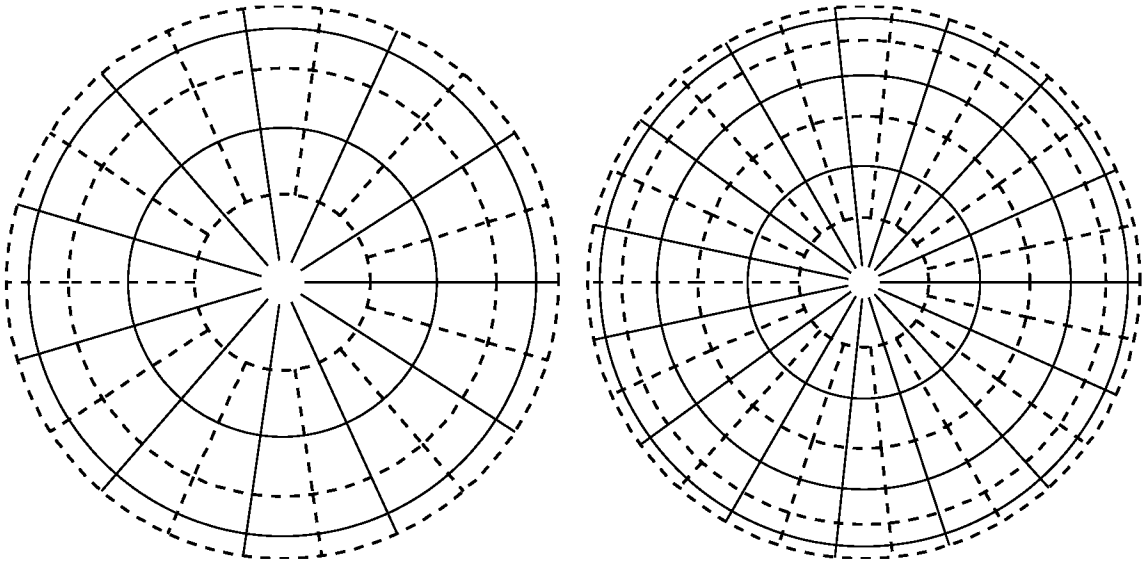

$n = 11$, R-net of type $C(5, 11)$ $n = 15$, R-net of type $C(7, 15)$

Figure 3.9: The finite volume discretization for $\sigma \equiv 1$. The primary grids (R-net) are in solid line and the dual grids (control volumes) are in dotted line.

and especially in the presence of noise, see Section 3.2.5) so proving such a result is not necessary for our algorithm to work.

3.3.2 Reconstructing averages of the conductivity

Given measurements $\mathcal{M}_n(\Lambda_\sigma^{DtN})$ of the DtN map for an unknown conductivity σ, we propose a reconstruction method based on an interpretation of the resistors in the R-net reduced model (see Section 3.2) of the EIT equation (1.1) as averages over grid cells of σ. Our method is an extension to two dimensions of the optimal grid inversion procedure of Borcea, Druskin and Knizhnerman [19, 20]. We present numerical results to validate our approach. Note that this is a computationally cheap procedure and that we improve upon it later in Section 3.4.

The reconstruction algorithm

Call the homogeneous conductivity $\sigma^0 \equiv 1$. Following Section 3.3.1, we construct the optimal grid for σ^0. Recall that the discretization is designed to give an exact match for the measurements $\mathcal{M}_n(\Lambda_{\sigma^0}^{DtN})$. If we assume that the grid depends weakly on the conductivity (we explain the reasons for this assumption in Section 3.3.3), we may approximate the averaging relations (3.2) and (3.3) by writing them on the grid for the reference conductivity σ^0,

$$\begin{aligned} R_{i,j} &\approx \int_{r_{i+1}^0}^{r_i^0} dt \left(t \int_{(j-1/2)h_\theta}^{(j+1/2)h_\theta} \sigma(t,\theta) d\theta \right)^{-1} &&= \frac{1}{\widehat{\sigma}_{i,j}} R_i^0, \\ \widehat{R}_{i,j+1/2} &\approx \int_{jh_\theta}^{(j+1)h_\theta} d\alpha \left(\int_{\widehat{r}_i^0}^{\widehat{r}_{i-1}^0} dt \frac{\sigma(t,\alpha)}{t} \right)^{-1} &&= \frac{1}{\sigma_{i,j+1/2}} \widehat{R}_i^0, \end{aligned} \tag{3.15}$$

where the R_i^0, $\widehat{R}_i^0$ are the resistors for the homogeneous conductivity σ^0 and the r_i^0, $\widehat{r}_i^0$ are the radii of the grid for σ^0. Here $j = 1, \ldots, n$ and the ranges for the index i are taken as in (3.2) and (3.3). Thus from the resistors it is elementary to estimate the averages $\sigma_{i,j+1/2}$, $\widehat{\sigma}_{i,j}$ of the conductivity, as appears in the following Algorithm.

Algorithm 3.15. Inputs: Measurements $\mathcal{M}_n(\Lambda_\sigma^{DtN})$ (Definition 3.2), for n odd. **Outputs:** Estimates of the averages $\sigma_{i,j+1/2}, \widehat{\sigma}_{i,j}$.

i. Calculate the resistors $R_i^0, \widehat{R}_i^0$ and grid for $\sigma^0 = 1$.

ii. Find the resistors $R_{i,j}, \widehat{R}_{i,j+1/2}$ that match the measurements $\mathcal{M}_n(\Lambda_\sigma^{DtN})$.

iii. Obtain averages of the conductivity over grid cells from (3.15) as follows,

$$\widehat{\sigma}_{i,j} \approx \frac{R_i^0}{R_{i,j}}, \quad \sigma_{i,j+1/2} \approx \frac{\widehat{R}_i^0}{\widehat{R}_{i,j+1/2}}.$$

Generally one is interested in recovering the conductivity rather than its averages. We remedy this in Section 3.4, where we also introduce a priori information about the conductivity σ.

Numerical results

We present results from an implementation of Algorithm 3.15 on synthetic data sets for the conductivities in Figure 3.10, that we define more precisely in Appendix C. To verify that we are reconstructing averages of the conductivity, we compare the following:

- Averages $\sigma_{i,j+1/2}, \widehat{\sigma}_{i,j}$ reconstructed from the measurements $\mathcal{M}_n(\Lambda_\sigma^{DtN})$ using Algorithm 3.15.

- Averages of the conductivity σ, computed on the grid for the reference conductivity σ^0 by numerical integration.

Reconstructions for noiseless measurements are shown in Figures 3.11 and 3.12. In our numerical experiments, we discretize the PDE on a fine uniform grid using finite volumes (as in Section 3.1). In that way, we obtain approximate pointwise values of the kernel of the DtN map at 100 equally spaced points of $\partial\Omega$, which are used to evaluate the integrals in equation (3.8) numerically and thus approximate the measurements $\mathcal{M}_n(\Lambda_\sigma^{DtN})$. Actually, the DtN map of a resistor network is the Schur complement of the Kirchhoff matrix with respect to the interior variables (see e.g. [36]). The Schur complement of a matrix with respect to a set of indices is the matrix that remains after doing a Gaussian elimination of the complementary set of indices.

In order to visualize the averages $\sigma_{i,j+1/2}, \widehat{\sigma}_{i,j}$, we interpret them as being pointwise values at the intersection between primary and dual grids, i.e. respectively $(r_i, (j + 1/2)h_\theta)$ and $(\widehat{r}_i, jh_\theta)$. Such pointwise values are then interpolated linearly by means

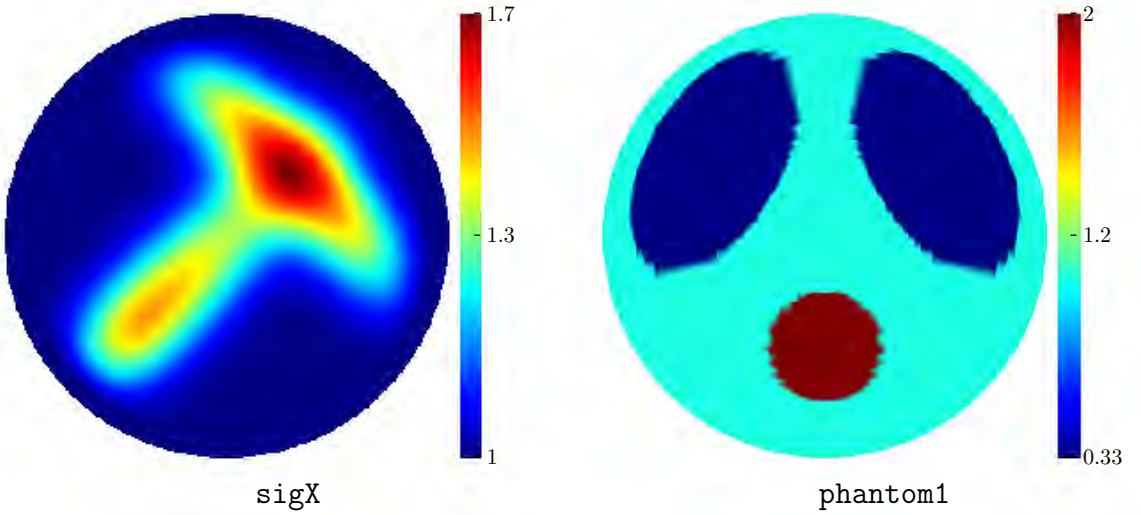

Figure 3.10: The conductivities used in the two dimensional numerics. See Appendix C for a precise definition.

of a Delaunay triangulation. Outside the convex hull of the evaluation points, we extrapolate linearly to get values for all $\mathbf{x} \in \Omega$. Finally, we plot the grids of the finite volumes discretization on top, with the convention that dotted lines represent the dual grid (control volumes) and solid lines the primary grid (R-net).

To simulate noise in our measurements we added a multiplicative Gaussian noise with zero average to the approximation of the kernel of the DtN map. In Table 3.1 we give the size of the networks to recover that are predicted by the SVD analysis of Section 3.2.5, for different noise levels. This heuristic gives only approximate network sizes, that do not always give positive resistors with the resistor finding algorithm we used (see Section 3.2.4).

Instead of using the method of Section 3.2.5, we preferred to find empirically the largest network that gives positive resistors for several realizations of the noise. We believe the discrepancies between the empirical network sizes and those in Table 3.1 are due to the instability of the resistor finding algorithm of Section 3.2.4. The reconstructions are shown in Figures 3.14 and 3.13.

	0.1%	0.5%	1%	5%
`sigX`	$C(7,15)$	$C(4,9)$	$C(3,7)$	$C(1,3)$
`phantom1`	$C(12,25)$	$C(8,17)$	$C(7,15)$	$C(3,7)$

Table 3.1: Network sizes for inversion found by the method discussed in Section 3.2.5 for certain noise levels and conductivities (see Appendix C).

3.3.3 Does the grid depend weakly on the conductivity?

In Algorithm 3.15 we made the assumption that the grid we use for inversion is essentially independent of the conductivity. By weak dependence we mean that given a compact set $\mathcal{S}$ of sufficiently similar conductivities, Algorithm 3.15 on the grid $r_i^0, \widehat{r}_i^0$ for a reference conductivity $\sigma^0 \in \mathcal{S}$ gives reconstructed averages that are close to the true ones. We have several reasons to believe that the grid depends weakly on the conductivity:

- All the smooth conductivities we tried in our numerical experiments are sufficiently similar to the reference homogeneous conductivity $\sigma^0 \equiv 1$, since the reconstructed averages are close to the true averages.

- For the 1D inverse spectral problem of Chapter 2, the weak dependence was proved rigorously by Borcea et al. [20]. Their result is asymptotic as the number of measurements increases.

To rigorously prove weak dependence of the grid on the conductivity we need to show that a necessary and sufficient condition for the convergence of Algorithm 3.15 is that the grid used for inversion is asymptotically close (as the number of measurements increases) to the grid for the reference homogeneous conductivity. So far, the only result we can prove is necessity. The remaining of this Section is devoted to state and prove our necessity result Proposition 3.16.

Let $r_i, \widehat{r}_i$ be a grid used in Algorithm 3.15, not necessarily the same as the grid $r_i^0, \widehat{r}_i^0$ for the homogeneous medium. In Proposition 3.16 we consider the following

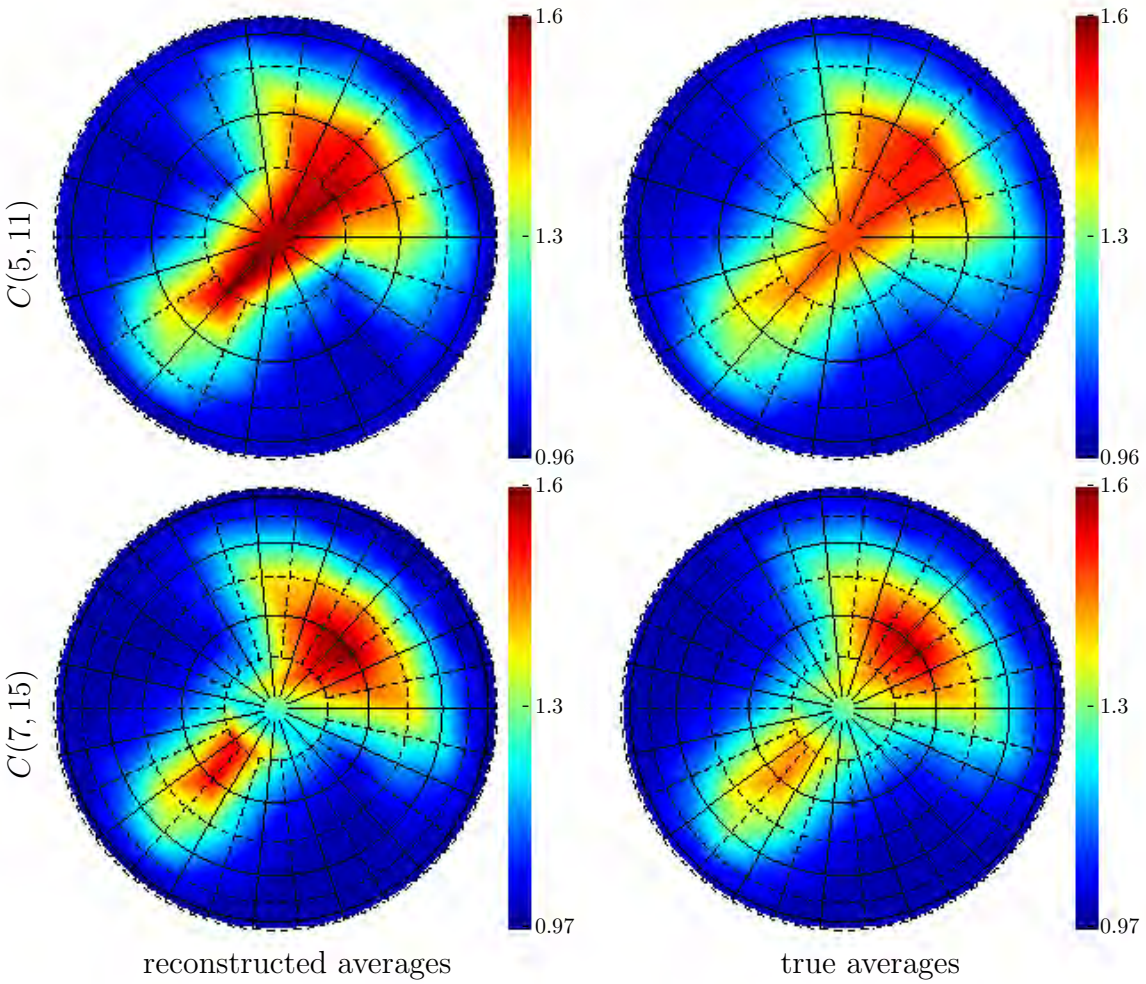

Figure 3.11: Left: reconstructions of local averages of the smooth conductivity `sigX` (defined in Appendix C) using Algorithm 3.15. Right: true averages of `sigX` on the grid for the reference conductivity $\sigma^0 \equiv 1$.

convergence notion. Given a compact set $\mathcal{S}$ of conductivities, the reconstructed conductivity of Algorithm 3.15 converges to the true one if,

$$\max_{\sigma\in\mathcal{S}} \max_{j\in\{1,\dots,n\}} \frac{1}{h_\theta} \left| \int_{(j-\frac{1}{2})h_\theta}^{(j+\frac{1}{2})h_\theta} \int_{r_{i+1}}^{1} \frac{dtd\theta}{t\sigma(t,\theta)} - \sum_{p=1}^{i} R_{p,j} \right| < \epsilon_l, \quad \text{for } i = 1,\dots,\lceil l/2 \rceil\,.$$
$$\max_{\sigma\in\mathcal{S}} \max_{j\in\{1,\dots,n\}} \frac{1}{h_\theta} \left| \int_{jh_\theta}^{(j+1)h_\theta} \int_{\widehat{r}_i}^{1} \sigma(t,\theta) \frac{dtd\theta}{t} - \sum_{p=2}^{i} \widehat{R}^{-1}_{p,j+\frac{1}{2}} \right| < \epsilon_l, \quad \text{for } i = 2,\dots,\lfloor l/2 \rfloor + 1, \tag{3.16}$$

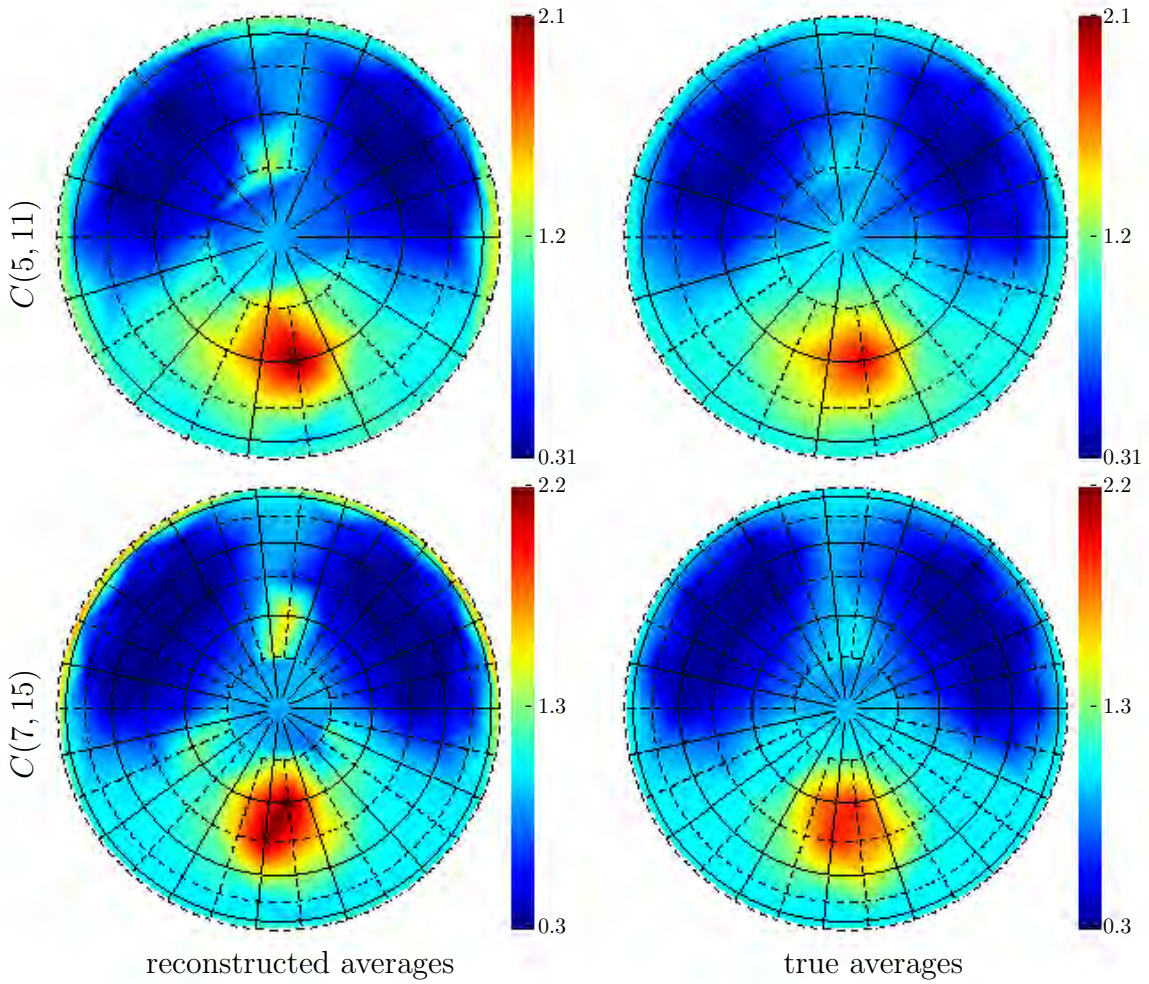

Figure 3.12: Left: reconstructions of local averages of the piecewise constant conductivity `phantom1` (defined in Appendix C) using Algorithm 3.15. Right: true averages of `phantom1` on the grid for the reference conductivity $\sigma^0 \equiv 1$.

where as the number of layers $l \to \infty$, we have $\epsilon_l > 0$ and $\epsilon_l \to 0$. Having $l \to \infty$ is equivalent to having the number of measurements $n \to \infty$, since to get uniqueness of the R-net reduced model (Corollary 3.8), we require that $n = 2l + 1$.

So far we have not defined a reconstructed conductivity. The only information from the unknown σ we can expect from Algorithm 3.15 are averages and this is precisely the only information about the reconstructed conductivity that appears in (3.16), through the resistor sums. This weak convergence notion was essentially

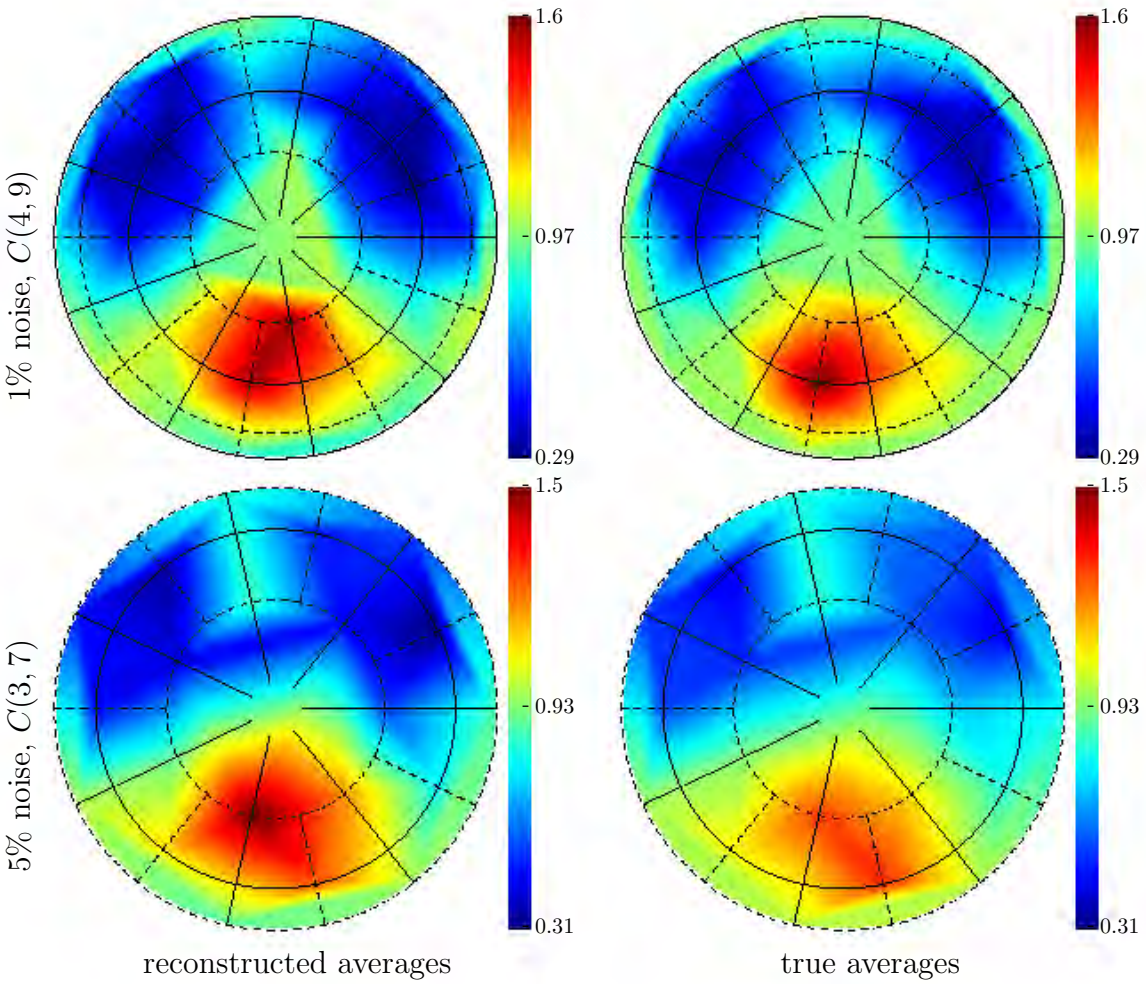

Figure 3.13: Left: reconstructions of local averages of the piecewise constant conductivity `phantom1` (defined in Appendix C) using Algorithm 3.15 with noisy data. Right: true averages of `phantom1` on the grid for the reference conductivity $\sigma^0 \equiv 1$.

introduced in [19, §4] for the 1D inverse spectral problem of Chapter 2.

Proposition 3.16. *Let $\mathcal{S}$ be a compact set of conductivities containing $\sigma^0 \equiv 1$. Let $R_{i,j}, \widehat{R}_{i,j+\frac{1}{2}}$ be the resistors obtained from measurements $\mathcal{M}_n(\Lambda_\sigma^{DtN})$. For any choice*

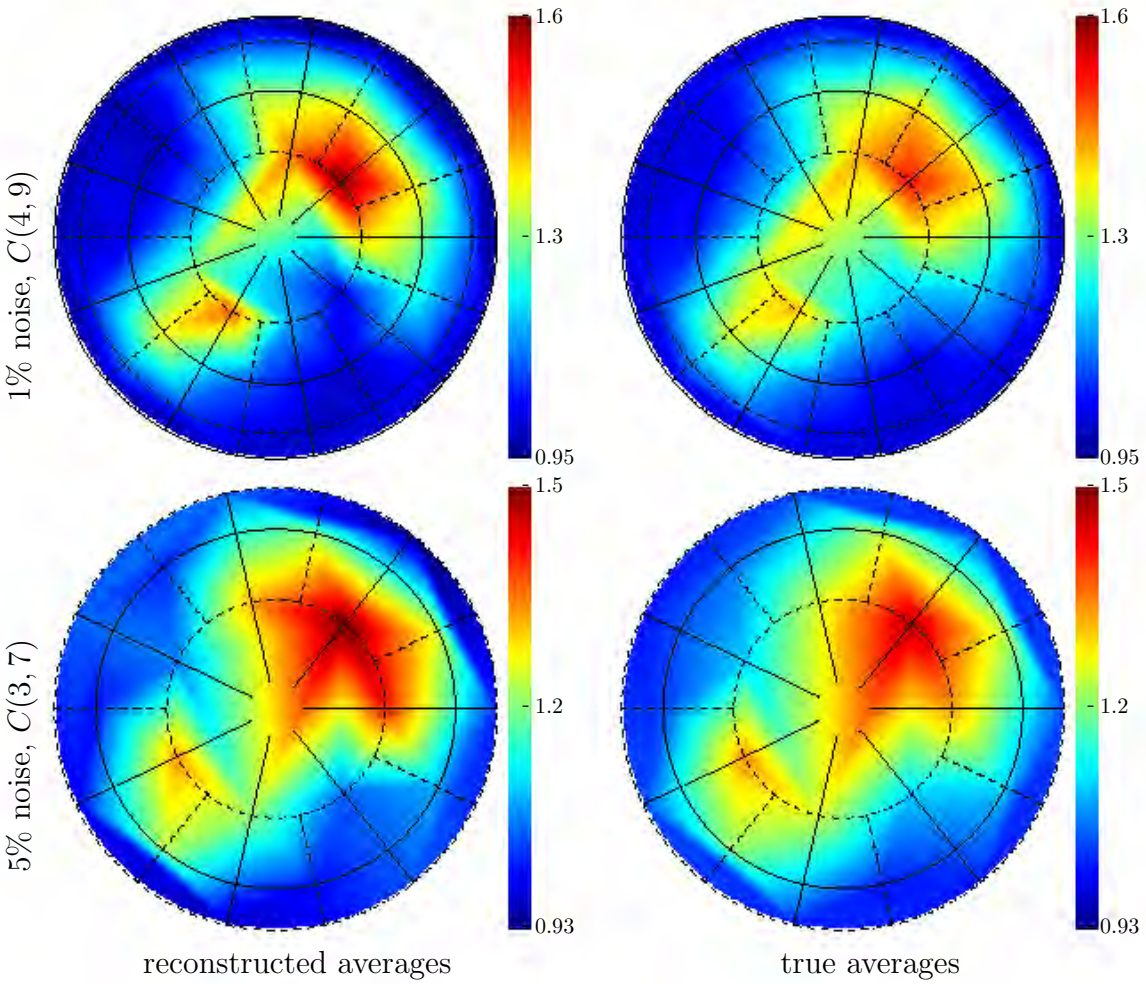

Figure 3.14: Left: reconstructions of local averages of the smooth conductivity `sigX` (defined in Appendix C) using Algorithm 3.15 with noisy data. Right: true averages of `sigX` on the grid for the reference conductivity $\sigma^0 \equiv 1$.

of positive radii $r_i, \widehat{r}_i$ *we have,*

$$\max_{\sigma\in\mathcal{S}} \max_{j\in\{1,\dots,n\}} \frac{1}{h_\theta} \left| \int_{(j-\frac{1}{2})h_\theta}^{(j+\frac{1}{2})h_\theta} \int_{r_{i+1}}^{1} \frac{dtd\theta}{t\sigma(t,\theta)} - \sum_{p=1}^{i} R_{p,j} \right| \geq \left| \ln(r_{i+1}) - \ln(r_{i+1}^0) \right|,$$
$$\max_{\sigma\in\mathcal{S}} \max_{j\in\{1,\dots,n\}} \frac{1}{h_\theta} \left| \int_{jh_\theta}^{(j+1)h_\theta} \int_{\widehat{r}_i}^{1} \frac{\sigma(t,\theta)}{t} dtd\theta - \sum_{p=2}^{i} \widehat{R}^{-1}_{p,j+\frac{1}{2}} \right| \geq \left| \ln(\widehat{r}_i) - \ln(\widehat{r}_i^0) \right|. \tag{3.17}$$

Proof. Observe that $\sigma^0 \equiv 1$ belongs to $\mathcal{S}$. Hence the left hand side of the first

inequality in (3.17) is larger than,

$$\frac{1}{h_\theta}\left|\int_{(j-\frac{1}{2})h_\theta}^{(j+\frac{1}{2})h_\theta}\int_{r_{i+1}}^{1}\frac{dtd\theta}{t}-\sum_{p=1}^{i}R_p^0\right|=\frac{1}{h_\theta}\left|\int_{(j-\frac{1}{2})h_\theta}^{(j+\frac{1}{2})h_\theta}\int_{r_{i+1}}^{r_{i+1}^0}\frac{dtd\theta}{t}\right|=\left|\ln(r_{i+1})-\ln(r_{i+1}^0)\right|.$$

Similarly, the left hand side of the second inequality in (3.17) is larger than,

$$\frac{1}{h_\theta}\left|\int_{jh_\theta}^{(j+1)h_\theta}\int_{\widehat{r}_i}^{1}\frac{dtd\theta}{t}-\sum_{p=2}^{i}\frac{1}{\widehat{R}_p^0}\right|=\frac{1}{h_\theta}\left|\int_{jh_\theta}^{(j+1)h_\theta}\int_{\widehat{r}_i}^{\widehat{r}_i^0}\frac{dtd\theta}{t}\right|=\left|\ln(\widehat{r}_i)-\ln(\widehat{r}_i^0)\right|. \qquad \square$$

Owing to Proposition 3.16, it follows that convergence in the sense (3.16) implies that the radii of the grid must be asymptotically close to the homogeneous grid, as the number of measurements $n \to \infty$. Here, the convergence of the radii is measured with the metric defined on $(0, 1]$ by $|\ln(a/b)|$. Finally, we note that Proposition 3.16 is modelled after [19, Proposition 4].

3.4 A Newton-type iterative algorithm for the inverse problem

We introduce in this section an iterative Gauss-Newton procedure that takes advantage of the R-net reduced model of Section 3.2 in two ways. First, the reconstruction obtained in Section 3.3.2 is used as an initial guess for the iterations. Then instead of minimizing the misfit in the DtN data, as would be done in traditional Output Least Squares, we minimize the *misfit in the reconstructions given by Algorithm 3.15*. This can be done efficiently because the latter algorithm is computationally inexpensive. In doing so, we hope to precondition the EIT problem by solving an inexpensive discrete problem. Moreover, the iterative procedure converges to a conductivity that basically has the same averages as those found by Algorithm 3.15 and therefore fits the data automatically.

Once the data fitting is done, we introduce a priori information in Section 3.4.3 by adding a correction in the orthogonal complement of the sensitivity functions that need to be computed for the Gauss-Newton procedure.

3.4.1 The Gauss-Newton iteration

Let us denote by $\Gamma_n : \mathcal{S} \to \mathbb{R}^{n(n-1)/2}$ the mapping[8] that takes us from the conductivity to the DtN map measurements and then to the averages[9] $\sigma_{i,j+1/2}, \widehat{\sigma}_{i,j}$ given by Algorithm 3.15.

Given measurements $\mathcal{M}_n(\Lambda^{DtN}_{\sigma_{true}})$ of an unknown conductivity σ_{true}, we use the Gauss-Newton method to find a conductivity minimizing,

$$\min_{\sigma\in\mathcal{S}} \frac{1}{2} \left\|\Gamma_n(\sigma) - \Gamma_n(\sigma_{true})\right\|_2^2 . \tag{3.18}$$

To be physically meaningful, the conductivity must remain positive. To enforce this constraint, we make the change of variables $\kappa = \ln(\sigma)$ (sometimes called "geometric programming"). We seek to compare in our cost functional quantities that are as similar as possible to our new variable κ, so we further take the logarithm of Γ_n. Therefore instead of minimizing (3.18), we consider the unconstrained optimization problem,

$$\min_{\kappa} \frac{1}{2} \left\|\widetilde{\Gamma}_n(\kappa) - \widetilde{\Gamma}_n(\kappa_{true})\right\|_2^2 , \tag{3.19}$$

where $\widetilde{\Gamma}_n \equiv \ln \circ \Gamma_n \circ \exp$ and $\kappa_{true} = \ln(\sigma_{true})$.[10] Since Algorithm 3.15 gives reconstructions that are close to the true conductivity, we hope that in some sense, the

[8] Implicitly, we have assumed there is some convention to order the averages as a vector of length $n(n-1)/2$. Recall the size of the network is fixed by the requirement that the reduced R-net model is uniquely recoverable, see Section 3.2.2.

[9] By Algorithm 3.15, the averages are essentially rescalings of the resistors.

[10] Let $\rho_n(\kappa)$ be the mapping that takes from a log-conductivity to the corresponding resistors. Then $\Gamma_n(\kappa) = \rho_n(0)/\rho_n(\kappa)$, where the division is understood componentwise. Thus measuring the misfit in $\widetilde{\Gamma}_n(\kappa)$ is the same as measuring the misfit in the log-resistors.

mapping $\widetilde{\Gamma}_n$ is close to the identity.

We can compute sensitivity functions for the mapping $\widetilde{\Gamma}_n$ with respect to perturbations in the log-conductivity and obtain the formal expansion around some reference log-conductivity κ^0,

$$\widetilde{\Gamma}_n(\kappa) = \widetilde{\Gamma}_n(\kappa^0) + D\widetilde{\Gamma}_n[\kappa^0]\delta\kappa + \cdots, \tag{3.20}$$

where κ is the perturbed log-conductivity, $D\widetilde{\Gamma}_n[\kappa^0]$ is the formal Jacobian of $\widetilde{\Gamma}_n$ at κ^0 and $\delta\kappa = \kappa - \kappa^0$. By a similar argument to the inverse spectral spectral problem (see Section 2.3.3), we expect the sensitivity functions to be weak approximations of characteristic functions of cells. Our computations confirm that the sensitivity functions are reasonably well localized, as appears in Figure 3.15. For the latter computations, the kernel of the DtN map is approximated pointwise on 100 equally spaced points of $\partial\Omega$ and smoothed box functions define the measurement operator.

The Gauss-Newton method applied to (3.19), consists in finding the new iterate $\kappa^{(k+1)}$ from the previous iterate $\kappa^{(k)}$ by

$$\kappa^{(k+1)} = \kappa^{(k)} + \left(D\widetilde{\Gamma}_n[\kappa^{(k)}]\right)^{\dagger}\left(\widetilde{\Gamma}_n(\kappa_{true}) - \widetilde{\Gamma}_n(\kappa^{(k)})\right), \tag{3.21}$$

where $\left(D\widetilde{\Gamma}_n[\kappa^{(k)}]\right)^{\dagger}$ is the pseudo-inverse[11] of $D\widetilde{\Gamma}_n[\kappa^{(k)}]$. This iteration amounts to finding the update $\delta\kappa = \kappa^{(k+1)} - \kappa^{(k)}$ as the minimal L^2 norm solution to the normal equations,

$$D\widetilde{\Gamma}_n^*[\kappa^{(k)}]D\widetilde{\Gamma}_n[\kappa^{(k)}]\delta\kappa = D\widetilde{\Gamma}_n^*[\kappa^{(k)}]\left(\widetilde{\Gamma}_n(\kappa_{true}) - \widetilde{\Gamma}_n(\kappa^{(k)})\right),$$

where $D\widetilde{\Gamma}_n^*[\kappa^{(k)}]$ is the adjoint of $D\widetilde{\Gamma}_n[\kappa^{(k)}]$. Thus in the iteration (3.21) we find the *orthogonal projection* of the update $\delta\kappa = \kappa^{(k+1)} - \kappa^{(k)}$ onto the span of the sensitivity

[11] The pseudo-inverse, also called the Moore-Penrose generalized inverse, can be defined in the context of Hilbert spaces. See e.g. [50, §2].

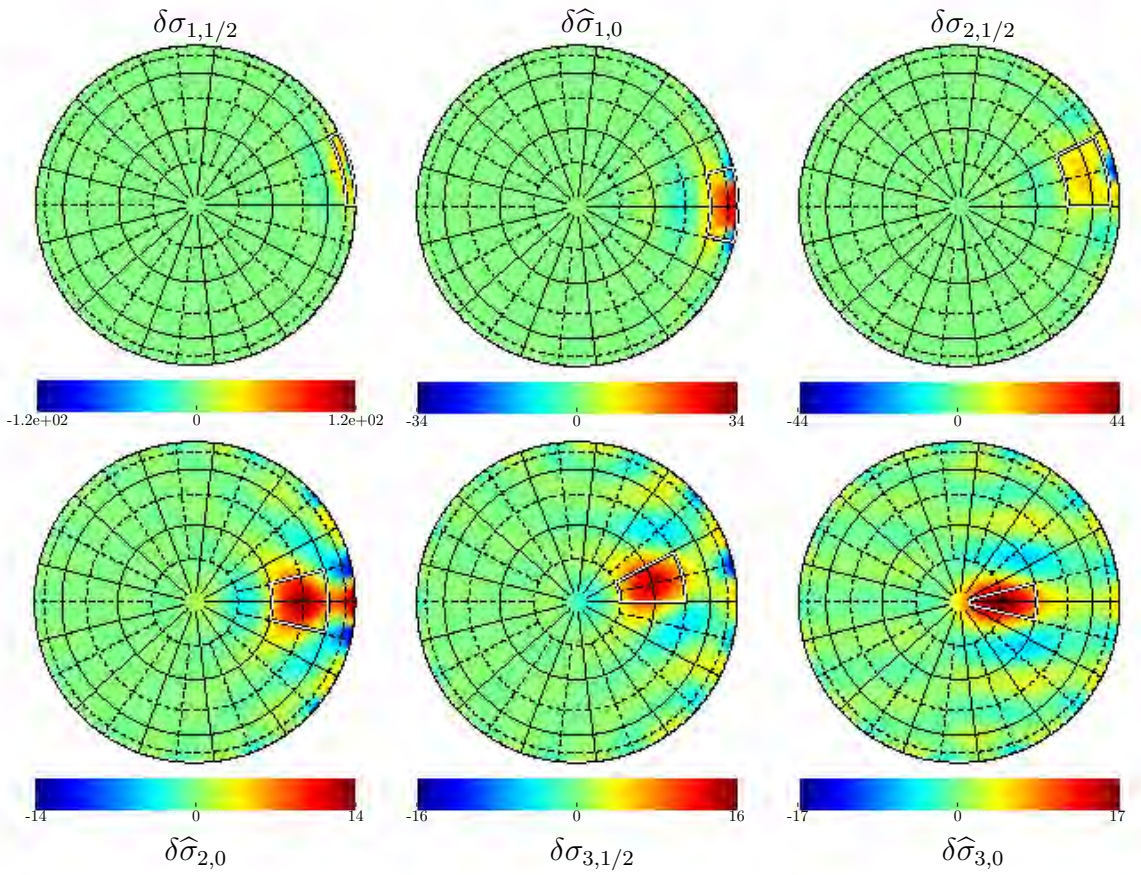

Figure 3.15: Sensitivity functions for the reconstructed averages of Algorithm 3.15 to perturbations in the conductivity. The resistor network here is $C(6, 13)$ and the reference conductivity is $\sigma^0 \equiv 1$. Since there is a $2\pi/13$ rotational symmetry, only sensitivities for $\sigma_{i,1/2}$ and $\widehat{\sigma}_{i,0}$ are plotted. All the sensitivity functions integrate to 1 (numerically). The cells where the corresponding resistor is averaged are highlighted.

functions.

We start the iterations with a linear interpolation of the averages found by Algorithm 3.15, which in most cases is already close to the true conductivity (Section 3.3.2). The choice of a good initial iterate is helpful in the convergence of the Gauss-Newton method, because of the local convergence properties of the method. The complete algorithm is summarized in Algorithm 3.17 and numerical experiments are included and discussed in Section 3.4.2.

Algorithm 3.17. Inputs: Measurements $\mathcal{M}_n(\Lambda^{DtN}_{\sigma_{true}})$ (Definition 3.2) for n odd and

some tolerance ϵ for the misfit. **Outputs:** A reconstructed conductivity σ^*.

1. Compute $\kappa^{(0)} = \ln(\sigma^{(0)})$, where $\sigma^{(0)}$ is a linear interpolation of the averages $\sigma_{i,j+1/2}, \widehat{\sigma}_{i,j}$ obtained by Algorithm 3.15 from the measurements $\mathcal{M}_n(\Lambda^{DtN}_{\sigma_{true}})$.

2. For $k = 0, 1, \ldots$ do,

   (a) $\kappa^{(k+1)} \leftarrow \kappa^{(k)} + \left(D\widetilde{\Gamma}_n[\kappa^{(k)}]\right)^\dagger \left(\widetilde{\Gamma}_n(\kappa_{true}) - \widetilde{\Gamma}_n(\kappa^{(k)})\right)$

   (b) If $\left\|\widetilde{\Gamma}_n(\kappa^{(k+1)}) - \widetilde{\Gamma}_n(\kappa_{true})\right\|_2 < \epsilon$, stop.

3. $\sigma^* \leftarrow \exp(\kappa^{(k+1)})$.

3.4.2 Numerical experiments for the Gauss-Newton algorithm

Implementation of the Gauss-Newton algorithm

In our numerical experiments, n is much smaller than the number of parameters used for κ. Thus the pseudo-inverse in the Gauss-Newton iteration (3.21) can be efficiently applied with the identity,

$$(D\widetilde{\Gamma}_n[\kappa^{(k)}])^\dagger = D\widetilde{\Gamma}_n^*[\kappa^{(k)}] \left(D\widetilde{\Gamma}_n[\kappa^{(k)}] D\widetilde{\Gamma}_n^*[\kappa^{(k)}]\right)^\dagger. \tag{3.22}$$

Furthermore, we observed that for the conductivities we considered, the Jacobian $D\widetilde{\Gamma}_n[\kappa^{(k)}]$ is full-rank to working precision and well-conditioned, so that the relatively small matrix $D\widetilde{\Gamma}_n[\kappa^{(k)}] D\widetilde{\Gamma}_n^*[\kappa^{(k)}]$ is invertible and the pseudo-inverse in (3.22) could be replaced by the inverse.

One usually recurs to globalization strategies such as line search or trust region to guarantee progress to the solution at each iteration of Algorithm 3.17 by essentially limiting the size of the update (3.21). We observed that such strategies were not

necessary and we believe this is because the initial iterate is already close to the true conductivity.

The iterations

We give in Figures 3.16 and 3.17 two typical reconstructions obtained by using Algorithm 3.17 on data collected with 100 "electrodes" tainted with 1% multiplicative noise with zero mean. We determine the size of the network empirically as the largest network that gives positive resistors that do not change substantially with the realizations of the noise. The PDE was discretized using the finite volumes method discussed in Section 3.1, on a grid with 100×100 dual cells of uniform size, with one degree of freedom for the conductivity per dual cell.

As can be seen from the reconstructions, numerical convergence occurs in only a few iterations, with the largest update occurring in the first iteration. For all practical purposes, this first iterate is already a good reconstruction. Also note that the conductivity values are better resolved than with the average reconstructions of Algorithm 3.15.

A non-linear preconditioning of the problem?

If we follow the traditional approach of measuring the misfit in the measurements directly and use the Gauss-Newton method to find a conductivity that fits the measurements, we would obtain iteration (3.21) where the Jacobian $D\mathcal{M}_n[\sigma]$ of the measurements appears instead of $D\Gamma_n(\sigma)$. Here we compare condition numbers (ratio of largest singular value to smallest) for $D\Gamma_n[\sigma]$ and $D\mathcal{M}_n[\sigma]$ and report them in Table 3.2.

The condition numbers of $D\Gamma_n[\sigma]$ are orders of magnitude smaller than those of $D\mathcal{M}_n[\sigma]$ and do not change considerably with n or the conductivity. This is why

	$\sigma \equiv 1$		$\sigma \equiv$ `sigX`		$\sigma \equiv$ `phantom1`	
n	$D\mathcal{M}_n[\sigma]$	$D\Gamma_n[\sigma]$	$D\mathcal{M}_n[\sigma]$	$D\Gamma_n[\sigma]$	$D\mathcal{M}_n[\sigma]$	$D\Gamma_n[\sigma]$
9	5.55e+02	4.81e+00	5.72e+02	4.80e+00	1.24e+03	4.48e+00
11	5.14e+03	6.01e+00	5.27e+03	5.92e+00	1.13e+04	5.67e+00
13	4.88e+04	7.89e+00	4.95e+04	7.78e+00	9.19e+04	7.56e+00

Table 3.2: Condition number of $D\Gamma_n[\sigma]$ (misfit in the $\sigma_{i,j}, \widehat{\sigma}_{i,j+1/2}$) compared to that of $D\mathcal{M}_n[\sigma]$ (misfit on the measurements directly) for different conductivities defined in Appendix C.

we say that measuring the misfit in the the reconstructions of Algorithm 3.15 is a preconditioning of the EIT problem. Nevertheless, having better condition numbers of the Jacobian does not mean that the Gauss-Newton method converges faster.

Note that in all the cases we considered, the matrices approximating these quantities were full-rank, so that when using identity (3.22), the condition number of the systems we need to solve to compute the Gauss-Newton update is actually the square of what appears in Table 3.2.

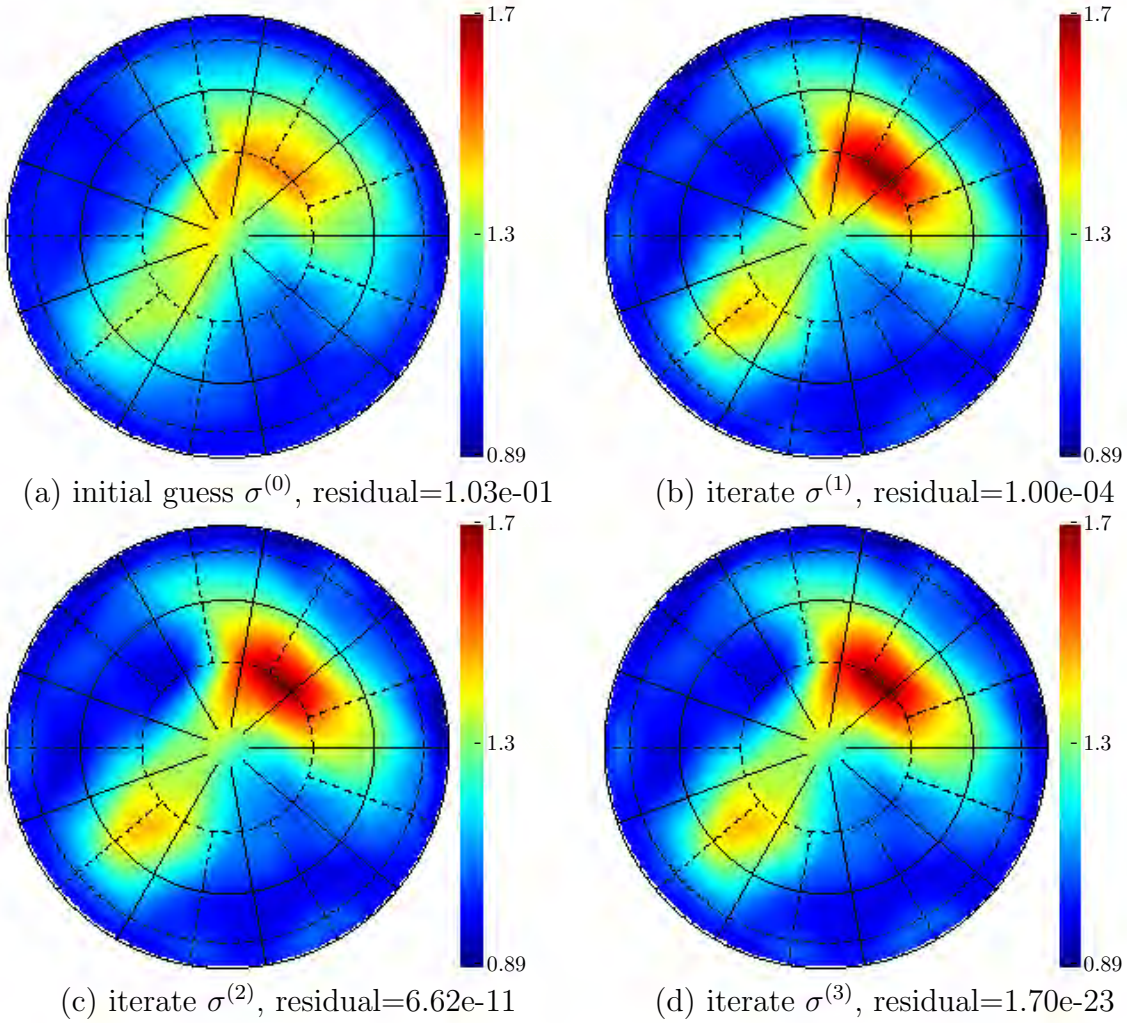

(a) initial guess $\sigma^{(0)}$, residual=1.03e-01

(b) iterate $\sigma^{(1)}$, residual=1.00e-04

(c) iterate $\sigma^{(2)}$, residual=6.62e-11

(d) iterate $\sigma^{(3)}$, residual=1.70e-23

Figure 3.16: Convergence history for Algorithm 3.17 on the conductivity `sigX` (see Appendix C), with 1% noise added. The initial guess (a) is given by Algorithm 3.15 on a $C(4, 9)$ network. The reported residual is the misfit $\|\widetilde{\Gamma}_n(\ln(\sigma)) - \widetilde{\Gamma}_n(\ln(\sigma_{true}))\|_2^2$.

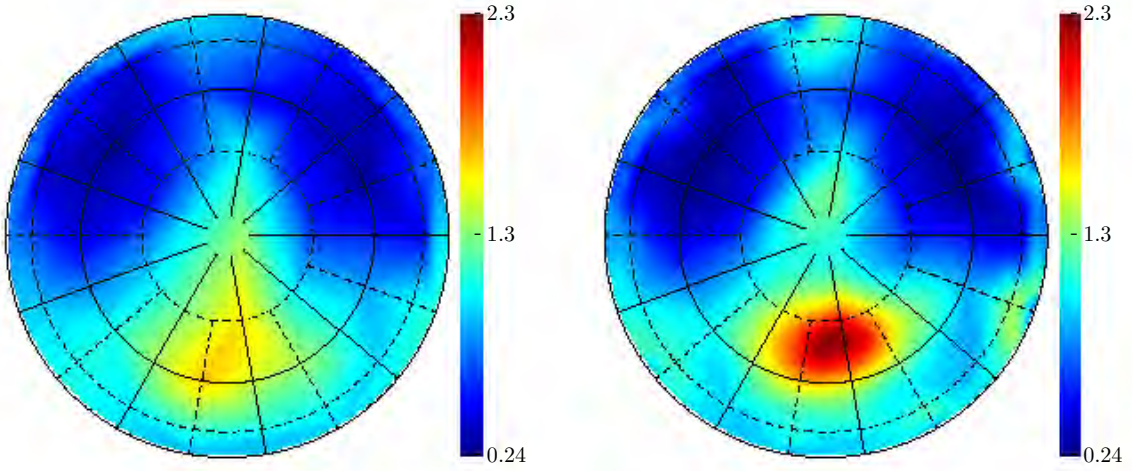

(a) initial guess $\sigma^{(0)}$, residual=7.61e-01

(b) iterate $\sigma^{(1)}$, residual=3.10e-03

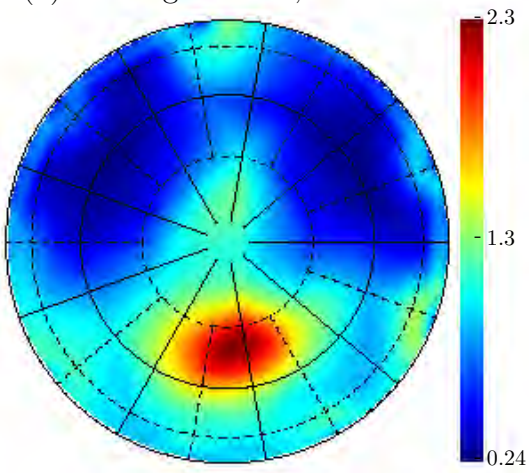

(c) iterate $\sigma^{(2)}$, residual=2.29e-08

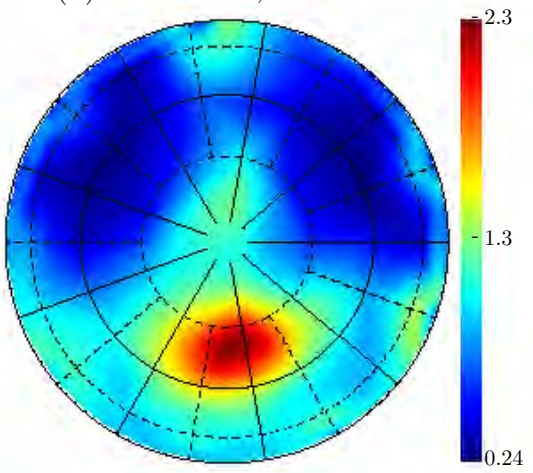

(d) iterate $\sigma^{(3)}$, residual=7.73e-18

Figure 3.17: Convergence history for Algorithm 3.17 on the conductivity `phantom1` (see Appendix C), with 1% noise added. The initial guess (a) is given by Algorithm 3.15 on a $C(4, 9)$ network. The reported residual is the resistor misfit $\|\widetilde{\Gamma}_n(\ln(\sigma)) - \widetilde{\Gamma}_n(\ln(\sigma_{true}))\|_2^2$.

3.4.3 Introducing a priori information about the solution

If a priori information about the solution is available, it should be taken into account, because the right prior generally improves the quality of the reconstructions. Here we assume that the prior is given in the form of a *penalty functional* $J(\sigma)$ that measures how far σ is from the desired prior. For example, if we expect that the true conductivity is piecewise constant, we can look for a conductivity that has a small total variation, i.e. $J(\sigma) = \mathrm{TV}(\sigma)$.

As the numerical results of Section 3.4.2 show, the Gauss-Newton iteration converges fast. In fact, after the first iteration, the corrections are so small that the image remains virtually unchanged. Therefore, for all practical purposes it is enough to keep the first Gauss-Newton iterate, which is the same as finding the minimal $L^2(\Omega)$ norm solution κ^{LS} to the linearized inverse problem,

$$D\widetilde{\Gamma}_n[\kappa^{(0)}](\kappa^{LS} - \kappa^{(0)}) = \widetilde{\Gamma}_n(\kappa_{true}) - \widetilde{\Gamma}_n(\kappa^{(0)}). \tag{3.23}$$

Clearly $\kappa = \kappa^{LS} + \delta\kappa$ is also a solution to the linearized inverse problem (3.23) provided that $\delta\kappa \in \mathrm{null}\,(D\widetilde{\Gamma}_n[\kappa^{(0)}])$. Therefore, we can add a priori information by simply looking for the correction $\delta\kappa$ in the orthogonal complement of the sensitivity functions (i.e. $\mathrm{null}\,(D\widetilde{\Gamma}_n[\kappa^{(0)}])$) that minimizes the penalty functional. This gives us the following constrained optimization problem,

$$\begin{aligned} \min_{\kappa} \quad & J(\kappa) \\ \text{subject to} \quad & D\widetilde{\Gamma}_n[\kappa^{(0)}](\kappa - \kappa^{LS}) = 0. \end{aligned} \tag{3.24}$$

The data fit of κ is to first order approximation the same as that of κ^{LS}. The procedure is summarized as follows.

Algorithm 3.18. Inputs: Measurements $\mathcal{M}_n(\Lambda_{\sigma_{true}}^{DtN})$ (Definition 3.2) for n odd and a penalty functional $J(\kappa)$ encoding the a priori information. **Outputs:** A reconstructed conductivity σ^*.

i. Compute $\kappa^{(0)} = \ln(\sigma^{(0)})$, where $\sigma^{(0)}$ is a linear interpolation of the averages $\sigma_{i,j+1/2}, \widehat{\sigma}_{i,j}$ obtained by Algorithm 3.15 from the measurements $\mathcal{M}_n(\Lambda_{\sigma_{true}}^{DtN})$.

ii. Carry out the first iteration of Algorithm 3.17, that is compute the least squares solution to the linearized EIT problem with misfit measured in the outputs of Algorithm 3.15:

$$\kappa^{LS} \leftarrow \kappa^{(0)} + \left(D\widetilde{\Gamma}_n[\kappa^{(0)}]\right)^{\dagger} \left(\widetilde{\Gamma}_n(\kappa_{true}) - \widetilde{\Gamma}_n(\kappa^{(0)})\right).$$

iii. Find the reconstructed log-conductivity $\kappa^* = \ln(\sigma^*)$ as a minimizer of (3.24).

The idea of solving an optimization problem similar to (3.24) is not new, actually it was considered for example, by Dobson and Santosa [42] with $J(\sigma)$ being a TV penalty functional. The biggest difference is that in their approach the sensitivities of the data to perturbations in the conductivity are used directly as constraints. This is problematic because such sensitivity matrices have a large condition number, so some SVD truncation is needed [42]. In the optimization problem (3.24), the sensitivity matrix (or numerical approximation of $D\widetilde{\Gamma}_n[\kappa^{(0)}]$) has a small condition number for two reasons: (1) the size of the reduced model (the R-net) is relatively small and (2) we apply the non-linear measurements-to-resistors mapping (which "preconditions" in some sense the problem, see Section 3.4.2).

Also because the number of resistors we look for is small, there are only a few constraints in the optimization problem (3.24). This can be exploited by the optimization algorithm to obtain reconstructions efficiently, as we show next.

3.4.4 Numerical experiments with a priori information

We implemented the method of the previous section with the functional J_{TV}, which favours blocky reconstructions and is defined as follows

$$J_{TV}(\kappa) = TV(\kappa), \quad \text{where} \quad TV(\kappa) = \int_\Omega \|\nabla\kappa(\mathbf{x})\|_2 \, d\mathbf{x}.$$

We note that with the functional J_{TV}, and without any assumptions on $D\widetilde{\Gamma}_n[\kappa^{(0)}]$ a minimizer of (3.24) is defined up to an additive constant. However we observed numerically that constants do not belong to the range of the sensitivity functions, thus the minimizer of (3.24) is unique.

Implementation strategies

To solve the problem (3.24) we resort to an SQP (Sequential Quadratic Programming) method where the KKT (Karush-Kuhn-Tucker) systems are solved using the range space approach [91, Chap. 18]. This method is well suited for our optimization problem, because we have only a few linear constraints, and the Hessian of the Lagrangian of (3.24) is readily available, positive definite and sparse. For the size of the problems we considered (up to 10^4 variables for the conductivity), sparse direct methods (such as UMFPACK in Matlab) are efficient in solving the systems involving the Hessian, that need to be computed at each iteration of the optimization algorithm.

To make the convergence global, we controlled the size of the step with a line search strategy on an ℓ_1 type merit function [91, p544].

Moreover, to minimize the non-differentiable functional J_{TV} we recurred to the standard trick of approximating the absolute value by a smooth functional,

$$\mathrm{TV}(\kappa) \approx \int_\Omega \sqrt{\|\nabla\kappa(\mathbf{x})\|_2^2 + \beta^2} d\mathbf{x},$$

with $\beta = 0.1$. We also used the Quasi-Newton approximation to the Hessian of the TV functional (i.e. the part of the Hessian that has second derivatives is ignored), that is further regularized by adding 10^{-2} to the diagonal entries.

The resulting numerical method to minimize (3.24) with the J_{TV} functional is very similar to the so called lagged diffusivity method [112, p136], modified to take into account the constraints.

Noiseless reconstructions

We stopped the iterations when the norm of the gradient of the Lagrangian was reduced by $5 \cdot 10^{-2}$, which in all our test cases occurred in no more than 15 SQP iterations. As can be seen in Figure 3.18, the typical convergence that we observed justify our stopping criterion: much of the progress in reducing the objective function is done at the beginning so it is best to terminate the iterations early.

To validate our approach on the ideal noiseless data case, we present in Figure 3.19 reconstructions with such data. The PDE was discretized on a uniform finite volumes grid with 100×100 dual cells (see Section 3.1) and measurements are taken at 50 equally spaced "electrodes", that are lumped into fewer measurements to regularize the problem. The conductivity is sought after on a uniform grid with 50×50 cells to avoid committing an inverse crime.

3.4.5 Comparison of our method to output least squares

We compare our approach to traditional output least squares (OLS) in Figure 3.20. In there, both methods are given noisy data collected at 50 "electrodes".

To be more specific, let N be the number of electrodes and $\mathcal{M}_N(\Lambda_\sigma^{DtN})$ the measured DtN map. In our implementation of the OLS method, we seek the log-

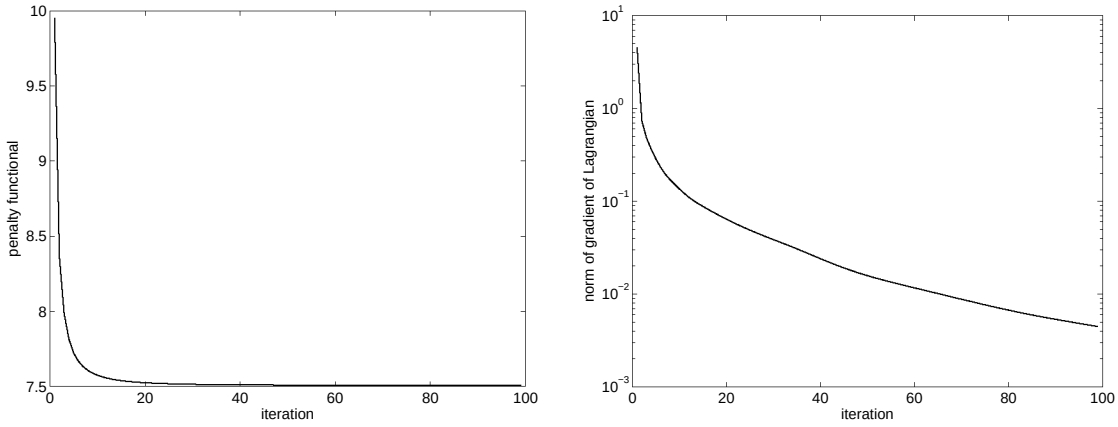

(a) Penalty functional. (b) Norm of gradient of the Lagrangian.

Figure 3.18: Typical convergence history of the SQP algorithm for minimizing (3.24) with a TV penalty functional.

conductivity κ^* minimizing,

$$\min_{\kappa} \quad \frac{1}{2} \left\| \mathcal{M}_N(\Lambda^{DtN}_{\exp(\kappa)}) - \mathcal{M}_N(\Lambda^{DtN}_{\sigma_{true}}) \right\|_F^2 + \alpha TV(\kappa), \tag{3.25}$$

where $\| \cdot \|_F$ is the Frobenius norm for matrices. We determine empirically the regularization parameter α by minimizing (3.25) for different values of α.

To minimize (3.25) we use the Quasi-Newton approximation to the Hessian of the TV functional and we further regularize the Hessian by adding 10^{-3} to the diagonal entries. For the globalization strategy of the iterations, we use Armijo line search. The stopping criterion for the operations was to achieve a relative reduction of the norm of the gradient of at least 10^{-2}.

Finally for making the comparison as fair as possible, the conductivity is discretized on the same 50×50 cells of uniform size. This makes the Hessian of the objective function in (3.25) a 2501×2501 dense matrix that is formed explicitly in our code.

The times included in Figures 3.19 and 3.20 correspond to wall-clock times for obtaining reconstructions in Matlab r2006a on a Pentium 4 Linux PC with 2GB of

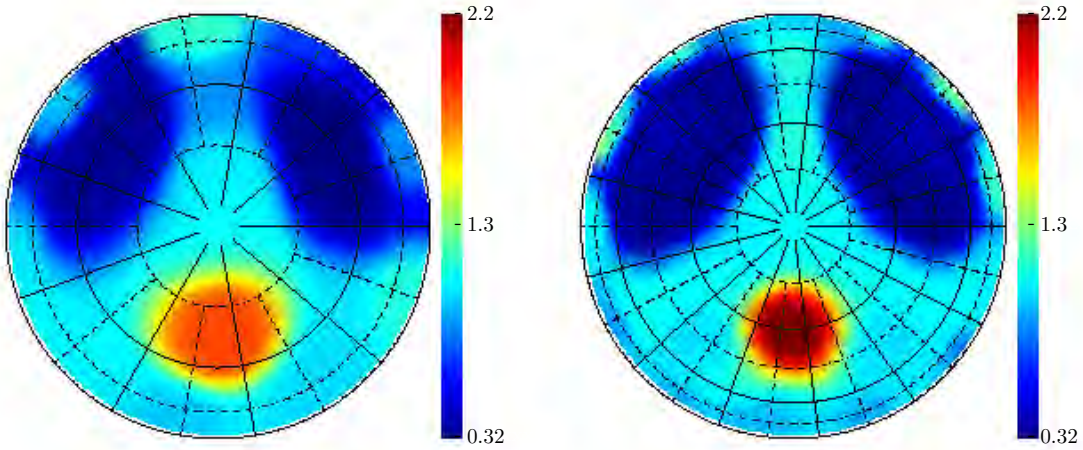

10 iterations, 6.0s 6 iterations, 5.4s

Figure 3.19: Reconstructions from noiseless data using Algorithm 3.18 with TV penalty functional, for the conductivity `phantom1` (see Appendix C).

RAM. We remark that Algorithm 3.18 is roughly 5 times faster than the traditional OLS approach. However in our OLS implementation, close to 50% of the time is spent forming the Hessian and solving for the Newton updates, while the other 50% corresponds to the forward problem and derivative computations. Thus, OLS is more expensive than our approach even if we could find a more efficient way of computing the updates (e.g. with a Krylov based iterative solver). The computational advantage of our approach is that we do not need to compute *at each iteration* the forward problem plus derivatives.

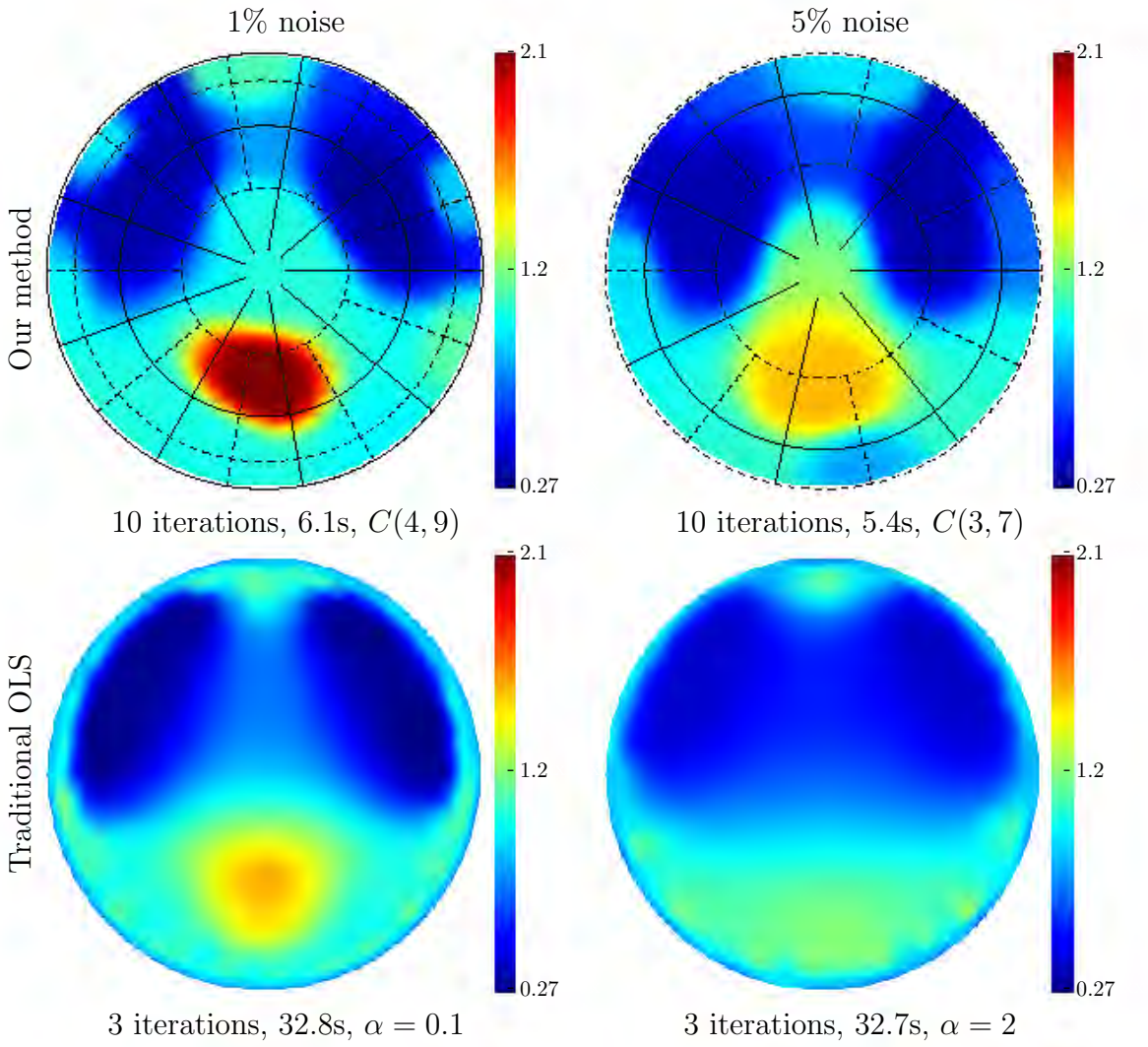

Figure 3.20: Comparison of the method of Section 3.4.3 with traditional output least squares.

Chapter 4

Summary and future work

4.1 Summary

In Chapter 3, we extended a finite differences based method for inverse Sturm-Liouville problems [19, 20] to EIT in dimension two. We obtained a simple inversion algorithm that efficiently estimates averages of the conductivity over grid cells and that is simple to implement. A deep rift between inverse Sturm-Liouville problems and EIT is that the latter is severely ill-posed. We cope with the ill-posedness in EIT in two ways. First, we determine as many parameters as we can expect to recover given the noise level in the measurements. Second, we acknowledge the spatial resolution limits inherent to the EIT problem by using a grid that is refined near the boundary of measurements.

Since both the simple inversion algorithm for inverse Sturm-Liouville problems and its extension to EIT are inexpensive, we use them as non-linear transformations of the measurements (Sections 2.4 and 3.4). So we setup a Gauss-Newton iterative procedure to minimize the misfit in the reduced model parameters instead of the conventional misfit in the measurements. We observed for both problems that the condition number of the Jacobian of the mapping taking from conductivity to reduced

model parameters was significantly smaller compared to that of the mapping going from the conductivity to the measurements. This leads us to believe that this non-linear transformation preconditions, in some sense, the problem. The iterative procedure converged quickly and allowed us to introduce a priori information about the true solution in a straightforward and efficient manner, without significantly changing the data fit (Sections 2.4.3 and 3.4.3) .

4.2 Future work

First, it may be possible to extend the simple reconstruction algorithm of Section 3.3 to EIT for low-frequency electric measurements. In this case, one is interested in finding the complex conductivity of the medium (also called impedance, see e.g. [18]) from voltage and electric current measurements at the boundary. A first step towards solving this problem would be to determine if at a fixed frequency it is possible to find a network of electric impedances (which play the role of the resistor network) in a unique way from the measurements. Perhaps the reconstruction algorithm could be also extended to the anisotropic case, where the solution is unique up to a smooth diffeomorphism of the domain that is the identity at the boundary (see e.g. [8]).

Sparsity is a notion that naturally arises when studying the resolution limits of inverse problems. Indeed, if we know that we cannot resolve all the details of the conductivity in EIT, it does not make sense to discretize the unknown with too many parameters. Thus we should look for a sparse reconstruction, meaning that it can be represented with only a few basis functions. A simple way of enforcing sparsity is to limit the number of parameters that we look for with the measurement precision, which is precisely what is done in e.g. [54, 28] and in Chapter 3. However, the unknown remains discretized on the characteristic functions of a grid. This maybe

be satisfactory for the smooth and piecewise constant conductivities we have worked with, but is bound to fail in applications such as crack detection, where the inhomogeneities are typically small. Thus we want to explore the use of better adapted libraries of functions (e.g. ridgelets [24]) for parametrizing the conductivity and use the regularizing properties of sparsity that Daubechies et al. [37] have demonstrated at least for linear inverse problems.

The common theme between the iterative methods introduced in Chapters 2 and 3 is that we use a reduced model of the differential equation that is uniquely recoverable from the data as a "preconditioner" in a Newton-type iterative procedure. However, such a model may not even exist for other inverse problems, and the interpretation of the reduced model parameters as a discretization may not be possible either. Therefore, we would like to explore relaxations to this requirement that would give more flexibility to the methods we have developed. For example, is it possible to devise a similar iterative method by simply assuming a reduced model that does not fit the data exactly?

Appendix A

Optimal finite difference grids for the forward problem

In this Thesis we have only seen optimal grids in the context of an inversion method. To complete the picture, we give a brief overview of the existing work on optimal grids for the forward problem, which was the original purpose of optimal grids.

First proposed by Druskin [44], optimal grids are a second order finite difference scheme with grid steps chosen to minimize the error in the impedance function (2.6). The grid that is used is essentially the same staggered finite difference grid that we presented in Section 2.2.1. The key observation is that the impedance function (2.14) of the finite difference approximation is also a rational function. Thus the problem of finding the grid steps that minimize the error in the impedance function is essentially a rational approximation problem. In this respect, Ingerman et al. [63] obtain the grid steps from Zolotarev's closed form, best rational approximation of the inverse square root function on an interval [1, 93]. This particular impedance arises in the case of a constant conductivity. For other impedance functions, Druskin and Knizhnerman [45] use Padé approximants to find close-to-optimal grid steps. Either of the two choices gives exponential convergence *locally* at the point where the impedance is defined ($z = 0$ in (2.3)), and only second order convergence globally.

Another advantage is that at least in the high frequency limit ($\omega^2 \gg 1$), using the grid designed for the homogeneous medium (for the grid construction see Section 2.2.3) yields exponential accuracy of the impedance function [19, §5]. Exponential rates can also be achieved with spectral methods. Actually Druskin and Moskow [46] established for elliptic problems the equivalence of optimal grids to a spectral Galerkin-Petrov finite element method.

The main advantage of optimal grids is that they can dramatically reduce the number of points needed to achieve a certain accuracy in the impedance function. This discretization method has been applied to efficiently solve an elliptic problem coming from Maxwell's equation in a geophysical application [38]. With a slight modification to the rational approximation problem, optimal grids have also been applied to hyperbolic problems (wave propagation) [9, 10] and to reduce the computational cost of Berenger's Partially Matched Layers [11] (non-reflecting boundary conditions for wave propagation).

Appendix B

Working with DtN map measurements

In this Appendix we complement Chapter 3 with some details we omitted. First in Section B.1 we explain why trying to find the size of the network from the noise level does not work when considering the DtN map measurements. Then we show in Section B.2 how convex duality relations can be used to transform NtD to DtN map measurements *exactly*. Finally in Section B.4 we show what we mean by measurement lumping, which is a discrete approximation to the measured DtN map.

B.1 The singular functions of the DtN map difference do not always become smoother as the singular values increase

To obtain the size of the network from the noise level, the key observation in Section 3.2.5 was that for the NtD map difference the largest singular values correspond to the smoothest singular vectors. This observation does not hold for the DtN map as we show next with a simple example.

Consider the DtN map difference $\Lambda_\sigma^{DtN} - \Lambda_{\sigma^0}^{DtN}$ for two conductivities σ and σ^0 that we assume are equal to a constant on a neighborhood of the boundary. From the bounds given in [54, AIII] it can be shown that the DtN map difference is a compact operator with rapidly decaying singular values. This happens even if the DtN maps

by themselves are unbounded operators. Moreover, the singular values of the DtN map difference are $\mathcal{O}(k\alpha^{2k})$.

In Example B.1, we give two simple conductivities σ and σ^0 for which the leading singular functions of the difference $\Lambda_\sigma^{DtN} - \Lambda_{\sigma^0}^{DtN}$ are not the smoothest ones. The same behavior is illustrated for a more realistic conductivity in Figure B.2. Therefore, we cannot make the assumption that the most significant part of the data is low frequency and can be represented with only a few points on the boundary.

Example B.1. Let $\sigma^0 \equiv 1$ and σ be,

$$\sigma(r,\theta) = \begin{cases} a & \text{if } 0 \leq r < \alpha \\ 1 & \text{if } \alpha \leq r \leq 1. \end{cases}$$

The singular values s_k of $\Lambda_\sigma^{DtN} - \Lambda_{\sigma^0}^{DtN}$, associated with the singular functions $\sin(k\theta)$ and $\cos(k\theta)$ can be computed [65] to be,

$$s_k = k\frac{1+\mu(a)\alpha^{2k}}{1-\mu(a)\alpha^{2k}} - k,$$

where $\mu(z) = z - 1/z + 1$. We display in Figure B.1 the singular values for $a = 4$ and $\alpha = 0.95$ in an non-standard way, as a function of the *frequency* k of the respective singular functions. Clearly, the largest singular values do not correspond to the lowest frequencies.

B.2 Converting NtD map measurements to DtN map measurements with convex duality

In dimension two, the electric current density $\mathbf{j}$ is divergence free, so there is a scalar field h such that $\mathbf{j} = \nabla^\perp h$, where $\nabla^\perp \equiv (\partial/\partial y, -\partial/\partial x)^T$. The current density is

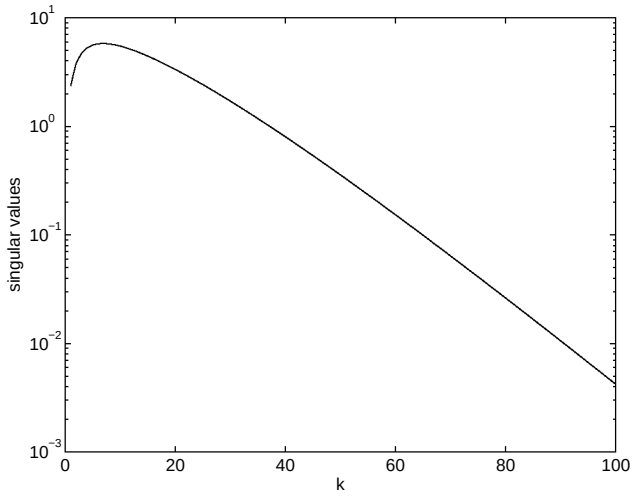

Figure B.1: Singular values of the DtN map difference for $\sigma^0 \equiv 1$ and σ defined as in Example B.1, with respect to the *frequency* of the singular function.

related to the electric potential u through Ohm's law (see e.g. [18, §2.1])

$$\sigma \nabla u = \mathbf{j} = \nabla^{\perp} h, \tag{B.1}$$

where σ is the electric conductivity.

Now recall that the DtN map is defined as $\Lambda_{\sigma}^{DtN} f = \mathbf{n} \cdot (\sigma \nabla u)$ where u solves the differential equation with Dirichlet boundary conditions,

$$\nabla \cdot [\sigma \nabla u] = 0 \text{ in } \Omega \quad \text{and} \quad u|_{\partial\Omega} = f.$$

By the duality relation (B.1) we have that h solves the differential equation with Neumann boundary conditions,

$$\nabla \cdot \left[\frac{1}{\sigma} \nabla h \right] = 0 \text{ in } \Omega \quad \text{and} \quad \mathbf{n} \cdot \left(\frac{1}{\sigma} \nabla h \right) = -\mathbf{n} \cdot \nabla^{\perp} u \text{ on } \partial\Omega.$$

By using the duality relation (B.1) again we get that $\Lambda_{\sigma}^{DtN} f = \mathbf{n} \cdot \nabla^{\perp} h$. If we assume that the domain Ω is the unit disk as we did in Chapter 3, the tangential derivative

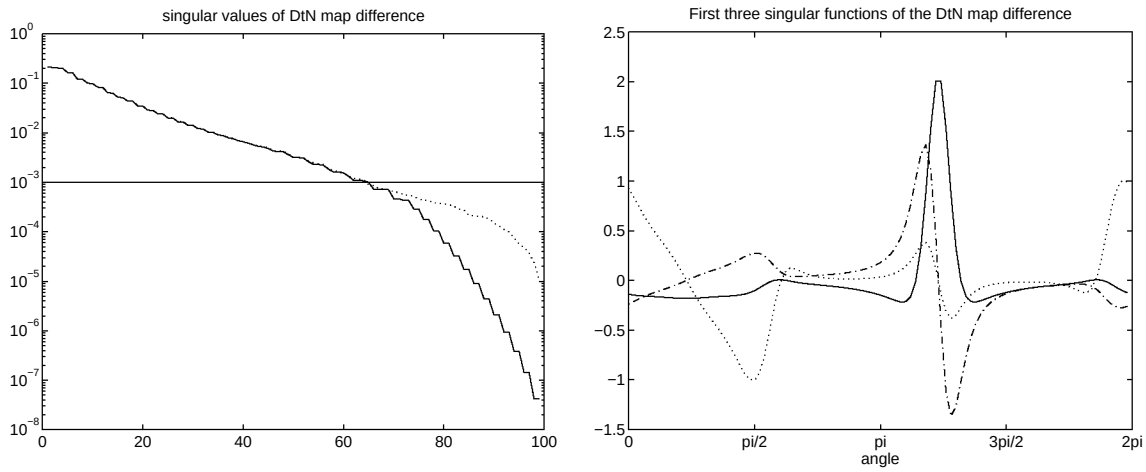

(a: Singular values) (b: Leading singular vectors)

Figure B.2: (a) Singular values of the DtN difference map for conductivities `sigX` (defined in Section 3.3) and $\sigma^0 \equiv 1$. We include singular values for the true (solid line) and noisy (dotted line) difference maps. The noise level $\delta = 10^{-3}$ is also displayed. (b) The three leading singular vectors, normalized such that $\|I_k\|_{L^2} = 1$. The leading singular function I_1 is in solid line, I_2 in dashed line and I_3 in dotted line.

takes the form $\mathbf{n} \cdot \nabla^\perp \equiv -\partial/\partial\theta$ where θ is the angle parametrizing the unit circle in the usual way. Therefore the NtD map of $1/\sigma$ and the DtN map of σ are related via the duality relation,

$$\Lambda_\sigma^{DtN} = -\frac{\partial}{\partial\theta}\Lambda_{1/\sigma}^{NtD}\frac{\partial}{\partial\theta}. \tag{B.2}$$

The numerical reconstructions methods of Chapter 3 assume the measured DtN map defined in (3.8) is known. We now show using the duality relation (B.2) that NtD map measurements consistent with the so called "shunt electrode model" [100] can be transformed into DtN map measurements.

Let $\psi_1, \psi_2, \cdots, \psi_{2n}$ be $2n$ nonnegative functions in $H^{-1/2}(\partial\Omega)$ with disjoint supports numbered in circular order around the boundary and such that $\int_{\partial\Omega} \psi_i d\mathbf{x} = 1$. We assume that the NtD map measurements are in the form of the *measured NtD*

map $\mathcal{M}_{2n}(\Lambda_\sigma^{NtD}) \in \mathbb{R}^{2n\times 2n}$ that is defined componentwise by,

$$\left(\mathcal{M}_{2n}(\Lambda_\sigma^{NtD})\right)_{i,j} = \begin{cases} \left\langle \psi_i, \Lambda_\sigma^{NtD}\psi_j \right\rangle & \text{if } i \neq j \\ -\sum_{i=1,p\neq i}^{2n} \left\langle \psi_i, \Lambda_\sigma^{NtD}\psi_p \right\rangle & \text{otherwise,} \end{cases} \tag{B.3}$$

where $\langle\cdot,\cdot\rangle$ is the $H^{-1/2}(\partial\Omega), H^{1/2}(\partial\Omega)$ duality pairing.

Let I_i be the smallest connected component of $\partial\Omega$ containing $\operatorname{supp}\psi_{2i}$ and $\operatorname{supp}\psi_{2i-1}$ and the functions $\widetilde{\phi}_i$ be defined for $i = 1,\ldots,n$ by,

$$\widetilde{\phi}_i(\theta) = \int_{\alpha_i}^{\theta} \psi_{2i-1}(s) - \psi_{2i}(s)ds,$$

where α_i is the angle of some point in the complement of I_i in $\partial\Omega$. Thus since the functions ψ_k integrate to one, we have $\operatorname{supp}\widetilde{\phi}_i = I_i$. Furthermore, the functions $\widetilde{\phi}_i$ are nonnegative because the ψ_k are numbered by increasing θ. Let us define $\beta_i = \int_{\partial\Omega}\widetilde{\phi}_i d\mathbf{x}$. The functions $\phi_i \equiv \widetilde{\phi}_i/\beta_i \in H^{1/2}(\partial\Omega)$ meet all the requirements outlined in Definition 3.2 to define a measured DtN map. In particular they have disjoint supports, therefore by the duality relation (B.2) we have for $i \neq j$,

$$\begin{aligned} \left\langle \phi_i, \Lambda_{1/\sigma}^{DtN}\phi_j \right\rangle &= -\left\langle \phi_i, \left(\frac{\partial}{\partial\theta}\Lambda_\sigma^{NtD}\frac{\partial}{\partial\theta}\right)\phi_j \right\rangle = \left\langle \frac{\partial\phi_i}{\partial\theta}, \Lambda_\sigma^{NtD}\frac{\partial\phi_j}{\partial\theta} \right\rangle \\ &= \frac{1}{\beta_i\beta_j}\left\langle \psi_{2i} - \psi_{2i-1}, \Lambda_\sigma^{NtD}(\psi_{2j} - \psi_{2j-1}) \right\rangle. \end{aligned} \tag{B.4}$$

Thus by doing a numerical tangential derivative of the NtD data for σ we can extract a measured DtN map for $1/\sigma$. We illustrate the process with Figure B.3. The matrix version of (B.4) is surprisingly simple:

$$\mathcal{M}_n(\Lambda_{1/\sigma}^{DtN}) = \mathcal{Z}(\mathbf{D}^T\mathcal{M}_{2n}(\Lambda_\sigma^{NtD})\mathbf{D}), \tag{B.5}$$

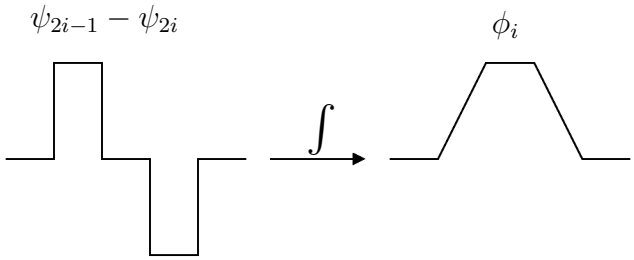

Figure B.3: How n measurement functions ϕ_i for the DtN map could be obtained from $2n$ measurement functions ψ_k of the NtD map.

where $\mathcal{Z}(\mathbf{A}) := \mathbf{A} - \operatorname{diag}(\mathbf{A1})$ and $\mathbf{D} \in \mathbb{R}^{2n\times n}$ is the matrix given columnwise by

$$\mathbf{D} = [\beta_1(\mathbf{e}_1 - \mathbf{e}_2), \beta_2(\mathbf{e}_3 - \mathbf{e}_4), \ldots, \beta_n(\mathbf{e}_{2n-1} - \mathbf{e}_{2n})].$$

Another immediate consequence of (B.4) is that we can formulate corollaries to the results we obtained in Section 3.2.3 on the consistency of DtN map measurements with the R-net model. Specifically, it would be possible to derive necessary conditions for the NtD map based on the necessary conditions of Ingerman and Morrow [62].

B.3 The mollified DtN map

We consider a particular case of the measurement operator introduced in Definition 3.2, where the functions ϕ_i are all constructed from a "mother" nonnegative function ϕ, with $\operatorname{supp}\phi \subset (-1, 1)$ and integrating to one. Let $\phi^{(n)}$ be the rescaled ϕ such that $\phi^{(n)}(\theta) = (n/\pi)\phi(\theta n/\pi)$. Parametrize the unit circle $\partial\Omega$ as usual by an angle $\theta \in [0, 2\pi)$, so that all $\mathbf{x} \in \partial\Omega$ can be written $\mathbf{x}(\theta)$, and let $\theta_j = 2\pi j/n$.

Definition B.2. We define the measured DtN map $\mathcal{M}[n, \phi](\Lambda_\sigma)$ as in Definition 3.2 with test functions ϕ_j,

$$\phi_j(\theta) = \phi^{(n)}(\theta - \theta_j). \tag{B.6}$$

In a slight abuse of notation, we use $\phi_j(\theta)$ instead of $\phi_j(\mathbf{x}(\theta))$. By construction,

we have that the $\operatorname{supp}\phi_j \subset \theta_j + (-\pi/n, \pi/n)$ are disjoint and that $\int_{\partial\Omega} \phi_j d\mathbf{x} = 1$.

When the mother function ϕ is smooth, then $\mathcal{M}[n,\phi](\Lambda_\sigma)$ can be seen as pointwise measurements of a mollified[1] DtN map,

$$\Lambda^{DtN}[\sigma,\phi^{(n)}] = \Lambda_\sigma^{DtN} * \left(\check{\phi}^{(n)} \otimes \check{\phi}^{(n)}\right), \tag{B.7}$$

where $\check{\phi}^{(n)}(\theta) = \phi^{(n)}(-\theta)$, the symbol $\otimes$ denotes the tensor product and the convolution $f * g$ is understood in the distribution sense (see e.g. [52, Chap. 5]). The mollified kernel is then a smooth function defined for $(\alpha,\beta) \in [0,2\pi) \times [0,2\pi)$ by,

$$K[\sigma,\phi^{(n)}](\alpha,\beta) = \left\langle \phi^{(n)}(\,\cdot\, - \alpha), \Lambda_\sigma^{DtN}\phi^{(n)}(\,\cdot\, - \beta)\right\rangle, \tag{B.8}$$

therefore for $i \neq j$,

$$K[\sigma,\phi^{(n)}](\theta_i,\theta_j) = \langle \phi_i, \Lambda_\sigma \phi_j\rangle = \left(\mathcal{M}[n,\phi](\Lambda_\sigma)\right)_{i,j}.$$

Also, since ϕ satisfies $\int_{-1}^{1}\phi(t)dt = 1$, the mollified map is, in some sense, an approximation to the true DtN map. Moreover, as the true DtN map, the mollified DtN integrates to zero:

$$\begin{aligned}\left\langle \Lambda^{DtN}[\sigma,\phi^{(n)}], 1\right\rangle &= \left\langle \Lambda_\sigma^{DtN} * \left(\check{\phi}^{(n)} \otimes \check{\phi}^{(n)}\right), 1\right\rangle \\ &= \left\langle \check{\phi}^{(n)} \otimes \check{\phi}^{(n)}, \left\langle \Lambda_\sigma^{DtN}, 1\right\rangle\right\rangle = 0.\end{aligned} \tag{B.9}$$

B.4 Lumping of the measurements

From measurements $\mathcal{M}[N,\psi](\Lambda_\sigma^{DtN})$ taken at N "electrodes" we want to approximate measurements $\mathcal{M}[n,\phi](\Lambda_\sigma^{DtN})$ taken at $n \ll N$ electrodes. We propose a simple

[1] In distribution theory, this is also called regularization; see e.g. [52, §5.2]. To avoid confusions with regularization of inverse problems, we prefer not to use this terminology.

approximation that is *guaranteed* to be the DtN map of a resistor network with n boundary points, at least for measurements devoid of noise.

Let $\phi_j(\theta) = \phi^{(n)}(\theta - 2\pi j/n)$. Clearly when $i \neq j$, the entries of the measured DtN map can be approximated by

$$\begin{aligned}\left(\mathcal{M}[n,\phi](\Lambda_\sigma^{DtN})\right)_{i,j} &= \left\langle \phi_i, \Lambda_\sigma^{DtN}\phi_j \right\rangle \\ &\approx \left\langle \phi_i, \Lambda^{DtN}[\sigma,\psi^{(N)}]\phi_j \right\rangle,\end{aligned} \tag{B.10}$$

which is the same as approximating $\mathcal{M}[n,\phi](\Lambda_\sigma^{DtN})$ with $\mathcal{M}[n,\phi * \psi^{(N/n)}](\Lambda_\sigma^{DtN})$. If ψ is smooth, there are only ordinary integrals involved. We can then use $\mathcal{M}[N,\psi](\Lambda_\sigma^{DtN})$ to approximate $\left\langle \phi_i, \Lambda_\sigma^{DtN}\phi_j \right\rangle$ with some Cartesian product numerical integration rule (see e.g. [73, §6.1.4]):

$$\begin{aligned}\left\langle \phi_i, \Lambda_\sigma^{DtN}\phi_j \right\rangle &\approx \int_{I_i\times I_j} \phi_i(\mathbf{x})\phi_j(\mathbf{y})K[\sigma,\psi^{(N)}](\mathbf{x},\mathbf{y})d\mathbf{x}d\mathbf{y} \\ &\approx \sum_{p,q=1}^{N} \Phi_{i,p}\Phi_{j,q}K[\sigma,\psi^{(N)}](\mathbf{x}_p,\mathbf{x}_q),\end{aligned} \tag{B.11}$$

where $\mathbf{x}_j = \mathbf{x}(2\pi j/N)$, and $\Phi_{i,p}$ are the coefficients in an integration rule designed such that,

$$\int_{\partial\Omega} f(\mathbf{x})\phi_i(\mathbf{x})d\mathbf{x} \approx \sum_{p=1}^{N} \Phi_{i,p} f(\mathbf{x}_p), \tag{B.12}$$

We can put the approximation in matrix form,

$$\mathcal{M}[n,\phi](\Lambda_\sigma^{DtN}) \approx \mathcal{Z}\left(\mathbf{\Phi}\mathcal{M}[N,\psi]\left(\Lambda_\sigma^{DtN}\right)\mathbf{\Phi}^T\right), \tag{B.13}$$

where $\mathcal{Z}(\mathbf{A}) := \mathbf{A} - \mathrm{diag}\left(\mathbf{A}\mathbf{1}\right)$ and $\mathbf{\Phi} \in \mathbb{R}^{n\times N}$ has entries $\Phi_{i,j}$. It is worth noting that because of the condition $\int_{\partial\Omega}\phi_i(\mathbf{x})d\mathbf{x} = 1$, if the integration rules (B.12) are exact for constants, then $\mathbf{\Phi}\mathbf{1} = \mathbf{1}$.

The following lemma gives mild sufficient conditions for the approximation (B.13) to be the DtN map of a well-connected resistor network. This is a discrete analogous of the consistency result in Section 3.2.3.

Lemma B.3. *The approximation* $\mathcal{Z}\left(\mathbf{\Phi}\mathcal{M}[N,\psi]\left(\Lambda_\sigma^{DtN}\right)\mathbf{\Phi}^T\right)$ *to* $\mathcal{M}[n,\phi](\Lambda_\sigma^{DtN})$ *is the DtN map of a well-connected resistor network with* n *boundary points if the following conditions hold,*

i. The matrix $\mathbf{\Phi}$ *has nonnegative entries.*

ii. The sets of indices $I_i = \{j \mid \Phi_{i,j} > 0\}$*, are disjoint and numbered in circular order when laid down on a circle.*

Proof. By construction $\mathbf{A} := \mathcal{Z}\left(\mathbf{\Phi}\mathcal{M}[N,\psi]\left(\Lambda_\sigma^{DtN}\right)\mathbf{\Phi}^T\right)$ is an $n\times n$ symmetric matrix with zero row sum. Moreover by a discrete analogous of Lemma 3.11, all circular minors of $\mathbf{A}$ can be shown to be totally negative using the total negativity of the circular minors of $\mathcal{M}[N,\psi]\left(\Lambda_\sigma^{DtN}\right)$ and the properties above. Therefore $\mathbf{A}\in\Omega_n$ (see Definition 3.4), which means that $\mathbf{A}$ is the DtN map of a well-connected resistor network. □

Since the $\phi_j(\theta) = \phi^{(n)}(\theta - 2\pi j/n)$ are nonnegative and have disjoint supports, the conditions in Lemma B.3 can be easily satisfied if N is large enough.

Appendix C

Supplement for the two dimensional numerical experiments

Here we define conductivities that we used throughout the numerics of Chapter 3, as well as the smoothed box function that we use in the definition of the measured DtN map (Section 3.2.1).

C.1 Conductivity definitions

We depict in Figure 3.10 the conductivities used in the numerical experiments of Chapter 3. The precise definition of each conductivity follows.

- Conductivity "`sigX`" (Figure 3.10 left)

  Smooth function that is the superposition of two Gaussian bell functions. Specifically, the conductivity is given by

  $$\sigma(\mathbf{x}) = 1 + \frac{1}{2}\psi(\|\mathbf{x}\|_2)\exp(-\|\mathbf{A}(\mathbf{x}-\mathbf{a})\|_2^2) + \frac{1}{2}\psi(\|\mathbf{x}\|_2)\exp(-\|\mathbf{B}(\mathbf{x}-\mathbf{b})\|_2^2),$$

  where $\mathbf{a} = (0.3, 0.3)^T$, $\mathbf{b} = (-0.4, -0.4)^T$ and the matrices $\mathbf{A}$ and $\mathbf{B}$ are,

$$\mathbf{A} = \mathbf{Q}\,\mathrm{diag}\,(\sqrt{20}, 1)\,\mathbf{Q}^T, \quad \mathbf{B} = \mathbf{Q}\,\mathrm{diag}\,(1, \sqrt{20})\,\mathbf{Q}^T, \quad \mathbf{Q} = \frac{-1}{\sqrt{2}}\begin{bmatrix} 1 & 1 \\ 1 & -1 \end{bmatrix}.$$

The function $\psi(t)$ is a smooth cutoff function that ensures $\sigma|_{\partial\Omega} = 1$ by having $\psi(t) = 0$ for $t \geq 0.99$ and $\psi(t) = 1$ for $t \leq 0.5$. The smooth transition from 0 to 1 on $[0.5, 0.99]$ is obtained by an affine mapping of the function $\exp(1 + 1/s^2)$ defined on $[0, 1]$.

- Conductivity "`phantom1`" (Figure 3.10 right)

  A piecewise constant conductivity that represents a simplified chest phantom with conductivities relative to the background close to those of the human body during expiration [70, §5.1]. The background conductivity is 1. The lungs are simulated by two ellipses with conductivity $1/3$ and the heart has conductivity 2. These conductivities are dimensionless since we have divided by the conductivity of the background medium.

C.2 The smoothed box function

We recall from Section 3.2.1 that the measured DtN map $\mathcal{M}_n(\Lambda_\sigma)$ consists of measurements taken with n non-negative functions ϕ_i defined on the boundary $\partial\Omega$ and that have disjoint supports. In the numerics, all the ϕ_i are patterned from a single function and we explain how this is done.

We parametrize the boundary $\partial\Omega$ by an angle $\theta \in [0, 2\pi]$, and by a slight abuse of notation $\phi_i(\theta)$ represents $\phi_i(\mathbf{x}(\theta))$. Then the functions ϕ_i are constructed from a single function $\phi(t)$ with $\operatorname{supp}\phi \subset (-1, 1)$, by setting

$$\phi_i(\theta) = (n/\pi)\phi((n/\pi)(\theta - 2i\pi/n)).$$

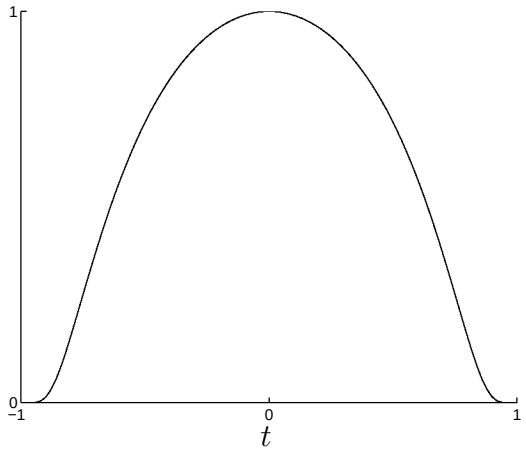

Figure C.1: The smoothed box function $\phi(t)$ we use to define the measured DtN map, rescaled to have values in $[0, 1]$.

This guarantees that the ϕ_i have disjoint supports since $\operatorname{supp} \phi_i \subset 2i\pi/n + (-\pi/n, \pi/n)$.

With this choice we are sure to get a layered resistor network from a layered conductivity. Indeed, when the conductivity σ is layered, the measured DtN map is a circulant matrix because of the $n-$fold rotational symmetry of the setup.

The particular function ϕ we chose is the smoothed box function depicted in Figure C.1, rescaled so that $\int_{-1}^{1} \phi(t)dt = 1$. The function $\phi(t)$ appearing in Figure C.1 is such that $\phi(t) = 1$ for $|t| \leq 0.1$ and $\phi(t) = 0$ for $|t| \geq 0.9$. The smooth transition from 0 to 1 on $[0.1, 0.9]$ and $[-0.9, -0.1]$ is obtained by an affine mapping of the function $\exp(1 + 1/s^2)$ defined on $[0, 1]$.

Bibliography

[1] N. I. Achieser. *Theory of approximation*. Dover Publications Inc., New York, 1992. ISBN 0-486-67129-1. Translated from the Russian and with a preface by Charles J. Hyman, Reprint of the 1956 English translation.

[2] G. Alessandrini. Stable determination of conductivity by boundary measurements. *Appl. Anal.*, 27(1-3):153–172, 1988. ISSN 0003-6811.

[3] G. Alessandrini. Singular solutions of elliptic equations and the determination of conductivity by boundary measurements. *J. Differential Equations*, 84(2): 252–272, 1990. ISSN 0022-0396.

[4] G. Alessandrini. Examples of instability in inverse boundary-value problems. *Inverse Problems*, 13(4):887–897, 1997. ISSN 0266-5611. doi:10.1088/0266-5611/13/4/001.

[5] A. L. Andrew. Asymptotic correction and inverse eigenvalue problems: an overview. *ANZIAM J.*, 46((C)):C1–C14, 2004/05. ISSN 1446-1811. URL `http://anziamj.austms.org.au/V46/CTAC2004/Andr/`.

[6] U. M. Ascher and E. Haber. Grid refinement and scaling for distributed parameter estimation problems. *Inverse Problems*, 17(3):571–590, 2001. ISSN 0266-5611. doi:10.1088/0266-5611/17/3/314.

[7] U. M. Ascher and E. Haber. A multigrid method for distributed parameter estimation problems. *Electron. Trans. Numer. Anal.*, 15:1–17 (electronic), 2003. ISSN 1068-9613. URL `http://etna.mcs.kent.edu/vol.15.2003/index.html`. Tenth Copper Mountain Conference on Multigrid Methods (Copper Mountain, CO, 2001).

[8] K. Astala, L. Päivärinta, and M. Lassas. Calderón's inverse problem for anisotropic conductivity in the plane. *Comm. Partial Differential Equations*, 30(1-3):207–224, 2005. ISSN 0360-5302. doi:10.1081/PDE-200044485.

[9] S. Asvadurov, V. Druskin, and L. Knizhnerman. Application of the difference Gaussian rules to solution of hyperbolic problems. *J. Comput. Phys.*, 158(1): 116–135, 2000. ISSN 0021-9991. doi:10.1006/jcph.1999.6410.

[10] S. Asvadurov, V. Druskin, and L. Knizhnerman. Application of the difference Gaussian rules to solution of hyperbolic problems. II. Global expansion. *J. Comput. Phys.*, 175(1):24–49, 2002. ISSN 0021-9991. doi:10.1006/jcph.2001.6878.

[11] S. Asvadurov, V. Druskin, M. N. Guddati, and L. Knizhnerman. On optimal finite-difference approximation of PML. *SIAM J. Numer. Anal.*, 41(1):287–305 (electronic), 2003. ISSN 1095-7170. doi:10.1137/S0036142901391451.

[12] J. A. Barceló, T. Barceló, and A. Ruiz. Stability of the inverse conductivity problem in the plane for less regular conductivities. *J. Differential Equations*, 173(2):231–270, 2001. ISSN 0022-0396. doi:10.1006/jdeq.2000.3920.

[13] D. C. Barnes. The inverse eigenvalue problem with finite data. *SIAM J. Math. Anal.*, 22(3):732–753, 1991. ISSN 0036-1410. doi:10.1137/0522044.

[14] H. Ben Ameur and B. Kaltenbacher. Regularization of parameter estimation by adaptive discretization using refinement and coarsening indicators. *J. Inverse Ill-Posed Probl.*, 10(6):561–583, 2002. ISSN 0928-0219.

[15] H. Ben Ameur, G. Chavent, and J. Jaffré. Refinement and coarsening indicators for adaptive parametrization: application to the estimation of hydraulic transmissivities. *Inverse Problems*, 18(3):775–794, 2002. ISSN 0266-5611. doi:10.1088/0266-5611/18/3/317.

[16] D. Boley and G. H. Golub. A survey of matrix inverse eigenvalue problems. *Inverse Problems*, 3(4):595–622, 1987. ISSN 0266-5611. doi:10.1088/0266-5611/3/4/010.

[17] L. Borcea. A nonlinear multigrid for imaging electrical conductivity and permittivity at low frequency. *Inverse Problems*, 17(2):329–359, 2001. ISSN 0266-5611. doi:10.1088/0266-5611/17/2/312.

[18] L. Borcea. Electrical impedance tomography. *Inverse Problems*, 18:R99–R136, 2002. doi:10.1088/0266-5611/18/6/201. Topical Review.

[19] L. Borcea and V. Druskin. Optimal finite difference grids for direct and inverse Sturm-Liouville problems. *Inverse Problems*, 18(4):979–1001, 2002. ISSN 0266-5611. doi:10.1088/0266-5611/18/4/303.

[20] L. Borcea, V. Druskin, and L. Knizhnerman. On the continuum limit of a discrete inverse spectral problem on optimal finite difference grids. *Comm. Pure Appl. Math.*, 58(9):1231–1279, 2005. ISSN 0010-3640. doi:10.1002/cpa.20073.

[21] G. Borg. Eine Umkehrung der Sturm-Liouvilleschen Eigenwertaufgabe. Bestimmung der Differentialgleichung durch die Eigenwerte. *Acta Math.*, 78:1–96, 1946. ISSN 0001-5962.

[22] R. M. Brown. Global uniqueness in the impedance-imaging problem for less regular conductivities. *SIAM J. Math. Anal.*, 27(4):1049–1056, 1996. ISSN 0036-1410. doi:10.1137/0527057.

[23] A.-P. Calderón. On an inverse boundary value problem. In *Seminar on Numerical Analysis and its Applications to Continuum Physics (Rio de Janeiro, 1980)*, pages 65–73. Soc. Brasil. Mat., Rio de Janeiro, 1980.

[24] E. J. Candès and D. L. Donoho. Recovering edges in ill-posed inverse problems: optimality of curvelet frames. *Ann. Statist.*, 30(3):784–842, 2002. ISSN 0090-5364. doi:10.1214/aos/1028674842. Dedicated to the memory of Lucien Le Cam.

[25] K. Chadan, D. Colton, L. Päivärinta, and W. Rundell. *An introduction to inverse scattering and inverse spectral problems*. SIAM Monographs on Mathematical Modeling and Computation. Society for Industrial and Applied Mathematics (SIAM), Philadelphia, PA, 1997. ISBN 0-89871-387-0. With a foreword by Margaret Cheney.

[26] M. Cheney, D. Isaacson, J. Newell, S. Simske, and J. Goble. Noser: An algorithm for solving the inverse conductivity problem. *Internat. J. Imaging Systems & Technol.*, 2:66–75, 1990. URL `http://www.rpi.edu/~cheney/downloads.html`.

[27] M. Cheney, D. Isaacson, and J. C. Newell. Electrical impedance tomography. *SIAM Rev.*, 41(1):85–101 (electronic), 1999. ISSN 1095-7200. doi:10.1137/S0036144598333613.

[28] E. Cherkaeva and A. C. Tripp. Inverse conductivity problem for inaccurate measurements. *Inverse Problems*, 12(6):869–883, 1996. ISSN 0266-5611. doi:10.1088/0266-5611/12/6/005.

[29] M. T. Chu. Inverse eigenvalue problems. *SIAM Rev.*, 40(1):1–39 (electronic), 1998. ISSN 1095-7200. doi:10.1137/S0036144596303984.

[30] M. T. Chu and G. H. Golub. Structured inverse eigenvalue problems. *Acta Numer.*, 11:1–71, 2002. ISSN 0962-4929.

[31] M. T. Chu and G. H. Golub. *Inverse eigenvalue problems*. Numerical Mathematics and Scientific Computation. Oxford University press, 2005.

[32] C. F. Coleman and J. R. McLaughlin. Solution of the inverse spectral problem for an impedance with integrable derivative. I, II. *Comm. Pure Appl. Math.*, 46(2):145–184, 185–212, 1993. ISSN 0010-3640.

[33] R. Courant and D. Hilbert. *Methods of mathematical physics. Vol. I.* Interscience Publishers, Inc., New York, N.Y., 1953.

[34] E. Curtis, E. Mooers, and J. Morrow. Finding the conductors in circular networks from boundary measurements. *RAIRO Modél. Math. Anal. Numér.*, 28 (7):781–814, 1994. ISSN 0764-583X.

[35] E. B. Curtis and J. A. Morrow. *Inverse Problems for Electrical Networks*, volume 13 of *Series on Applied Mathematics*. World Scientific, 2000.

[36] E. B. Curtis, D. Ingerman, and J. A. Morrow. Circular planar graphs and resistor networks. *Linear Algebra Appl.*, 283(1-3):115–150, 1998. ISSN 0024-3795. doi:10.1016/S0024-3795(98)10087-3.

[37] I. Daubechies, M. Defrise, and C. De Mol. An iterative thresholding algorithm for linear inverse problems with a sparsity constraint. *Comm. Pure Appl. Math.*, 57(11):1413–1457, 2004. ISSN 0010-3640. doi:10.1002/cpa.20042.

[38] S. Davydycheva, V. Druskin, and T. Habashy. An efficient finite-difference scheme for electromagnetic logging in 3d anisotropic inhomogeneous media. *Geophysics*, 68:1525–1536, 2003. doi:10.1190/1.1620626.

[39] C. de Boor and G. H. Golub. The numerically stable reconstruction of a Jacobi matrix from spectral data. *Linear Algebra Appl.*, 21(3):245–260, 1978. ISSN 0024-3795. doi:10.1016/0024-3795(78)90086-1.

[40] D. C. Dobson. *Stability and Regularity of an Inverse Elliptic Boundary Value Problem*. PhD thesis, CAAM Dept., Rice University, jun 1990. URL `http://www.caam.rice.edu/caam/content/techrep.html`.

[41] D. C. Dobson. Estimates on resolution and stabilization for the linearized inverse conductivity problem. *Inverse Problems*, 8(1):71–81, 1992. ISSN 0266-5611. doi:10.1088/0266-5611/8/1/005.

[42] D. C. Dobson and F. Santosa. An image-enhancement technique for electrical impedance tomography. *Inverse Problems*, 10(2):317–334, 1994. ISSN 0266-5611. doi:10.1088/0266-5611/10/2/008.

[43] V. Druskin. The unique solution of the inverse problem of electrical surveying and electrical well-logging for piecewise-continuous condutivity. *Izvestiya Earth Physics*, 18(1):51–53, 1982.

[44] V. Druskin. Spectrally optimal finite-difference grids in unbounded domains. Research Note EMG-002-97-22, Schlumberger-Doll Research, 1997.

[45] V. Druskin and L. Knizhnerman. Gaussian spectral rules for the three-point second differences. I. A two-point positive definite problem in a semi-infinite domain. *SIAM J. Numer. Anal.*, 37(2):403–422 (electronic), 2000. ISSN 1095-7170. doi:10.1023/A:1016600805438.

[46] V. Druskin and S. Moskow. Three-point finite-difference schemes, Padé and the spectral Galerkin method. I. One-sided impedance approximation. *Math. Comp.*, 71(239):995–1019 (electronic), 2002. ISSN 0025-5718. doi:10.1090/S0025-5718-01-01349-7.

[47] V. Druskin, L. Borcea, and L. Knizhnerman. On the sensitivity of Lanczos recursions to the spectrum. *Linear Algebra Appl.*, 396:103–125, 2005. ISSN 0024-3795. doi:10.1016/j.laa.2004.08.031.

[48] V. L. Druskin. Uniqueness of the determination of three-dimensional underground structures from surface measurements for a stationary or monochromatic field source. *Izv. Akad. Nauk SSSR Ser. Fiz. Zemli*, 3:63–69, 1985. ISSN 0002-3337.

[49] H. Dym and H. P. McKean. *Gaussian processes, function theory, and the inverse spectral problem*. Academic Press [Harcourt Brace Jovanovich Publishers], New York, 1976. Probability and Mathematical Statistics, Vol. 31.

[50] H. W. Engl, M. Hanke, and A. Neubauer. *Regularization of Inverse Problems*. Kluwer Academic Publishers, 1996.

[51] G. B. Folland. *Introduction to partial differential equations*. Princeton University Press, Princeton, NJ, second edition, 1995. ISBN 0-691-04361-2.

[52] F. G. Friedlander. *Introduction to the theory of distributions*. Cambridge University Press, Cambridge, second edition, 1998. ISBN 0-521-64015-6; 0-521-64971-4. With additional material by M. Joshi.

[53] I. M. Gel′fand and B. M. Levitan. On the determination of a differential equation from its spectral function. *Amer. Math. Soc. Transl. (2)*, 1:253–304, 1955.

[54] D. G. Gisser, D. Isaacson, and J. C. Newell. Electric current computed tomography and eigenvalues. *SIAM J. Appl. Math.*, 50(6):1623–1634, 1990. ISSN 0036-1399. doi:10.1137/0150096.

[55] G. H. Golub and C. F. Van Loan. *Matrix computations*. Johns Hopkins Studies in the Mathematical Sciences. Johns Hopkins University Press, Baltimore, MD, third edition, 1996. ISBN 0-8018-5413-X; 0-8018-5414-8.

[56] A. Greenbaum. Behavior of slightly perturbed Lanczos and conjugate-gradient recurrences. *Linear Algebra Appl.*, 113:7–63, 1989. ISSN 0024-3795. doi:10.1016/0024-3795(89)90285-1.

[57] J. Hadamard. Sur les problèmes aux dérivées partielles et leur signification physique. *Bull. Univ. Princeton*, 13:49–52, 1902.

[58] O. H. Hald. Inverse eigenvalue problems for Jacobi matrices. *Linear Algebra and Appl.*, 14(1):63–85, 1976. doi:10.1016/0024-3795(76)90064-1.

[59] O. H. Hald. The inverse Sturm-Liouville problem and the Rayleigh-Ritz method. *Math. Comp.*, 32(143):687–705, 1978. ISSN 0025-5718. URL `http://links.jstor.org/sici?sici=0025-5718%28197807%2932%3A143%3C687%3ATISPAT%3E2.0.CO%3B2-X`.

[60] H. Hochstadt. On the construction of a Jacobi matrix from spectral data. *Linear Algebra and Appl.*, 8:435–446, 1974. doi:10.1016/0024-3795(74)90077-9.

[61] H. Hochstadt. On the well-posedness of the inverse Sturm-Liouville problems. *J. Differential Equations*, 23(3):402–413, 1977. ISSN 0022-0396. doi:10.1016/0022-0396(77)90119-X.

[62] D. Ingerman and J. A. Morrow. On a characterization of the kernel of the Dirichlet-to-Neumann map for a planar region. *SIAM J. Math. Anal.*, 29(1): 106–115 (electronic), 1998. ISSN 1095-7154. doi:10.1137/S0036141096300483.

[63] D. Ingerman, V. Druskin, and L. Knizhnerman. Optimal finite difference grids and rational approximations of the square root. I. Elliptic problems. *Comm. Pure Appl. Math.*, 53(8):1039–1066, 2000. ISSN 0010-3640. doi:10.1002/1097-0312(200008)53:8¡1039::AID-CPA4¿3.0.CO;2-I.

[64] D. V. Ingerman. Discrete and continuous Dirichlet-to-Neumann maps in the layered case. *SIAM J. Math. Anal.*, 31(6):1214–1234 (electronic), 2000. ISSN 1095-7154. doi:10.1137/S0036141097326581.

[65] D. Isaacson. Distinguishability of conductivities by electric current computed tomography. *IEEE Trans. on Medical Imaging*, MI-5(2):91–95, 1986.

[66] B. Kaltenbacher. On the regularizing properties of a full multigrid method for ill-posed problems. *Inverse Problems*, 17(4):767–788, 2001. ISSN 0266-5611. doi:10.1088/0266-5611/17/4/313. Special issue to celebrate Pierre Sabatier's 65th birthday (Montpellier, 2000).

[67] B. Kaltenbacher and J. Schicho. A multi-grid method with a priori and a posteriori level choice for the regularization of nonlinear ill-posed problems. *Numer. Math.*, 93(1):77–107, 2002. ISSN 0029-599X. doi:10.1007/s002110100375.

[68] B. Kaltenbacher, M. Kaltenbacher, and S. Reitzinger. Identification of nonlinear *B-H* curves based on magnetic field computations and multigrid methods for ill-posed problems. *European J. Appl. Math.*, 14(1):15–38, 2003. ISSN 0956-7925. doi:10.1017/S0956792502005089.

[69] P. Kaup, F. Santosa, and M. Vogelius. A method for imaging corrosion damage in thin plates from electrostatic data. *Inverse Problems*, 12:279–293, 1996. doi:10.1088/0266-5611/12/3/008.

[70] K. Knudsen, J. Mueller, and S. Siltanen. Numerical solution method for the dbar-equation in the plane. *J. Comput. Phys.*, 198(2):500–517, 2004. ISSN 0021-9991. doi:10.1016/j.jcp.2004.01.028.

[71] R. Kohn and M. Vogelius. Determining conductivity by boundary measurements. *Comm. Pure Appl. Math.*, 37(3):289–298, 1984. ISSN 0010-3640.

[72] R. V. Kohn and M. Vogelius. Determining conductivity by boundary measurements. II. Interior results. *Comm. Pure Appl. Math.*, 38(5):643–667, 1985. ISSN 0010-3640.

[73] A. R. Krommer and C. W. Ueberhuber. *Computational integration*. Society for Industrial and Applied Mathematics (SIAM), Philadelphia, PA, 1998. ISBN 0-89871-374-9.

[74] N. Levinson. The inverse Sturm-Liouville problem. *Mat. Tidsskr. B.*, 1949: 25–30, 1949.

[75] B. M. Levitan. *Inverse Sturm-Liouville problems*. VSP, Zeist, 1987. ISBN 90-6764-055-7. Translated from the Russian by O. Efimov.

[76] L. Liu. *Stability estimates for the two-dimensional inverse conductivity problem*. PhD thesis, Department of Mathematics, University of Rochester, New York, 1997.

[77] B. D. Lowe, M. Pilant, and W. Rundell. The recovery of potentials from finite spectral data. *SIAM J. Math. Anal.*, 23(2):482–504, 1992. ISSN 0036-1410. doi:10.1137/0523023.

[78] H. R. MacMillan, T. A. Manteuffel, and S. F. McCormick. First-order system least squares and electrical impedance tomography. *SIAM Journal of Numerical Analysis*, 42(2):461–483, 2004. doi:10.1137/S0036142902412245.

[79] H. R. MacMillan, T. A. Manteuffel, and S. F. McCormick. First-order system least squares and electrical impedance tomography: part II. URL `http://amath.colorado.edu/pub/fosls/`. Unpublished manuscript, 2004.

[80] N. Mandache. Exponential instability in an inverse problem for the Schrödinger equation. *Inverse Problems*, 17(5):1435–1444, 2001. ISSN 0266-5611. doi:10.1088/0266-5611/17/5/313.

[81] V. A. Marčenko. Concerning the theory of a differential operator of the second order. *Doklady Akad. Nauk SSSR. (N.S.)*, 72:457–460, 1950.

[82] M. Marletta and R. Weikard. Weak stability for an inverse Sturm-Liouville problem with finite spectral data and complex potential. *Inverse Problems*, 21 (4):1275–1290, 2005. ISSN 0266-5611. doi:10.1088/0266-5611/21/4/005.

[83] S. F. McCormick and J. G. Wade. Multigrid solution of a linearized, regularized least-squares problem in electrical impedance tomography. *Inverse Problems*, 9 (6):697–713, 1993. ISSN 0266-5611. doi:10.1088/0266-5611/9/6/007.

[84] J. R. McLaughlin. Analytical methods for recovering coefficients in differential equations from spectral data. *SIAM Rev.*, 28(1):53–72, 1986. ISSN 0036-1445. doi:10.1137/1028003.

[85] J. R. McLaughlin. Stability theorems for two inverse spectral problems. *Inverse Problems*, 4(2):529–540, 1988. ISSN 0266-5611. doi:10.1088/0266-5611/4/2/015.

[86] M. Molinari, B. H. Blott, S. J. Cox, and G. J. Daniell. Adaptive mesh refinement in electrical impedance tomography. *Physiological Measurement*, 22: 91–96, 2001. doi:10.1088/0967-3334/22/1/312.

[87] M. Molinari, B. H. Blott, S. J. Cox, and G. J. Daniell. Optimal imaging with adaptative mesh refinement in electrical impedance tomography. *Physiological Measurement*, 23(1):121–128, 2002. doi:10.1088/0967-3334/23/1/311.

[88] A. I. Nachman. Reconstructions from boundary measurements. *Ann. of Math. (2)*, 128(3):531–576, 1988. ISSN 0003-486X. URL `http://links.jstor.org/sici?sici=0003-486X%28198811%292%3A128%3A3%3C531%3ARFBM%3E2.0.CO%3B2-%23`.

[89] A. I. Nachman. Global uniqueness for a two-dimensional inverse boundary value problem. *Ann. of Math. (2)*, 143(1):71–96, 1996. ISSN 0003-486X. URL `http://links.jstor.org/sici?sici=0003-486X%28199601%292%3A143%3A1%3C71%3AGUFATI%3E2.0.CO%3B2-E`.

[90] F. Natterer. A discrete Gelfand-Levitan theory. URL `http://wwwmath1.uni-muenster.de/num/Preprints/1998/natterer_3/index.html`. Electronic, from the author's webpage, 1989.

[91] J. Nocedal and S. J. Wright. *Numerical Optimization*. Operations Research. Springer, 1999.

[92] R. L. Parker. The inverse problem of resistivity sounding. *Geophysics*, 142: 2143–2158, 1984.

[93] P. P. Petrushev and V. A. Popov. *Rational approximation of real functions*, volume 28 of *Encyclopedia of Mathematics and its Applications*. Cambridge University Press, Cambridge, 1987. ISBN 0-521-33107-2.

[94] J. Pöschel and E. Trubowitz. *Inverse spectral theory*, volume 130 of *Pure and Applied Mathematics*. Academic Press Inc., Boston, MA, 1987. ISBN 0-12-563040-9.

[95] W. Rundell and P. E. Sacks. The reconstruction of Sturm-Liouville operators. *Inverse Problems*, 8(3):457–482, 1992. ISSN 0266-5611. doi:10.1088/0266-5611/8/3/007.

[96] A. Seagar, Y. Yeo, and R. Bates. Full-wave computed tomography, part 2: resolution limits. *IEE Proceedings Pt. A, Science, Measurement and Technology*, 131(8):616–622, November 1984.

[97] A. Seagar, D. Barber, and B. Brown. Theoretical limits to sensitivity and resolution in impedance imaging. *Clinical Physics and Physiological Measurement*, 8(4A):13–31, 1987. doi:10.1088/0143-0815/8/4A/003.

[98] T. I. Seidman. A convergent approximation scheme for the inverse Sturm-Liouville problem. *Inverse Problems*, 1(3):251–262, 1985. ISSN 0266-5611. doi:10.1088/0266-5611/1/3/009.

[99] E. Somersalo, M. Cheney, D. Isaacson, and E. Isaacson. Layer stripping: a direct numerical method for impedance imaging. *Inverse Problems*, 7(6):899–926, 1991. ISSN 0266-5611. doi:10.1088/0266-5611/7/6/011.

[100] E. Somersalo, M. Cheney, and D. Isaacson. Existence and uniqueness for electrode models for electric current computed tomography. *SIAM J. Appl. Math.*, 52(4):1023–1040, 1992. ISSN 0036-1399. doi:10.1137/0152060.

[101] T.-J. Stieltjes. Recherches sur les fractions continues. *Ann. Fac. Sci. Toulouse Sci. Math. Sci. Phys.*, 8(4):J1–J122, 1894. ISSN 0996-0481. URL `http://www.numdam.org/item?id=AFST_1894_1_8_4_J1_0`.

[102] T.-J. Stieltjes. Recherches sur les fractions continues [Suite et fin]. *Ann. Fac. Sci. Toulouse Sci. Math. Sci. Phys.*, 9(1):A5–A47, 1895. ISSN 0996-0481. URL `http://www.numdam.org/item?id=AFST_1895_1_9_1_A5_0`.

[103] Z. Q. Sun. On an inverse boundary value problem in two dimensions. *Comm. Partial Differential Equations*, 14(8-9):1101–1113, 1989. ISSN 0360-5302.

[104] Z. Q. Sun. The inverse conductivity problem in two dimensions. *J. Differential Equations*, 87(2):227–255, 1990. ISSN 0022-0396.

[105] Z. Q. Sun and G. Uhlmann. Generic uniqueness for an inverse boundary value problem. *Duke Math. J.*, 62(1):131–155, 1991. ISSN 0012-7094. doi:10.1215/S0012-7094-91-06206-X.

[106] J. Sylvester and G. Uhlmann. A uniqueness theorem for an inverse boundary value problem in electrical prospection. *Comm. Pure Appl. Math.*, 39(1):91–112, 1986. ISSN 0010-3640.

[107] J. Sylvester and G. Uhlmann. A global uniqueness theorem for an inverse boundary value problem. *Ann. of Math. (2)*, 125(1):153–169, 1987. ISSN 0003-486X. URL `http://links.jstor.org/sici?sici=0003-486X%28198701%292%3A125%3A1%3C153%3AAGUTFA%3E2.0.CO%3B2-7`.

[108] J. Sylvester and G. Uhlmann. Inverse boundary value problems at the boundary–continuous dependence. *Comm. Pure Appl. Math.*, 41(2):197–219, 1988. ISSN 0010-3640.

[109] W. Symes. Inverse boundary value problems and a theorem of Gel′fand and Levitan. *J. Math. Anal. Appl.*, 71(2):379–402, 1979. ISSN 0022-247X. doi:10.1016/0022-247X(79)90199-9.

[110] L. N. Trefethen and D. Bau, III. *Numerical linear algebra*. Society for Industrial and Applied Mathematics (SIAM), Philadelphia, PA, 1997. ISBN 0-89871-361-7.

[111] G. Uhlmann. Developments in inverse problems since Calderón's foundational paper. In *Harmonic analysis and partial differential equations (Chicago, IL, 1996)*, Chicago Lectures in Math., pages 295–345. Univ. Chicago Press, Chicago, IL, 1999. URL `http://www.math.washington.edu/~gunther/publications/`.

[112] C. R. Vogel. *Computational Methods for Inverse Problems*. Frontiers in Applied Mathematics. SIAM, 2002.